Synthesis and Characterization of Thin Ceramic-Carbonate Dual-Phase Membranes for Carbon Dioxide Separation

by

Bo Lu

A Dissertation Presented in Partial Fulfillment
of the Requirements for the Degree
Doctor of Philosophy

Approved April 2014 by the
Graduate Supervisory Committee:

Jerry Y.S. Lin, Chair
Peter Crozier
Mary Laura Lind
Marcus Herrmann
Erica Forzani

ARIZONA STATE UNIVERSITY

May 2014

ABSTRACT

High temperature CO_2 perm-selective membranes offer potential for uses in various processes for CO_2 separation. Recently, efforts are reported on fabrication of dense ceramic-carbonate dual-phase membranes. The membranes provide selective permeation to CO_2 and exhibit high permeation flux at high temperature. Research on transport mechanism demonstrates that gas transport for ceramic-carbonate dual-phase membrane is rate limited by ion transport in ceramic support. Reducing membrane thickness proves effective to improve permeation flux. This dissertation reports strategy to prepare thin ceramic-carbonate dual-phase membranes to increase CO_2 permeance. The work also presents characteristics and gas permeation properties of the membranes.

Thin ceramic-carbonate dual-phase membrane was constructed with an asymmetric porous support consisting of a thin small-pore ionic conducting ceramic top-layer and a large pore base support. The base support must be carbonate non-wettable to ensure formation of supported dense, thin membrane. Macroporous yttria-stabilized zirconia (YSZ) layer was prepared on large pore $Bi_{1.5}Y_{0.3}Sm_{0.2}O_{3-\delta}$ (BYS) base support using suspension coating method. Thin YSZ-carbonate dual-phase membrane (d-YSZ/BYS) was prepared via direct infiltrating Li/Na/K carbonate mixtures into top YSZ layers. The thin membrane of 10 μm thick offered a CO_2 flux 5-10 times higher than the thick dual-phase membranes.

$Ce_{0.8}Sm_{0.2}O_{1.9}$ (SDC) exhibited highest CO_2 flux and long-term stability and was chosen as ceramic support for membrane performance improvement. Porous SDC layers were co-pressed on base supports using SDC and BYS powder mixtures which provided better sintering comparability and carbonate non-wettability. Thin SDC-carbonate dual-phase membrane (d-SDC/SDC60BYS40) of 150 μm thick was synthesized on SDC60BYS40. CO_2 permeation flux for d-SDC/SDC60BYS40 exhibited increasing dependence on temperature and partial pressure gradient. The flux was higher than other SDC-based dual-phase membranes. Reducing membrane thickness proves effective to increase CO_2 permeation flux for the dual-phase membrane.

The chapters in the dissertation are modified versions of the following papers published or to be submitted for publication:

Chapter 2

Lu, B., Lin, Y. S. (2011). Sol–gel synthesis and characterization of mesoporous yttria-stabilized zirconia membranes with graded pore structure. *Journal of Material Science*, 46, 7056-7066.

Chapter 3

Lu, B., Lin, Y. S. (2013). Synthesis and characterization of thin ceramic-carbonate dual-phase membranes for carbon dioxide separation. *Journal of Membrane Science*, 444, 402-411.

Chapter 4

Norton, T. T., Lu, B., Lin, Y. S. (2014). Carbon dioxide permeation properties and stability of samarium doped ceria-carbonate dual-phase membrane**.** *Journal of Membrane Science*, submitted.

Chapter 5

Lu, B., Lin, Y. S. (2014). Asymmetric thin samarium doped cerium oxide-carbonate dual-phase membrane for carbon dioxide separation. *AIChE Journal*, to be submitted.

Dedication

To my parents
Xinmin Lu
Xiumei Zhu

Thanks for your love and support

ACKNOWLEDGEMENTS

First, I would like to take the opportunity to thank my parents. Without whose substantial support, I would not come to a place tens of thousands miles away from my hometown to pursue my degree. Their love and encouragements always being a momentum pushed me forward and helped me go through hard times during my study in last 6 years. I would like to say "thank you" from the bottom of my heart to my father-Xinmin Lu and my mother-Xiumei Zhu.

I would like to thank my advisor, Dr. Jerry Lin, for his guidance and support for my graduate study. Dr. Lin let me join his group in 2008 and helped me transfer from my previous biological background to a brand new area-membrane study. He gave me opportunity to do exciting and interesting research. I learned a great deal-not only academic research but also other aspects such as management skills, leadership, logical thinking and so on-from him. All the knowledge will be beneficial for the rest of my life. I fully appreciate the support that he gave to me throughout my time here.

I would like to thank Dr. Peter Crozier, Dr. Mary Laura Lind, Dr. Marcus Herrmann and Dr. Erica Forzani for their willingness to serve on my committee. Thanks them for lending their expertise and making recommendations on solving difficulties and improving quality of my work. I would also like to thank Fred Pena. He helped me repair broken setups and give advice on designing new equipments. His kind heart facilitated my research progress.

Finally, I would like thank all the current and former group members in Dr. Lin's group that I have had the pleasure to work with: Dr. Matthew Anderson, Dr. Jay Kniep, Dr. Shriya Seshadri, Dr. Carrie Eggen, Dr. Ding Wang, Dr. Tyler Norton, Dr. Haibing Wang, Dr. Zebao Rui, Dr. Jose Ortiz-Landeros, Dr. Zhenxia Zhao, Dr. Chaoji, Dr. Xiaoping Liang, Dr. Xueliang Dong, Dr. Xiaojuan Hu, Dr. Defei Liu, Dr. Wanliang Mi, Teresa Rosa , Xiaoli Ma, Nick Linneen, Alex Kasik, Yang Liu, Joshua James, Huifeng Zhang, and Stewart Mann. Special thanks go to Dr. Tyler Norton for his contribution to the work documented in Chapter 4.

I highly appreciate the US Department of Energy, the National Science Foundation, and Science Foundation Arizona for the financial support of this work.

TABLE OF CONTENTS

Page

CHAPTER Page

CHAPTER Page

CHAPTER Page

LIST OF TABLES

Table Page

LIST OF FIGURES

Figure Page

Figure Page

Figure Page

Figure Page

CHAPTER 1

GENERAL INTRODUCTION

1.1 Introduction

Emission of carbon dioxide (CO_2) and other greenhouse gases into atmosphere has caused subsequent environmental problems such as global warming. Global CO_2 emission from coal combustion is predicted to increase from 9 Gton/year in 2000 to 32 Gton/year in 2050 [MTI Interdisciplinary Study, 2007]. Flue gas from coal-fired power plants is one of the main contributors to the problem [Merkel et al., 2010]. The success in CO_2 removal is to capture it directly from the flue gas. Flue gas is primarily composed of carbon dioxide and nitrogen, with temperature ranging from a few hundred to over thousand degree C depending on the locations of the gas within the plant. Acidic compounds such as sulfur oxide (SO_x) and nitride oxide (NO_x) are also present making CO_2 separation complicated and difficult.

It is highly desirable to separate carbon dioxide without cooling down the flue gas considering energy and capital cost. However, harsh environment-high temperature and acidic atmosphere-where flue gas comes out makes it hard and expensive to fulfill. Separation methods such as absorption, adsorption, cryogenic distillation and membrane process have been studied for the purpose. At present, amine solvent absorption and cryogenic distillation are most commonly used techniques for CO_2 separation from flue gas [Aaron & Tsouris, 2005]. Both methods can achieve high purity CO_2 streams.

However, amine solvents are expensive and absorption is not a continuous process due to requirement of regeneration or recharging. Cryogenic distillation is highly energy consumable because gas must be cooled considerably for separation. Therefore new and better technologies are needed for carbon dioxide separation.

Three strategies are considered to capture CO_2 from coal-combustion process [Figueroa et al., 2008]: post-combustion, oxy-combustion and pre-combustion. In the post-combustion process, CO_2 is removed from flue gas after combustion. In the oxy-combustion, oxygen is separated from air and then goes through combustion with fossil fuels. The process generates a nearly sequestration-ready CO_2-enriched stream. In the pre-combustion process, carbon in the fuel is removed or separated prior to combustion process. After reforming or shift reaction, high pressure CO_2 and H_2 streams are produced for separation. Membrane process exhibits the potential applied in all three processes. It is a continuous, steady state process and capable of handling high throughput stream that makes it especially useful for gas separation. Oxygen permeable membranes are suitable for air separation for oxy-combustion. H_2 or CO_2 selective membranes could be used in pre-combustion process for separation after reforming or water gas shift reaction. Both inorganic and polymeric membranes are studied for post-combustion process operated in the temperature range of 50-150^oC.

The majority of academic research on membrane process for carbon dioxide separation is focused on the polymer membrane due to low cost and ease of fabrication

[Powell and Qiao, 2006, Bernado et al., 2009]. However, polymer membranes are unstable in acidic condition and at high temperature. Plasticization of polymer in pressurized flow system also limits its application in industrial process. Inorganic membranes have drawn attentions due to its harsh environmental withstanding and stable properties compared to polymeric membranes.

The chapter will present a review on inorganic membranes for CO_2 separation especially of CO_2/N_2 mixtures. Inorganic membranes have shown capability of withstanding severe conditions at high temperature and pressure and acidic environment. The membranes can be broken into two categories: porous and dense. A brief review is given on status of microporous (carbon, silica and zeolite) and traditional dense (lithium zirconate/silicate) membranes for carbon dioxide separation first. The following is a detailed review on dense, carbonate dual-phase membranes (metal, ceramic) for high temperature CO_2 separation. Thin ionic-conducting membranes for gas separation are the last part. Membrane with reduced thickness demonstrates better gas separation and permeation performance. The chapter concludes with the objective of the work: identify synthesis and characteristics of the thin dual-phase membranes. Gas permeation properties through the membranes are studied as well.

1.2 Inorganic membranes

Inorganic membranes are often comprised of metals, glasses, or ceramic materials and have better mechanical, chemical, and especially thermal stability over the polymer

counterparts [Hsieh 1996, Lin et al., 2002]. Most research has focused on the use of microporous membrane (i.e., carbon, silicas, and zeolites) to take advantage of their molecular sieving ability to separate CO_2 from N_2 [Lin, 2001; Shekhawat et al. 2003, Bounaceur et al, 2006; Yang et al, 2008; Scholes et al., 2010; Anderson et al., 2012]. A few groups also reported gas separation using the dense membranes [Kawamura et al., 2005, Yamaguchi et al., 2007].

1.2.1 Microporous carbon membranes

A considerable amount of work has been performed on microporous carbon membrane for CO_2 and N_2 separation. The membranes are made via pyrolysis/carbonization of thermosetting polymer precursors such as polyacrylonitriles, polyimides, phenolic resins, polyfurfuryl alcohol (PFA), and polyvinyl chloride on porous substrates [Koresh and Sofer, 1983]. Pyrolysis is heating the polymers at high temperature up to 1000^{o}C in an inert or vacuum environment to burn off everything except the elemental carbon matrix. The matrix left creates a network of pores by which the actual membrane is formed. In addition to the precursors used, adjusting the heating rate, pyrolysis temperature and sintering atmosphere help to fabricate the carbon membranes with well-controlled morphology and pore structure with narrow pore size distribution [Lin et al., 2002]. This makes them ideal candidates for separating gases with similar kinetic diameters, as is the case between CO_2 and N_2. Carbon also having good CO_2 sorption characteristics strengthens its separation capability.

Microporous carbon membranes for CO_2 and N_2 separation have been prepared by the pyrolysis of polyamic films derived from 3, 3', 4, 4'-biphenylteracarboxylic dianhydride (BPDA) and 4, 4'-oxydianline (ODA) [Hayashi et al., 1995], BPDA-ODA polymer precursor with 2.4-diaminotoluene [Yamamoto, et al., 1997], PFA [Shiflett and Folye, 2000, Wang et al., 2000] and polyelectrolyte/polyimide blend [Barsema et al., 2005]. These carbon membranes were obtained by coating a thin polymer film on a porous disk or tubular support followed by pyrolysis at high temperature. Recently, cesium-incorporated carbon membranes were developed to improve separation performance under humid conditions [Kai et al., 2009]. A cardo-type polyimide was chosen as the precursor. Cesium carbonate (Cs_2CO_3) was chosen as a Cs source and blended with precursor solution. Carbonization was conducted at 600°C for 3 h under a nitrogen atmosphere. The Cs-incorporated carbon membranes achieved CO_2 permeance and separation factor ($\alpha CO_2/N_2$) of 9.8×10^{-9} mol/m^2/s/Pa and 44, respectively, and were greater than values for the original carbon membranes of 1.1×10^{-9} mol/m^2/s/Pa and 11.

The microporous carbon membrane using polyetherimide as a precursor, were prepared with mesoporous silica as filler forming a composite membrane [Tseng et al., 2011]. Incorporation of silica SBA-15 into the carbon matrix appeared to generate a more porous structure. SBA-15/CMS composite membrane exhibited gas permeability higher than that of the pure CMS membrane, whereas its selectivity was the same. Hollow fiber carbon membranes were made from the cellulosic precursors [He and Hagg,

2011, He et al., 2011]. By optimizing operating parameters including pressure, temperature, retentate flow rate and feed CO_2 composition, a CO_2-purity of 90% was achieved with 60% CO_2 capture. All the membranes mentioned above are able to effectively separate CO_2 from N_2 at low temperatures where adsorption-controlled solution diffusion is the dominant transport mechanism. At high temperature, the selectivity is determined by the diffusivity variation between CO_2 and N_2. CMS membranes exhibit small selectivity (<5) at temperature above 150^{o}C [Anderson et al., 2012] indicate that pore size is not sufficiently small (< 0.4 nm) to show molecular sieving effects.

1.2.2 Microporous silica membranes

Microporous silica membranes are favorable candidates for gas separation due to their high thermal stability, porosity and unprecedented performance. Smaller pore size (0.3-0.4 nm) makes them effectively to separate CO_2 from N_2 with similar kinetic diameter. The porous silica membranes are often prepared by depositing a thin layer-tens of nanometers-onto a porous support by either sol-gel method [Uhlhorn et al., 1989, Kusakabe et al., 1999] or chemical vapor deposition (CVD) [Cooper and Lin, 2002].

The sol-gel method includes hydrolysis and condensation of a silica precursor, such as tetraethoxysilane (TEOS), to obtain a polymeric sol. Thin, microporous silica film is prepared by dip-coating the sol on the support. Pore structure of the membrane will be determined by the fractal structure and interpenetration of the silica clusters in the sol and

subsequent drying and calcination process. Ultra thin silica membranes with the thickness smaller than 100 nm could be obtained by controlling sol-gel concentration, dip-coating conditions and quality of the support [Uhlhorn et al., 1989, de Vos et al., 1999, Sakamoto et al., 2007].

Novel sol-gel dip-coating process was also developed to prepare dual-layer microporous silica membranes [Tsai et al., 2000]. A surfactant template silica (STS) intermediate layer was introduced on top of porous support to improve its 'surface finish' and to prevent a subsequently deposited microporous over-layer from penetrating into the support. Microporous silica top-layer prepared by the dual-layer process improved both flux and selectivity compared to membrane made by a single-layer process using only the microporous over-layer. Xomeritakis et al. synthesized microporous silica membranes via a traditional sol-gel chemistry and surfactant-assisted self-assembly combination method [Xomeritakis et al., 2007]. The membrane achieved a CO_2 permeance of 3.0×10^{-7} mol/m^2/s/Pa coupled with a CO_2/N_2 separation factor in excess of 80 at room temperature. Recently, sol-gel derived silica membranes were also developed on tubular support [Xomeritakis et al., 2009].

The CVD method involves decomposition or oxidation of a silica precursor, such as TEOS or $SiCl_4$, at the vapor phase in the supports pores or on the surface of the support [Okubo and Inoue, 1989, Sea and Lee, 2001]. The pore structure of the CVD silica is defined by the network opening of amorphous silica with a pore size down to 0.3

nm. The thickness of the membranes ranges from 100 nm to about a few micrometers that is larger than the sol-gel derived silica membranes. Hence the CVD silica membranes have smaller CO_2 permeance in the range of 10^{-10}-10^{-8} mol/m^2/s/Pa. However, silica membranes prepared by high temperature (>600^{o}C) CVD exhibit better stability than the sol-gel derived silica membranes.

Ultra-thin silica membranes were prepared on a Vycor® microporous glass tubing substrate via high temperature sub-atmospheric CVD [Cuffe et al., 2006]. The membranes achieved CO_2/N_2 selectivities of 36 and 75 at 600^{o}C for CVD temperature of 600^{o}C and 670^{o}C. A selectivity of 275 was also obtained when the CVD temperature was decreased to 500^{o}C. Oyama and co-workers [Gu and Oyama, 2007] prepared thermally stable microporous silica membranes by high temperature CVD method. The pore size of the synthesized membrane was 0.3 nm and the membrane exhibited CO_2 and N_2 permeances separately of 2.0×10^{-10} and 9.0×10^{-11} mol/m^2/s/Pa at 600^{o}C. CO_2/N_2 selectivity was only 2.22. In general, silca membranes achieve a permeance that is one to two orders of magnitude higher than carbon membranes at the expense of a lower separation factor of CO_2/N_2 [Anderson et al., 2012]. Similar to carbon membranes, separation performance of silica membranes significantly degrades at high temperature where gas transport is dominated by diffusivity variation of the gases.

1.2.3 Zeolite membranes

Zeolites are crystalline aluminosilicates consisting of different pore connectivities resulting from various connections of TO_4 tetrahedrals (T = Si or Al). Combination of molecular sieving capabilities and adsorption characteristics make the membranes particularly useful for CO_2 separation. The membranes are often prepared by *in situ* nucleation and crystal growth or seeded nucleation followed by secondary crystal growth on macroporous alumina support. Most zeolite membranes are at least 1 μm thick due to packing of zeolite crystallites with size larger than 100 nm.

Among all the zeolite membranes, FAU-type zeolite Y has received most attention for CO_2 separation [Kusakabe et al., 1997, Gu et al., 2005]. These membranes exhibited CO_2 permeance in the range of 10^{-7}-10^{-6} mol/m^2/s/Pa with CO_2/N_2 selectivity up to 100. Recently, zeolite Y membranes were synthesized on alumina supports with rapid and slow growth solutions by secondary growth method [White et al., 2010]. Membranes formed from the rapid growth solution were 2−2.5 μm thick, while for the slower growth solution, a composite structure was observed with a dense membrane of 350−600 nm thick covered by a rather thick porous zeolite layer (25 μm). Both membranes exhibited similar separation properties and achieved extremely high CO_2/N_2 selectivity over 500. The thicker membrane had lower permeance (2.0×10^{-9} mol/m^2/s/Pa).

Along with Y-type zeolite membranes, the MFI-type ZSM-5 membranes have also been investigated for CO_2/N_2 separation [Bernal et al., 2004]. Shin et al. [Shin et al.,

2005] prepared ZSM-5 zeolite membranes via hydrothermal-treating various porous α-alumina tubes in template reaction mixtures. The membranes were also surface-modified by dip-coating with polymeric silica sol which filled up the inter-crystalline voids to improve CO_2 separation efficiency. Modified ZSM-5 zeolite membrane obtained a CO_2/N_2 separation factor of 54.3 at 25°C and 14.9 at 100°C with reduced permeance of 3.6×10^{-8} mol/m^2/s/Pa. Other types of zeolite membranes studied for CO_2 and N_2 separation include SAPO-34 (silicoalumino-phosphate) [Poshusta et al., 2000, Venna and Carreon, 2011, Ping et al., 2012], LTA type A zeolite [Zhou et al., 2007] and DDR-type zeolite [Tomita et al., 2004].

The pore size of different zeolites decreases in the order: FAU (0.7 nm) > MFI (0.55 nm) > SAPO-34, LTA and DDR (0.4 nm). However, Y type zeolite membranes with the largest pore size exhibit better CO_2 separation capability than smaller pore zeolite membranes indicating that CO_2/N_2 separation for zeolite membranes is majorly determined by surface chemistry rather than pore size. At room temperature, zeolite membranes shows better separation performance than microporous carbon and silica membranes considering both permeability and separation factor [Kusakabe et al., 1997]. High separation factors for zeolite membranes are generally achieved only when binary CO_2 and N_2 are used due to its characteristic sorption to CO_2 within the pores. Same as carbon and silica, zeolite membranes also suffer from decreasing CO_2/N_2 separation factor with increasing temperature above 200^{o}C [Anderson et al., 2012]. Figure 1.1

summarizes $\alpha CO_2/N_2$ dependence on permeation temperature for three microporous membranes. Selectivity decreases when temperature increases.

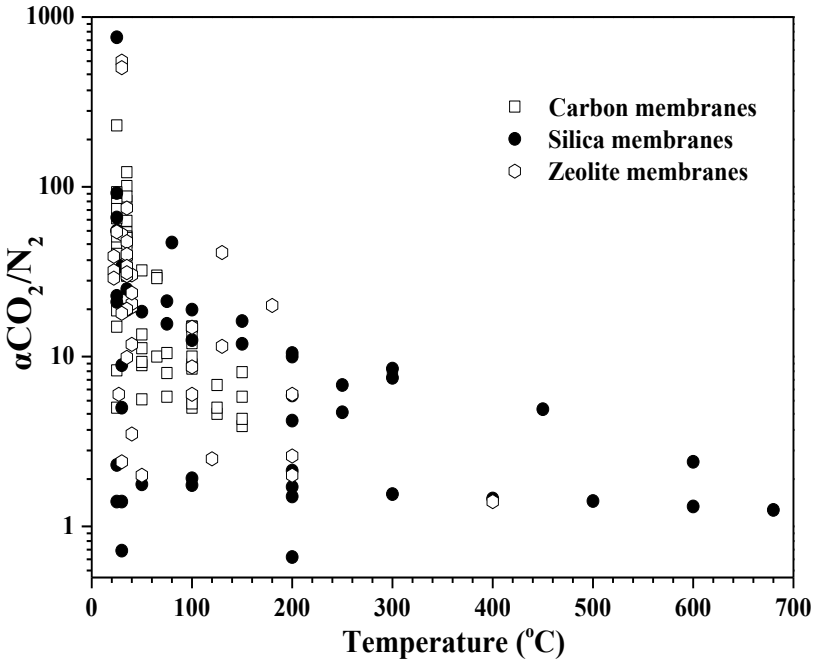

Figure 1.1 $\alpha CO_2/N_2$ dependence on permeation temperature for microporous membranes

1.2.4 Dense inorganic membranes

Inorganic microporous membranes mentioned above exhibit both good gas permeance and selectivity at low temperature. However, gas permeation through the membrane transferring from adsorption to diffusivity domination leads to decrease in membrane selectivity at high temperature. Dense inorganic membranes were developed for high temperature carbon dioxide separation. Original efforts were made on developing molten carbonate fuel cell (MCFC) [Abdel-Salam and Winnick, 1976, Kang and Winnick, 1985] and carbon dioxide separation became possible if external current is provided in MCFC without fuel injection.

Recent work reported use of dense lithium zirconate and lithium silicate membranes. Ida and Lin studied CO_2 sorption/desorption on pure and carbonates (Li/K) doped lithium zirconate (Li_2ZrO_3) [Ida and Lin, 2003]. Dense Li_2ZrO_3 membranes [Kawamura et al., 2005] were synthesized and Li_2ZrO_3 reversibly reacted with CO_2 forming Li_2CO_3 and ZrO_2 respectively capable of carrying CO_2 and conducting O_2 ion. Combination of selective reaction and electrolytes conduction made the membrane selective to CO_2. Yamaguchi et al. synthesized lithium silicate (Li_4SiO_4) membranes. The membranes were dipped and heat treated on porous alumina supports first and further coated with carbonate mixtures (20 mol% K_2CO_3 and 80 mol% Li_2CO_3) [Yamaguchi et al., 2007]. The membranes exhibited CO_2 permeance value around 10^{-8} mol/m^2/s/Pa and CO_2/N_2 selectivity only between 4 and 6 between 525 and 625^{o}C. Selective permeance of CO_2 through the membrane was possibly assisted by ionic diffusion through the liquid phase electrolyte and solid phase skeleton.

Both microporous and dense inorganic membranes show limited effectiveness for CO_2 separation at relatively high temperature. For some applications, such as solid fuel gasification and hydrogen production systems that desired to be operated in the high temperature regime (400-1100°C) or separation in acid flue gas (>350°C), an efficient CO_2 separation membrane that could maintain performance at high temperature is highly desirable. Recently, attempts at creating CO_2 perm-selective membranes at high temperature have turned to use dense, dual-phase carbonate membranes.

1.3 Dual-phase membranes

Lin's group [Chung et al., 2005] first came up with the idea of dense, dual-phase membranes. The membrane is consisting of an ionic or electronic conducting solid phase and a molten carbonate liquid phase as shown in Figure 1.2.

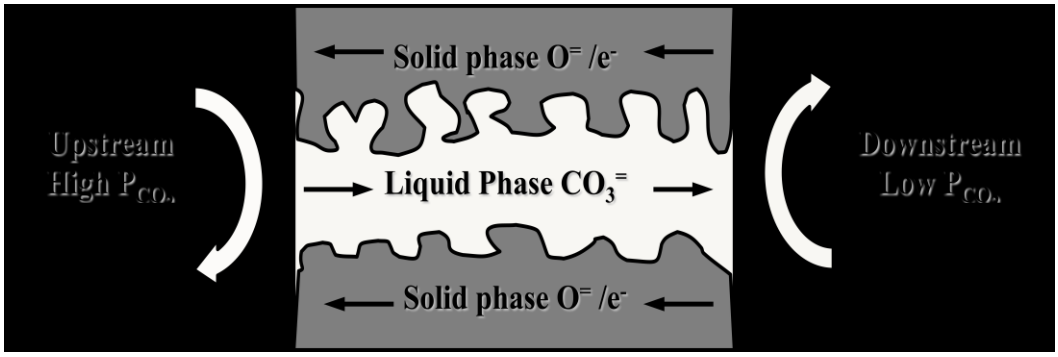

Figure 1.2 Concept of ceramic-carbonate dual-phase membrane for CO_2 separation

CO_2 permeates through the membrane driven by upstream and downstream partial pressure gradient. Oxygen ion or electron transports in the solid phase while carbonate ion transports in the liquid phase. The membrane is perm-selective to CO_2 guaranteed by its dense property and inability to ionize of other gases such as N_2.

1.3.1 Metal-carbonate dual-phase membranes

Original attempt at making dual-phase membrane was using electronic-conductive metal supports due to their high electronic conductivity (σ_e). Lin and coworkers first synthesized metal-carbonate dual-phase membrane by infiltrating eutectic carbonate mixtures (Li/Na/K) into a porous stainless steel support [Chung et al., 2005]. High temperature gas permeation tests were conducted from 450^{o}C to 750^{o}C and CO_2 and O_2 were applied as feed gas. CO_2 and O_2 ionized with electron in the support forming

CO_3^{2-} at the membrane surface as shown in Equation 1.1

$$CO_2 + \frac{1}{2}O_2 + 2e^- \leftrightarrow CO_3^{2-} \quad (1.1)$$

CO_2 partial pressure gradient across the membrane provided a driving force for the carbonate ions to transport through the molten carbonate phase of the membrane. On the permeate side, the reverse reaction took place releasing CO_2 and O_2. Inert gas such as N_2 could not permeate through the membrane due to its inability to ionize. At 650°C, a CO_2 permeation flux of 1.27×10^{-7} mol/s/cm^2 was measured with a CO_2/N_2 separation factor of 16. However, at temperatures over 650°C, stainless steel support would react with molten carbonates forming lithium iron oxides-$LiFe_5O_8$ and $LiFeO_2$-on the membrane surface [Chung et al., 2005]. The oxides had very low electronic conductivity [Biedenkopf et al., 2000] and stainless steel became ineffective in electron transport. Consequently, CO_2 and O_2 were unable to react with electrons and CO_2 permeance through the membrane dramatically decreased [Chung et al., 2005].

Xu et al. improved membrane performance by replacing stainless steel with metal silver (Ag) [Xu et al., 2012]. A maximum CO_2 flux of 7.09×10^{-3} mol/s/m^2 was achieved at 650°C. However, a similar drop in gas permeance was observed at higher temperature that was believed to cause by loss of molten carbonate from silver support [Lehman et al., 1998, Xu et al., 2012]. Long-term stability test exhibited an initial increase in gas flux for the first 20 h, followed by a gradual decrease in the next 60 h. This transient behavior is explained based on the Ag sintering mechanism. Recently,

Zhang et al. improved membrane stability by using surface-modified metal silver with Al_2O_3 colloidal solution [Zhang et al., 2014]. After infiltration, formation of $LiAlO_2$ improved silver's wettability to molten carbonate [Zhu & Huang, 2012] and its sintering property. Loss of carbonate was mitigated and silver-carbonate dual-phase membrane maintained a CO_2 permeation flux of 3.55×10^{-3} mol/s/m^2 for 130 h at 650^{o}C.

Metal-carbonate dual-phase membrane exhibits high CO_2 permeation flux [Chung et al., 2005, Xu et al., 2012]. However, molten carbonates tending to react with metal supports at high temperature (>650^{o}C) prevent ion transport. Due to inability to conduct oxygen ion, O_2 has to be present in CO_2-rich side of the metal support to form carbonate ion and both gases will permeate through the membrane. Additional steps needed to remove O_2 from permeate products. Both limit application of metal-carbonate dual-phase membranes. To overcome the shortcomings, improvement was made by replacing metal supports with mixed or ionic conducting ceramics.

1.3.2 Ceramic-carbonate dual-phase membranes

Anderson and Lin first proposed use of ionic conducting ceramics as the solid phase for the dual-phase membranes [Anderson & Lin, 2006]. The membrane could let CO_2 permeate through at high temperature due to the transport of carbonate ion in the carbonate phase and oxygen ion in the ceramic phase as shown in Figure 1.1. During the permeation, on the CO_2 rich side of the membrane, CO_2 reacts with oxygen ion in the solid phase forming carbonate ion as shown in Equation 1.2

$$CO_2 + O^{2-} \leftrightarrow CO_3^{2-} \quad (1.2)$$

After transport through the membrane, on the CO_2 lean side, carbonate ion converts to CO_2 and released, oxygen ion transports back through the ceramic phase to maintain electronic neutrality of the membrane. No oxygen is needed in the feed gas and the membrane is perm-selective to CO_2 only.

Experimentally, ceramic-carbonate dual-phase membrane was originally synthesized with mixed ionic-electronic conducting (MIEC) ceramics. Lin and coworkers reported preparation of $La_{0.6}Sr_{0.4}Co_{0.8}Fe_{0.2}O_{3-\delta}$ (LSCF)-carbonate dual-phase membrane first [Anderson & Lin, 2010]. The material has a typical perovskite structure and exhibits particularly high electronic and ionic conductivity [Xu et al., 2004a, 2004b]. The membrane effectively separated CO_2 at high temperature. Maximum CO_2 permeation fluxes of 1.02, 1.89, 2.35 and 2.42×10^{-3} mol/s/m^2 were respectively achieved for the dual-phase membranes with thicknesses of 3.0, 1.5, 0.75 and 0.375 mm at 900^{o}C. The 0.375 mm thick membrane had a CO_2/Ar separation factor for at least 225. Long-term stability test showed that CO_2 permeance considerably decreased before reaching steady state for about 65 h at 800-900^{o}C (only 10-15% of original value).

Norton et al. found that reaction between CO_2 and ceramic phase cause flux decline [Norton et al., 2014]. CO_2 reacted with LSCF forming CoO and $SrCO_3$ at high temperature. Formation of metal oxide and carbonate layer on the membrane surface inhibits exchange between CO_2 and lattice oxygen. Formation of carbonate ion was

prevented and CO_2 transport slowed down. Presence of O_2 let $SrCO_3$ [Liu et al, 2002] decompose and a solid state reaction could lead to structure recovery for LSCF [Tan et al., 2012]. Membrane stability was dramatically improved using O_2 in the feed gas [Norton et al., 2014]. The LSCF-carbonate membrane maintained a CO_2 flux of 20.3×10^{-3} mol/s/m^2 for at least 600 h at 900^{o}C. However, oxygen would also permeation through the membrane and appears in the products.

Norton and Lin [Norton & Lin, 2014] also prepared the dual-phase membrane with another perovskite-type ceramic-$La_{0.85}Ce_{0.1}Ga_{0.3}Fe_{0.65}Al_{0.05}O_{3-\delta}$ (LCGFA)-to address stability issue. The material was found to be CO_2-tolerant for high temperature O_2 separation [Dong et al., 2009]. LCGFA-carbonate dual-phase membranes of 1.5 mm and 0.75 mm thick separately achieved CO_2 permeation flux of 0.18 and 0.33×10^{-3} mol/s/m^2 at 900^{o}C. The membrane maintained a stable CO_2 permeation flux of $0.156\text{-}0.18\times10^{-3}$ mol/s/m^2 for more than 275 hours when exposed to CO_2 rich atmosphere. LCGFA-carbonate dual-phase membrane exhibited a better stability but CO_2 permeation flux was very low compared to that of LSCF-carbonate membrane because it has a smaller ionic conductivity.

Efforts were also made to use ionic-conducting ceramics to modify membrane performance. Wade et al. prepared ceramic-carbonate dual-phase membranes with yttria-stabilized zirconia ($Y_{0.16}Zr_{0.84}O_{2-\delta}$, YSZ) and gadolinia doped ceria ($Ce_{0.9}Gd_{0.1}O_{2-\delta}$, GDC) via tape casting technique [Wade et al., 2011]. The membranes were around

200-400 μm thick. TGA/DSC results showed that both ceramics were chemically stable mixed with carbonates at high temperature except that YSZ irreversibly reacted with pure lithium carbonate mixture forming lithium zirconate [Nair et al., 2004]. High temperature permeation tests were conducted in the absence of O_2. YSZ-carbonate dual-phase membrane exhibited a CO_2 permeation flux of 1.01×10^{-3} mol/s/m^2 at 750^{o}C and GDC-carbonate dual-phase membrane achieved a flux of 1.52×10^{-3} mol/s/m^2 at 850^{o}C. Both membranes had a CO_2/He selectivity around 1-2 within 800 and 900^{o}C. CO_2 permeability through the membranes gradually increased in the first 10-12 h and maintained a stable value for the next 50-60 h.

Rui et al. used fluorite structure $Bi_{1.5}Y_{0.3}Sm_{0.2}O_{3-\delta}$ (BYS) as ceramic solid phase for dual-phase membrane due to its higher ionic conductivity [Rui et al., 2012]. BYS was found to be carbonate non-wettable and molten carbonates could not fill the support pores forming dense dual-phase membrane. A thin γ-Al_2O_3 layer was coated on the support to modify pore wettability and dense dual-phase membrane was successfully prepared via direct infiltration method. The membrane was around 50 μm thick. CO_2 permeation flux through the membrane increased with upstream and downstream partial pressure difference. BYS exhibited a reversible phase transform between low temperature rhombohedral and high temperature cubic fluorite structure around 580-700^{o}C [Watanabe & Kikuchi, 1986, Sammes et al., 1999]. BYS of cubic fluorite structure has a higher oxygen ionic conductivity than that of rhombohedral structure. At 650^{o}C, the

dual-phase membrane went along the phase change and exhibited a flux increase from 0.19 to 0.55×10^{-3} mol/s/m^2. The system then maintained stable flux over 40 hrs.

Recently, Zhang et al. reported synthesis of samarium doped ceria ($Ce_{0.8}Sm_{0.2}O_{1.9}$, SDC)-carbonate dual-phase membrane [Zhang et al., 2012]. SDC support was prepared from a combined "co-precipitation" and "sacrificial-template" synthesis [Zhang et al., 2011]. The support prepared in this way exhibited highly three-dimensional porous network and contained a vast number of intra- and interconnected channels for fast ion transport [Zhang et al., 2011, 2012]. SDC-carbonate dual-phase membranes with supported porosities of 30, 35, 40 and 50% were separately prepared and achieved CO_2 permeation flux of 1.93, 3.35 4.76 and 13.7×10^{-3} mol/s/m^2 at 700^{o}C. Recently, Lin and coworkers [Dong et al., 2013] prepared thin tubular SDC-carbonate dual-phase membrane. The membrane was constructed with an asymmetric SDC-SDC/BYS porous support which was made by a centrifugal slip-casting method. The membrane achieved a CO_2 flux of 11.6×10^{-3} mol/s/m^2 at 900^{o}C. Norton et al. [Norton et al., 2014] studied stability of SDC-carbonate membrane using a uniaxially pressing and sintering method. The membranes exhibited stable CO_2 permeation with CO_2:N_2 mixture or simulated syngas (50% CO, 35% CO_2, 10% H_2 and 5% N_2) feed at pressure ranging from 1 to 5 atm for various testing periods of time as along as up to 35 days. Gas permeation properties of the dual-phase membranes are summarized in Table 1.1.

Table 1.1

Permeation properties of ceramic-carbonate dual-phase membranes

Ceramic phase	Membrane thickness (μm)	T (°C)	CO_2 flux (10^{-3} mol/s/m^2)	Stability	σ_v (S/cm)	Ref.
LSCF	375	900	2.42	N/A	0.173	Anderson & Lin, 2010
LCGFA	1500	900	0.156-0.18	~ 275 h	0.002	Norton & Lin, 2013
YSZ	200-400	750	1.01	50-60 h	0.029	Wade et al., 2011
GDC	200-400	850	1.52	50-60 h	0.126	Wade et al., 2011
BYS	~ 50	650	0.49	~40 h	0.137	Rui et al., 2012
SDC[1]	1500	700	13.70	10-15 h	0.21	Zhang et al., 2012
SDC[2]	1500	950	6.41	~ 35 d	0.155	Norton et al., 2014
SDC[3]	150	900	11.60	N/A	0.107	Dong et al., 2013

SDC[1], prepared from a "co-precipitation" and "sacrificial-template" synthesis;

SDC[2], prepared from uniaxially pressing and sintering method;

SDC[3], prepared from centrifugal slip-casting method, tubular membrane.

Recent work on transport mechanism of the dual-phase membrane [Wade et al., 2007, Rui et al., 2009] exhibited that CO_2 permeation through ceramic-carbonate membranes at high temperature based on driving forces provided by the oxygen ion conducting phase of the ceramic support as well as the carbonate ion conducting phase of the molten carbonate phase and gave equation:

$$J_{CO_2} = \frac{kRT}{4F^2L} ln\left(\frac{P"_{CO_2}}{P\prime_{CO_2}}\right) \quad (1.3)$$

where k is a permeance coefficient (or referred to as total conductance) defined by [Ortiz-Landeros et al., 2013]:

$$k = \frac{\left(\frac{\varepsilon}{\tau}\right)_p \sigma_c \left(\frac{\varepsilon}{\tau}\right)_s \sigma_i}{\left(\frac{\varepsilon}{\tau}\right)_p \sigma_c + \left(\frac{\varepsilon}{\tau}\right)_s \sigma_i} \quad (1.4)$$

and R is the ideal gas constant, T is the system temperature, F is Faraday's constant, L is the membrane thickness, P'_{CO2} and $P"_{CO2}$ are the feed and sweep CO_2 partial pressures, respectively, ε and τ denote the porosity and tortuosity of either the molten carbonate phase which occupies the ceramic support pore (p) or the solid ceramic phase (s). Ionic conductivity in the molten carbonate phase is much higher than that in the ceramic phase ($\sigma_c >> \sigma_i$), Equation 1.4 could be simplified to

$$k = \left(\frac{\varepsilon}{\tau}\right)_s \sigma_i \quad (1.5)$$

From Equation 1.3 and 1.5, at the same experimental conditions, CO_2 permeation flux through the dual-phase membrane is determined by membrane thickness, ionic conductivity and pore structure (refer to $\left(\frac{\varepsilon}{\tau}\right)_s$) of solid ceramic phase.

Zhang et al. [Zhang et al., 2012] prepared SDC-carbonate dual-phase membranes using the supports of various open porosities. At 700°C, CO_2 permeation flux increases with the value of $\left(\frac{\varepsilon}{\tau}\right)_s$. Recently, Lin and coworkers [Ortiz-Landeros et al., 2013] systematically studied effect of $\left(\frac{\varepsilon}{\tau}\right)_s$ on CO_2 permeation flux. The dual-phase membranes were synthesized from porous LSCF supports sintered at different temperatures. High temperature permeation tests exhibited that CO_2 permeation flux

increased with $\left(\frac{\varepsilon}{\tau}\right)_s$ first and then decreased. At 900°C, when $\left(\frac{\varepsilon}{\tau}\right)_s$ is 0.26, the membrane achieved a CO_2 flux of 3.19×10^{-3} mol/s/m^2 which is two times larger than previously prepared LSCF-carbonated dual-phase membrane [Anderson & Lin, 2010] without pore structure optimization. The specific ceramic-carbonate dual-phase membrane has an optimum pore structure-$\left(\frac{\varepsilon}{\tau}\right)_s$-for gas permeation. Figure 1.3 summarizes CO_2 permeation flux as a function of $\left(\frac{\varepsilon}{\tau}\right)_s$ for different membranes.

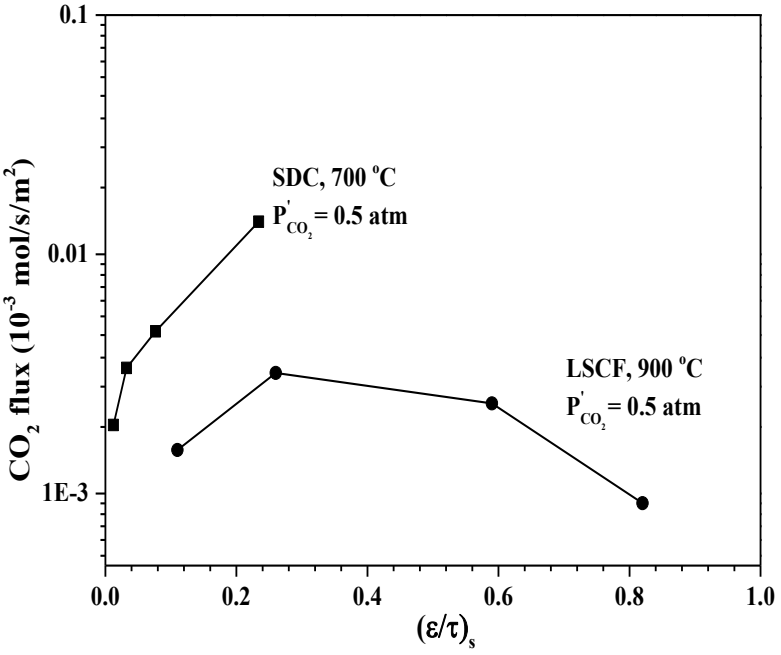

Figure 1.3 Effect of pore structure of ceramic phase-$\left(\frac{\varepsilon}{\tau}\right)_s$-on CO_2 permeation flux for ceramic-carbonate dual-phase membranes (membranes are around 1.5 mm thick, permeation tests were performed with CO_2: N_2 feed and 100 ml/min helium sweep)

When ceramic-carbonate dual-phase membranes have similar thickness and pore structure, rate-limiting step of CO_2 permeation through the membrane will be oxygen ionic conduction in the ceramic phase. Figure 1.4 compares CO_2 permeation flux for

various dual-phase membranes. All the membranes have a thickness around 1.5 mm and open porosity of 34-38%. The dual-phase membrane prepared from the ceramic with larger ionic conductivity exhibits a higher CO_2 permeation flux. Effects of pore structure and ionic conductivity of ceramic phase on CO_2 permeation through the dual-phase membranes have been studied, however, no research focused on thickness effect. Gas permeation of the dual-phase membrane is rate limited by ionic-conduction in solid phase, for ionic-conducting membranes, reducing membrane thickness would effectively increase gas permeation flux [Steele, 1987, Bouwmeester et al., 1992]. Thin dual-phase membrane forecasts a higher CO_2 flux.

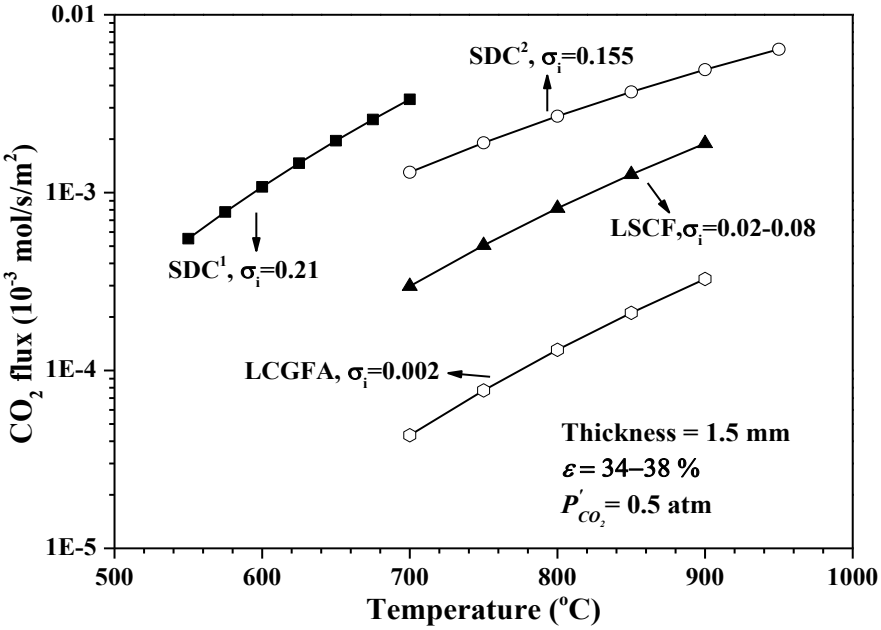

Figure 1.4 Effect of ionic conductivity in ceramic phase on CO_2 permeation flux for ceramic-carbonate dual-phase membranes (CO_2: N_2 feed and 100 ml/min helium sweep) (SDC[1], [Zhang et al., 2012]; SDC[2], [Norton et al., 2014])

1.4 Thin ionic-conducting membranes

1.4.1 Thin oxygen permeable membranes

Studies on the ionic-conducing membranes exhibited thickness effect. For oxygen permeable membranes, reducing thickness with various methods, such as sol gel [Kuper et al.,1992, Gurauskis et al., 2012], particle or suspension deposition [Meng et al., 1991, Wang & Barneet, 1993, Gurauskis et al., 2012], electrochemical vapor deposition (EVD) [Carolan & Michaels, 1990, Lin et al, 1990, Lin et al., 1992] and so on, is simple to achieve higher O_2 flux.

Mixed ionic and electronic perovskite structure materials were widely studied for high temperature oxygen permeation due to its promising ionic conductivity [Sunarso et al., 2008; Leo et al., 2009; Zhang et al., 2011]. Asymmetric-structured membranes of $La_{0.6}Ca_{0.4}CoO_3$ were synthesized via depositing a thin dense film [Watanabe et al., 2008] on a porous support. The $La_{0.6}Ca_{0.4}CoO_3$ porous support was fabricated using irregular-shaped precursor particles prepared through an oxalate method. A dense and crack-free membrane of 10 μm thick was formed on the porous support by coating a $La_{0.6}Ca_{0.4}CoO_3$ slurry and subsequent densification by sintering. The asymmetric membrane exhibited a high oxygen permeation flux of 1.2×10^{-2} mol/s/m^2 at 930 °C, which was four times higher than a typical sintered-disk type membrane (1200 μm).

Dense $Ba_{0.5}Sr_{0.5}Co_{0.8}Fe_{0.2}O_{3-\delta}$ (BSCF) ceramic membranes were prepared via glycine–nitrate route [Kovalevsky et al., 2011]. An asymmetric membrane consisting of

a dense layer sandwiched by two porous layers was proposed. A dense BSCF membrane of 170 μm thick was prepared intermediately between a 100 μm porous cover layer and 1.05 mm thick base support. At 900°C, oxygen permeation flux through thin dense membrane was found to be 1.5–1.8 times higher than thick symmetric one. Oxygen transport of dense BSCF membranes was predominantly controlled by surface exchange kinetics when the membrane thickness is smaller than 1.00 mm. Thin $La_{0.2}Sr_{0.8}Fe_{0.8}Ta_{0.2}O_{3-\delta}$ layers were deposited on porous substrates of the same composition [Gurauskis et al., 2012]. The thin layers were prepared by dip-coating technique. Dense and defect free layers with thickness in the range of 15–60 μm were obtained by a single dip coating deposition. Afterwards the second layer with pore former was deposited and resulted in a significantly enhanced surface area of the functional layer. The twice dip-coated membranes showed oxygen flux up to 6.4×10^{-2} mol/s/m^2 at 1000°C, about 50% increase in oxygen permeation [Gurauskis et al., 2012].

Recently, Liu et al. prepared a crack-free asymmetric tubular membrane made of $SrCo_{0.4}Fe_{0.5}Zr_{0.1}O_{3-\delta}$ perovskite oxide by a combined spin-spraying and co-sintering method [Liu et al., 2012], in which the slurry containing powders was sprayed on a rotating support tube and followed by sintering process. Asymmetric supports with the dense layer about 20 μm were prepared after sintering at 1250°C. SEM and nitrogen gas-tight test demonstrated that membrane surface was dense, continuous and crack-free. A high oxygen flux of 7.41×10^{-3} mol/s/m^2 was achieved at 800°C which was 2.35 times

that of symmetric membrane. Long-term oxygen permeation measurement (850°C, 200 h) showed that the asymmetric membrane could withstand low oxygen partial pressure environment. The oxygen transport is mainly controlled by surface exchange.

Oxygen ionic-conducting ceramics were also studied for O_2 permeation. Han et al. synthesized thin dense zirconia-yttria-ceria membranes via electrochemical vapor deposition synthesis [Han et al., 1997]. XRD results indicated successful doping and deposition of CeO_2 into ZrO_2-Y_2O_3 forming the films of 5-20 μm thick. The oxygen permeation flux through 9 μm ZrO_2-Y_2O_3-CeO_2 membranes at 1000°C were separately 1.6, 2.3 and 2.95×10^{-4} mol/s/m^2 for the membranes containing 5, 16 and 28% CeO_2. The permeation fluxes were much larger than those for thicker YSZ membranes. The oxygen permeation flux had a linear dependence on reciprocal film thickness indicating that oxygen permeation through the thin ZrO_2-Y_2O_3-CeO_2 membranes was rate limited by bulk transport.

More recently, the oxygen flux through supported thin $Ce_{0.9}Gd_{0.1}O_{1.95-\delta}$ (CGO) with 2 mol% of cobalt [Lobera, et al., 2011] was measured for oxygen separation in oxyfuel processes and syngas production. Membrane stability was compared to perovskite membranes which are prone to carbonation and/or decomposition when operated in CO_2-rich and reducing gas environments [Kharton et al., 2003, Arnold, et al., 2007]. A 27 μm dense GDC layer was synthesized on a porous GDC substrate. The supported membrane exhibited a maximum oxygen flux of 3.7×10^{-2} mol/s/m^2 at 1000°C when

diluted methane was used as sweep gas. The GDC membrane showed better stability in CO_2 (in contrast to tests on $La_{0.6}Sr_{0.4}Co_{0.2}Fe_{0.8}O_{3-\delta}$ membranes) and no detrimental effect on the oxygen flux was observed when CO_2 was present in the sweep gas. SEM analysis showed that membrane remained chemically stable after testing in CO_2.

1.4.2 Thin dual-phase membranes

Till now, there are no detailed studies reported on thin dual-phase membranes. Anderson and Lin [Anderson & Lin, 2010] prepared LSCF-carbonate dual-phase membranes with different thickness of 3.0, 1.5, 0.75 and 0.375 mm via SiC paper polishing. Norton and Lin synthesized LCGFA-carbonate dual-phase membranes of 1.5 and 0.75 mm by controlling the amount of green powders used for pressing [Norton & Lin, 2013]. Figure 1.5 shows dependence of CO_2 permeation flux on membrane thickness for two membranes.

For LSCF-carbonate dual-phase membrane, thinner membrane provided lower resistance for ionic transport hence achieving a higher flux. It was also noticed that the increase in CO_2 flux was not proportional to the extent of reduction in membrane thickness. For LCGFA-carbonate dual-phase membrane, the 0.75 mm thick dual-phase membrane has a permeation flux two times of that the 1.5 mm thick membrane indicating ionic transport effect. Recent studies demonstrate that CO_2 permeation through ceramic-carbonate dual-phase membrane is dominated by ionic transport [Wade et al., 2007, Rui et al., 2009, Ortiz-Landeros et al., 2013]. From the results above, reducing

thickness being effective to improve gas permeation flux for the ionic-conducting membrane, thin dual-phase membranes should give a better CO_2 permeation performance. However, the studies summarized in section 1.3 were mainly focused on the fabrication of thick membranes (1-2 mm). So far there are no synthesis and performance studies reported on thin dual-phase ceramic membranes for CO_2 separation.

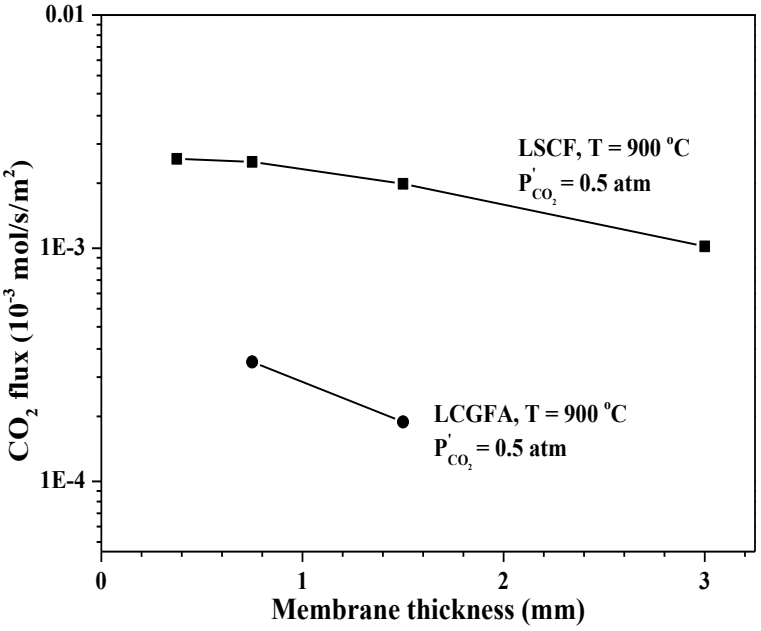

Figure 1.5 Dependence of CO_2 permeation flux on membrane thickness (permeation tests were performed with CO_2: N_2 feed and 100 ml/min helium sweep)

1.5 Research objective and significance

Ceramic-carbonate dual-phase membranes exhibited great potential for high temperature carbon dioxide separation and capture. As shown in Figure 1.6, performance of thick ceramic-carbonate dual-phase membranes significantly surpasses upper bond correlation for CO_2/N_2 separation [Robeson, 2008].

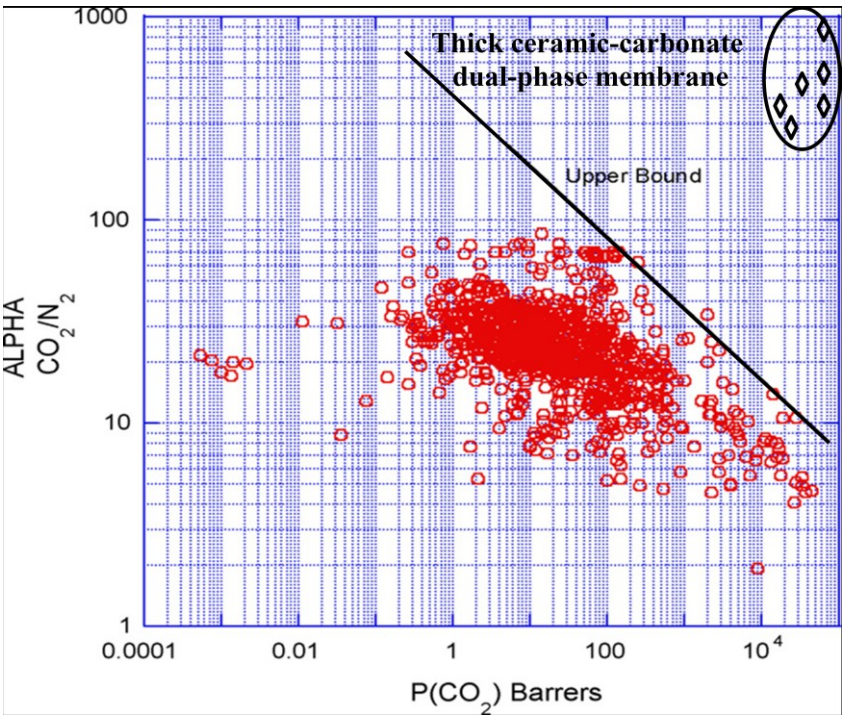

Figure 1.6 Upper bond correlation for CO_2/N_2 separation

Previous research indicated potential of the thinner membrane achieving a higher gas permeation flux. The objective of the dissertation is to present a systematic study on synthesis and improvement of thin ceramic-carbonate dual-phase membranes for high temperature CO_2 separation. The work will discuss preparation of thin dual-phase membranes with different ionic-conducting ceramics and thin film making methods. Gas permeation properties through the thin dual-phase membranes are studied as well. The research was conducted to achieve the following three specific objectives.

1.5.1 Research objective 1

Multi-layer asymmetric supports are commonly used to prepare thin ionic-conducting membranes [Watanabe et al., 2008, Liu et al., 2012]. The thin

ceramic-carbonate dual-phase membrane was proposed to prepare with an asymmetric support of multi-layer structure. The initial objective of the work was to study support synthesis. Ionic-conducing yttria stabilized zirconia (YSZ) demonstrated good chemical and mechanical stability and was used to make thin small-pore top-layer. Sol-gel and suspension coating methods were respectively used to prepare supported macroporous and mesoporous YSZ membranes. Membranes properties were characterized to identify feasibility of the method. The strategy developed for thin membrane making would be applied to thin ceramic-carbonate dual-phase membrane synthesis later.

1.5.2 Research Objective 2

The second objective of the dissertation was to study synthesis and characterization of thin ceramic-carbonate dual-phase membranes. Gas permeation properties through the membranes were reported as well. Asymmetric supports with a multi-layer structure were prepared from suspension coating method developed in objective 1. Macroporous $Y_{0.16}Zr_{0.84}O_{2-\delta}$ (YSZ) and $La_{0.6}Sr_{0.4}Co_{0.8}Fe_{0.2}O_{3-\delta}$ (LSCF) membranes were separately dip-coated on $B_{1.5}Y_{0.3}Sm_{0.2}O_{3-\delta}$ (BYS), $Y_{0.16}Zr_{0.84}O_{2-\delta}$ (YSZ) and α-alumina (ALU) supports. Thin dual-phase membranes were prepared via a direct infiltration method. The synthesized membranes were characterized to identify synthesis conditions for thin ceramic-carbonate dual-phase membrane. High temperature CO_2 permeation tests were performed on the membrane from 550 to 700^{o}C. The permeation results were used check extent of improvements by reducing membrane thickness.

1.5.3 Research objective 3

The final objective of the work was to optimize thin dual-phase membrane. CO_2 permeation stability of thick $Ce_{0.8}Sm_{0.2}O_{1.9}$ (SDC)-carbonate dual-phase membrane exposed to CO_2: N_2 or simulated syngas feed at high pressure was studied first. The membrane exhibited high CO_2 permeation flux and long-term stability. SDC was chosen as the solid phase for thin dual-phase membrane. The work of this part reported attempts at making thin SDC-carbonate dual-phase membranes with different methods. The findings provided new strategy for thin dual-phase membrane synthesis. Gas permeation studies were also performed.

The research objectives listed above present a significant contribution to dual-phase membrane research. Early studies on ceramic-carbonate dual-phase membranes only focused on bulk membranes and information on thin membranes was very limited. Studies of synthesis and permeation properties of thin ceramic-carbonate dual-phase membranes help perfect understanding of this kind of membrane.

1.6 Structure of the dissertation

The next chapters will serve to address the objectives mentioned above. Chapter 2 is to fulfill objective 1. Synthesis and characterization of multi-layer asymmetric supports prepared from coating porous YSZ layers on alumina supports is reported. Chapter 3 addresses objective 2. Thin YSZ-carbonate dual-phase membrane is successfully synthesized and gas permeation properties are briefly studied. Both

Chapters 4 and 5 fulfill the objective 3. Stability of bulk SDC-carbonate dual-phase membrane and thin membrane preparation are reported. Chapter 6 summarizes the work reported in this thesis and provides recommendations for future advancement of the dual-phase membrane for CO_2 capture.

CHAPTER 2

SOL-GEL SYNTHESIS AND CHARACTERIZATION OF MESOPOROUS YTTRIA STABILIZED ZIRCONIA MEMBRANES WITH GRADED PORE STRUCTURE

2.1 Introduction

As described in Chapter 1, to make thin ceramic-carbonate dual-phase membrane, asymmetric supports with a multi-layer structure should be prepared. Yttria stabilized zirconia (YSZ) is a widely used material because of its unique characteristics. YSZ has a better chemical stability in comparison to alumina and titania membranes [Bhave, 1991]. Compared with pure zirconia membranes which may form cracks due to the stresses developed associated with phase transformation from metastable tetragonal to stable monoclinic phase during heating treatment[Chang et al., 1994, Gopalan et al., 1995], YSZ membrane could maintain a stable cubic-fluorite structure between room temperature and 3000K. As a result, it is more promising for high temperature applications such as membrane reactors and gas separation by Knudsen flow.

YSZ membranes also exhibit a considerable oxygen ionic conductivity and an extreme low thermal conductivity at high temperature. Dense YSZ layers could be used as the electrolytes for solid oxide fuel cells, oxygen sensors and oxygen pumps [Mercera et al., 1991, Minh & Takahashi, 1995, Birkby & Stevens, 1996, Priyatham & Bauri, 2010] while porous ones could be applied as barriers for thermal insulation and insulated engine components [Thery et al., 2009, Hu et al., 2010, Hu et al. 2011]. YSZ mesoporous

membranes are attractive as the support, not only for ultra-thin dense YSZ, but also for other ceramic or metallic membranes because of their chemical inertness, ionic conductivity and thermal expansion coefficient which matches closely with that of many dense membrane materials [Kueper et al., 1992]. YSZ macroporous membrane could be used as an intermediate layer to improve the thermal stability of MFI-type zeolite membrane structure on porous alumina support [Kanezashi et al., 2007].

The sol-gel method is commonly used for fabrication of porous ceramic membranes [Bhave, 1991, Burggraaf et al., 1991]. YSZ mesoporous membranes made of sol-gel method were previously reported by several investigators [Wen et al., 1991, Herbert et al., 1991, Okubo & Nagamoto, 1995]. These studies were mainly focused on the phase and pore structures of YSZ. Recently, many researchers presented the synthesis and characterization of YSZ powders by the sol-gel process [Kuo et al., 2008, Farhikhten et al., 2010, Heshmatpour & Aghakhanpour, 2011]. However, information on preparing crack and defect-free membranes and permeation data is limited. A few researchers reported on the preparation of defect-free supported YSZ membranes [Okubo et al., 1996, Kim & Lin, 1998, Xia et al., 1999]. Okubo et al. synthesized YSZ membranes by mixing a particulate sol and a polymeric sol to improve the film formation process and the film property [Okubo et al, 1996]. Kim and Lin [Kim & Lin, 1998] reported synthesis of porous YSZ membranes with a particulate sol that was obtained by hydrolysis and peptization of zirconium *n*-propoxide. The YSZ layer was determined to

be pin-hole free by helium permeation tests. The zirconia sol used by Xia et al. was prepared by hydrolysis and condensation of zirconium tetra-*n*-propoxide [Xia et al, 1999]. For YSZ macroporous membrane, suspension coating followed by drying and calcination was a common process [Kim & Lin, 1999].

The mesoporous YSZ membranes described above were synthesized directly on macroporous alumina supports. In these membranes the mesoporous YSZ layers, which is only 1 to 3μm thick, is in direct contact with alumina support. For some applications of the mesoporous YSZ membranes, it is desirable to have an intermediate macroporous YSZ layer as a buffer between the thin mesoporous YSZ layer and less costly alumina support. One application is to use the mesoporous YSZ layer as the support for preparation of dual-phase membranes (with the pores infiltrated either by Pd [Kim & Lin, 2000] or carbonate [Anderson & Lin, 2010]), the macroporous intermediate layer would prevent infiltration of the second phase into alumina support, resulting in synthesis of thin dual-phase membranes for oxygen or carbon dioxide separation. The objective of chapter 2 is to report synthesis and characterization of asymmetric porous supports with multi-layer structure derived from YSZ. The three-layer mesoporous YSZ membranes with a macroporous YSZ intermediate layer on alumina support by the methods of sol-gel [Kim & Lin, 1998] and suspension coating [Kim & Lin 1999] are reported. Two-layer mesoporous and macroporous YSZ membranes on alumina support are also prepared.

2.2 Experimental

2.2.1 Suspension Preparation and YSZ Macroporous Membrane Synthesis

Porous α-alumina supports were made by pressing α-alumina powder (A16, Alcoa) into disk shape under 150 MPa of hydraulic pressure, followed by sintering at 1150°C for 30 h in programmable-temperature furnace. The alumina supports were polished sequentially by SiC polishing paper (Struers) #500, #800 and #1200, each for 5 min, after sintering. A stable YSZ suspension was made according to the previously reported procedures [Kim & Lin, 1999]. YSZ powders (8-mol% Y_2O_3-stabilized ZrO_2) (TZ-8Y, Tosoh Co., Tokyo, Japan), mixed with dilute nitric acid (pH= 3-4) at a weight ratio of 1:2, were ball milled in polyethylene (PE) pots with ZrO_2 balls 0.5 mm in diameter. The suspension was treated ultrasonically to break up the agglomerates and was then ball-milled for 7-10 days. After the ball-milling process, the YSZ suspension was diluted to 10 wt% by adding more dilute nitric acid.

Supported YSZ macroporous membranes were prepared by dip-coating a stable YSZ suspension on the α-alumina porous supports. Polyvinyl alcohol (PVA) was used as drying control chemical additive (DCCA) to prevent crack formation in the membranes during the drying step. PVA solution was prepared by dissolving 3 g of PVA (Fluka, MW=72,000) in 95 ml water and 5 ml of 1 M nitric acid. The optimum amount of PVA solution to be added into the suspension was determined to be at a volume ratio of 1:4. The YSZ suspension with PVA was dip-coated on alumina supports and dip-coated disks

were dried in air at a relative humidity (RH) of 50%-60% and a temperature of 40°C. After the drying process, the supported membrane was sintered in air at 1000°C for 3 h with a heating and cooling rate of 100°C per hour. The dip-coating, drying and sintering processes were repeated to ensure the preparation of crack-free supported YSZ macroporous membranes.

2.2.2 Sol Preparation and YSZ Mesoporous Membrane Synthesis

Mesoporous YSZ layer was coated on the macroporous YSZ/alumina supports, and for comparison on alumina supports, by the sol-gel method [Kin & Lin, 1998]. Stable 0.25 M zirconia sol was prepared by hydrolysis and condensation of 0.25 mol zirconium n-propoxide (Alfa, MW=327.56) in a water (900 ml)/isopropanol (500ml) solution. The white zirconia precipitates were filtered with vacuum suction and washed in water several times to remove the isopropanol. A small amount of water was added to help facilitate the filtering in the process. The filtered zirconia cake was diluted in 1 L of water and peptized with 125 ml 1 M nitric acid at 90-100°C overnight. The sol was ultrasonically treated for at least 30 minutes before it was used. A 0.07 M yttrium nitrate solution was made by mixing 2 g of $Y(NO_3)_3$(Alfa) with 95 mL water and 5 mL1 M nitric acid solution at 50°C. The PVA solution was prepared using the same procedure as the one that was previously mentioned. Hydroxypropyl cellulose (HPC) (Aldrich, MW=100,000) solution was prepared by dissolving 0.35 g powder in 95 mL water and 5 mL of 1 M nitric acid.

A solution-sol mixing method was used to coat the dopant on the grain surface of the zirconia membranes. The 0.07 M yttrium nitrate solution was mixed with the stable zirconia sol in a desired proportion to make 8 mol% YSZ. The optimum amount of DCCA at the specific concentration was found to be about 30% in volume of 0.25 M zironia sol [Kim & Lin, 1998]. The YSZ sol was made by mixing the zirconia sol, yttrium nitrate solution and DCCA with an approximate volume ratio of 35:11:11. The concentration of yttria-doped zirconia sol with DCCA was 0.154 M. Unsupported YSZ mesoporous membranes were made by pouring the sol into petri-dishes. Supported membranes were made by dip-coating YSZ sol on α-alumina support and supported YSZ macroporous membranes previously synthesized, respectively. The membranes were dried at the same condition as the YSZ macroporous membranes. The membranes were calcined at 450°C for 3 h with a heating and cooling rate of 0.5°C/min. For the supported membranes, the procedure of coating, drying and calcination was repeated to ensure the synthesis of crack-free membranes and formation of a membrane with the proper thickness. Some of the unsupported YSZ samples were further heat treated at 700°C for 30 h.

2.2.3 Characterization

The surface area, pore volume and pore size distribution of sol-gel derived YSZ powders were obtained from nitrogen ad(de)sorption isotherms using an adsorption porosimeter (Micrometrics, ASAP 2020). The phase structures of the membranes were

identified by X-ray diffractometry (XRD) (Bruker AXS, D8 Focus Diffractometer) with CuKα radiation. The morphology and thickness of supported mesoporous and macroporous YSZ membranes were studied by examining the cross section and top layer of the membrane disks using scanning electron microscopy (SEM) equipment (Philips, FEI XL30 FEG). Helium permeation through the membrane was measured by a steady-state permeation setup shown in Figure 2.1 to examine the quality of the membranes [Lin & Burggraaf, 1993].

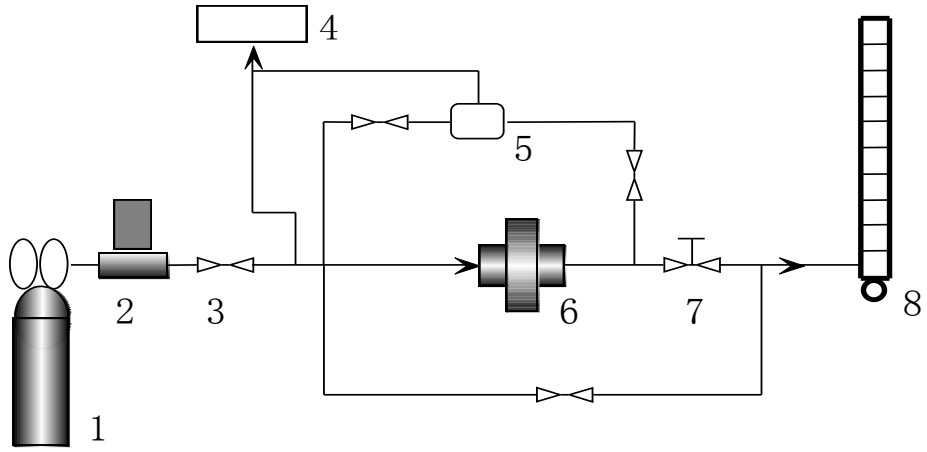

(1) Helium Cylinder; (2) Mass flow controller; (3) Valve; (4) Pressure Sensor; (5) Gas Reservoir; (6) Permeation Cell; (7) Needle Valve; (8) Bubble Flow Meter

Figure 2.1 Steady State Helium Permeation Setup

2.3 Results and Discussion

Good quality, macroporous YSZ membranes were obtained by dip-coating the YSZ suspension on the α-alumina support, followed by drying and heat-treatment. Figure 2.2 shows an XRD pattern of YSZ macroporous membrane prepared on an α-alumina

support. Peaks assigned to the 111, 200, 220, 311 and 400 deflections correspond to cubic YSZ [Garcia et al., 1998]. No XRD peaks for the alumina support can be seen due to the large thickness (at least 10 μm) of the YSZ layer.

Figure 2.3 shows the SEM images of surface and cross-section of a YSZ macroporous membrane on the alumina support prepared by dip-coating, drying and calcination for 3 times. It can be seen that a crack-free and uniform YSZ layer, of about 20 μm in thickness, was formed. The cross-sectional BE image shows a clear double layer structure in which the macroporous YSZ membrane can be distinguished from the α-alumina support due to the difference in the atomic weights.

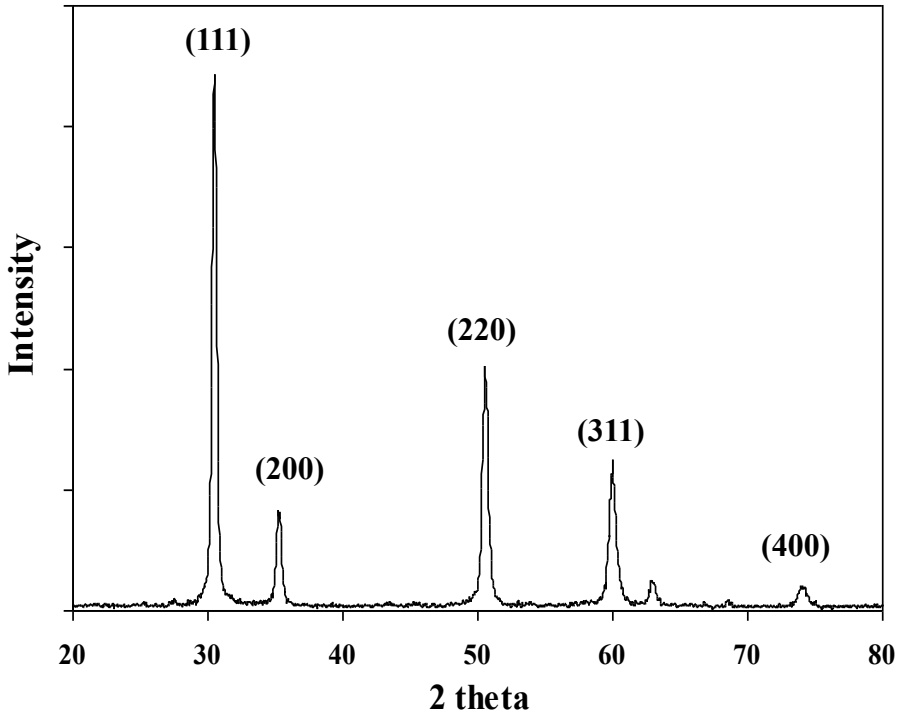

Figure 2.2 XRD pattern of YSZ macroporous membrane supported by α-alumina support after 3 times' dip-coating

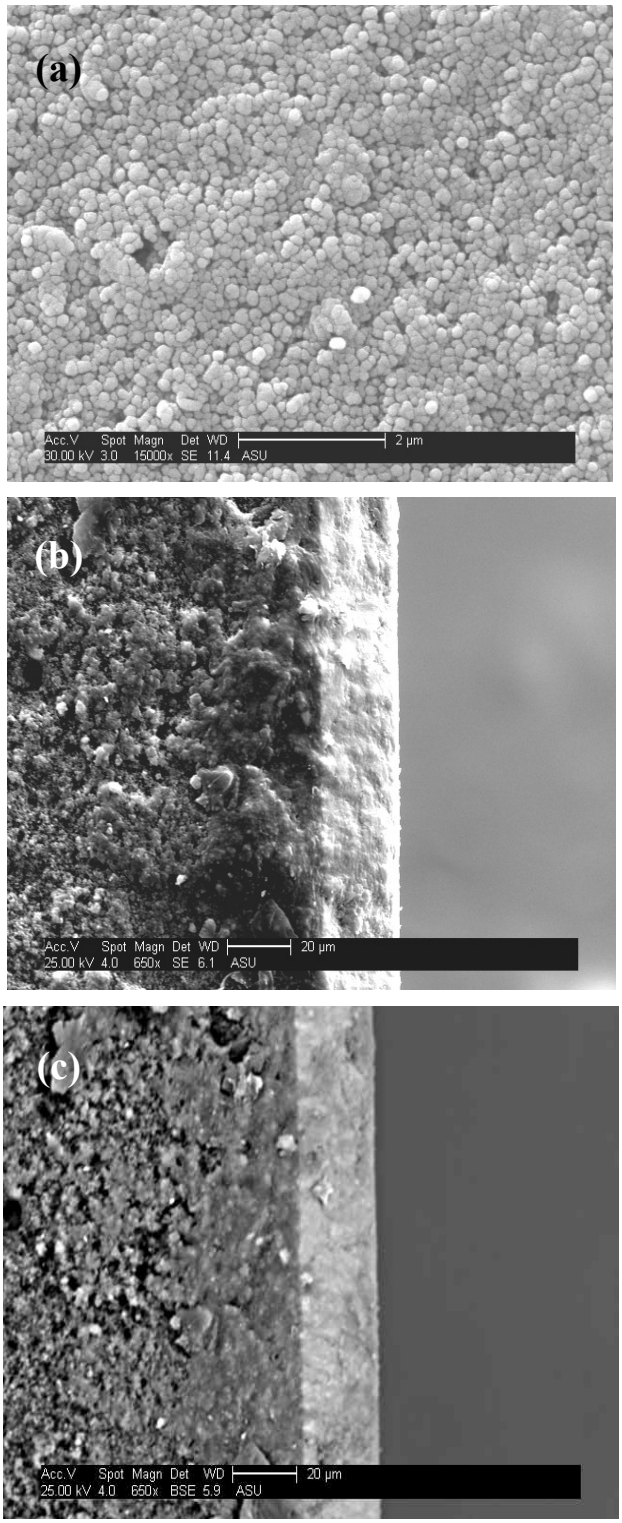

Figure 2.3 SEM images of the surface (a) and cross section of YSZ macroporous membrane (b) secondary-electron (SE) image and (c) backscattered-electron (BE) image)

Helium permeance data for the alumina support and for the supported macroporous YSZ membrane at different mean pressures cross the membrane are given in Figure 2.4. Coating of the YSZ layer caused about 5% reduction in helium permeance. The helium permeance data for the alumina support can be correlated by straight line as [Brinker & Scherer, 1990, Lin & Burggraaf, 1993]

$$\frac{F}{L} = \alpha + \beta P_{av} \tag{2.1}$$

Permeability coefficients α and β account for Knudsen flow and viscous flow, respectively, and can be used to calculate the pore radius of the membrane by:

$$r_p = 8.48\,(\frac{\beta}{\alpha})\sqrt{\frac{\mu^2 RT}{M_w}} \tag{2.2}$$

In these equations L is the disk thickness (m), M and μ are the molecular weight (kg/mol) and viscosity (kg/m/s) of the permeating gas (helium) and r_p is the average pore radius (m). The values for the permeation parameters obtained by linear regression and the pore size for the alumina support are given in Table 2.1.

The permeance for the supported YSZ layer was obtained from the flux data for the composite membrane (alumina support + YSZ layer) by the resistance-in-series model [Lin & Burggraaf, 1993]. For a given helium flow through the composite membrane at Q_i with an upstream pressure of P_h on the surface of the YSZ side, the permeance for the YSZ top-layer can be obtained by:

$$F_t = \frac{Q_i}{S(P_h - P_m)} \tag{2.3}$$

at the average pressure of $P_{av}=(P_h+P_m)/2$. Here P_m is obtained by:

$$P_m = \frac{\sqrt{\alpha_s^2 + 2\beta_s\left(\frac{Q_i}{S} + \alpha_s P_l + \frac{\beta_s}{2}P_l^2\right)} - \alpha_s}{\beta_s} \quad (2.4)$$

where the subscript "s" is for the properties for the support, and P_l is the pressure on the downstream surface (alumina support surface), and S is the membrane permeation area. The results for the permeance for the YSZ top-layer at various average pressures are plotted in Figure 2.4 (b). As shown the data can be correlated by a straight line from Equation 2.1. The values of the permeability coefficients for the YSZ top layer and the pore size calculated by Equation 2.2 are given in Table 2.1. Average pore diameter calculated for YSZ macroporous membrane is about 116 nm which is in agreement with previously reported results [Kim & Lin, 1999]. The pore size of the macroporous YSZ layer is close to that of the alumina support. Therefore it is suitable to coat mesoporous YSZ layer on the surface of the macroporous YSZ layer.

Table 2.1

Values of α, β and β/α for α-alumina support and 3 time-dip-coated top YSZ macroporous layer

Component	α (10^{-6} mol/m^2/s/Pa)	β (10^{-12} mol/m^2/s/Pa^2)	β/α ($\times 10^{-6}$ 1/Pa)	pore diameter (nm)
α-alumina support	1.33	0.92	0.69	180
YSZ top layer	31.51	14.29	0.45	116

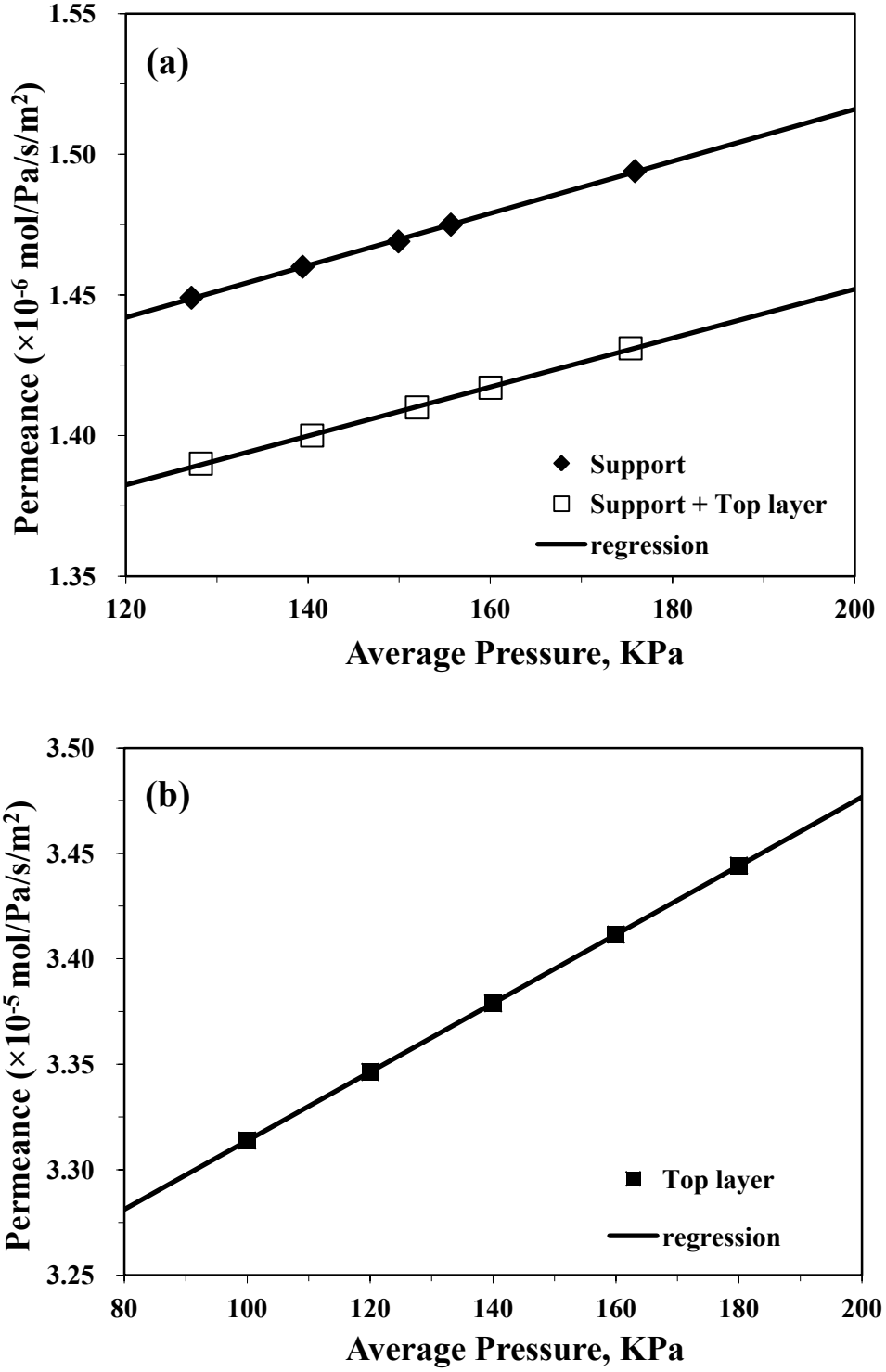

Figure 2.4 Helium permeance versus average pressure of a supported YSZ macroporous membrane (a) support and YSZ top layer and (b) calculated top layer

Stable zirconia sol was much more difficult to obtain [2] due to the extremely rapid reaction of zirconia alkoxide with water. The most important conditions for synthesis of zirconia sol include: (1) the dilution degree of the metal alkoxide, (2) the amount of water used for hydrolysis of the alkoxide and (3) the peptization conditions. Kim and Lin developed a promising method to make stable zirconia sol based on the conditions above [Kim & Lin, 1998] and it was followed in this work. Environmental humidity was strictly controlled and steam formed during the experiment was removed to prevent the reaction between metal alkoxide and water.

Figure 2.5 shows pore size distribution (PSD) of unsupported mesoporous YSZ membranes after calcination at 450°C for 3 h and after further heat treatment at 700°C for 30 h. The PSD after calcination is rather narrow, but becomes much broader with an increased pore size after further heat treatment. The pore structure data of the YSZ mesoporous membrane are consistent with previous results [Kim & Lin, 1998] and are shown in Table 2.2. Figure 2.6 shows the XRD data of unsupported YSZ mesoporous membranes after calcination and further heat treatment. The peak positions of mesoporous YSZ membranes are consistent with those of macroporous YSZ membranes.

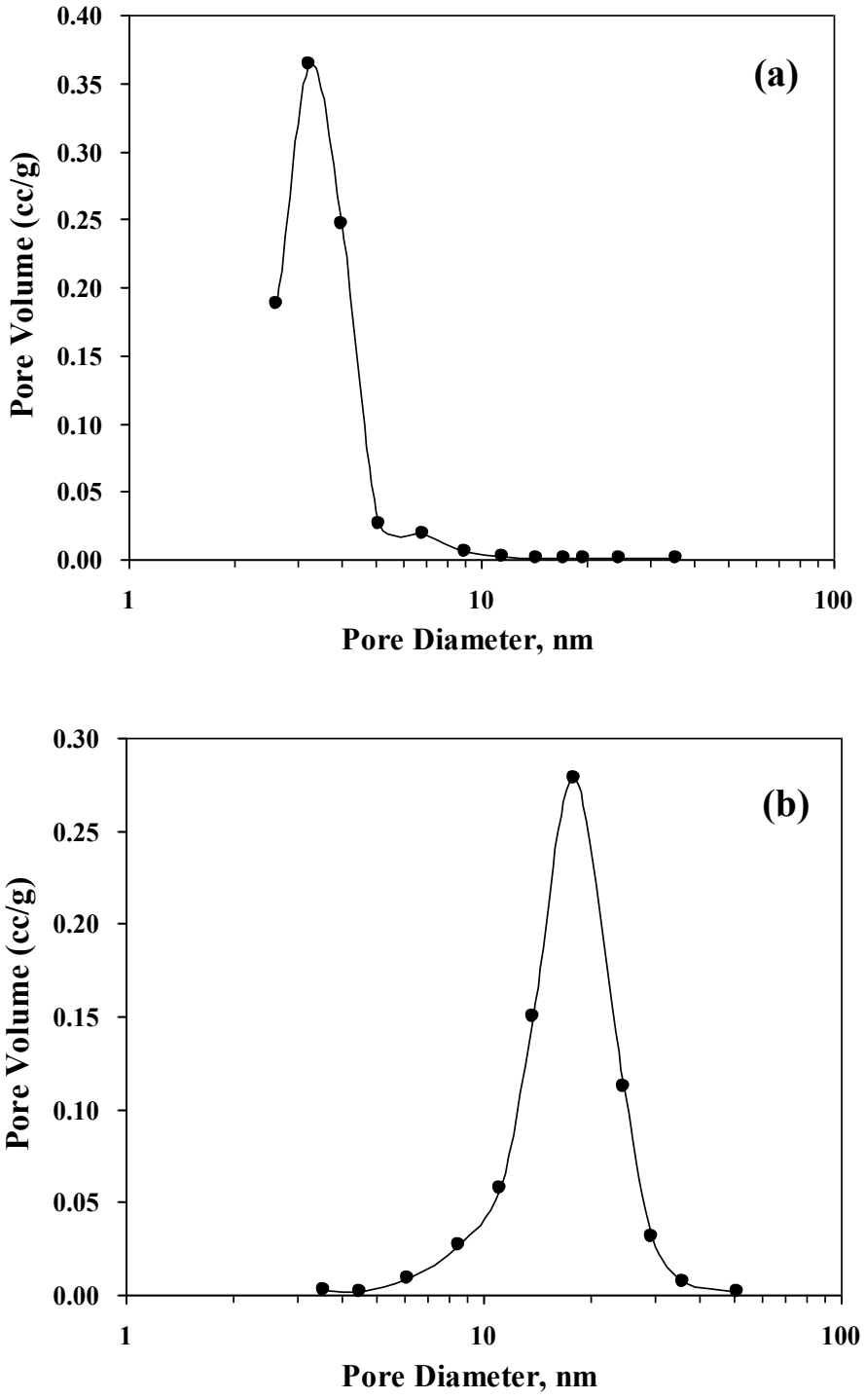

Figure 2.5 Pore size distributions of unsupported YSZ sol membranes after calcination at 450°C for 3 h (a) and after further heat treatment at 700°C for 30 h

Table 2.2

Pore structure data of YSZ membranes calcination at 450°C for 3 h (a) and after further heat treatment at 700°C for 30 h

	After calcination	After sintering
Pore size (nm)	3.3	22.3
Surface area (m^2/g)	110.2	14.7
Pore volume (cc/g)	0.087	0.081

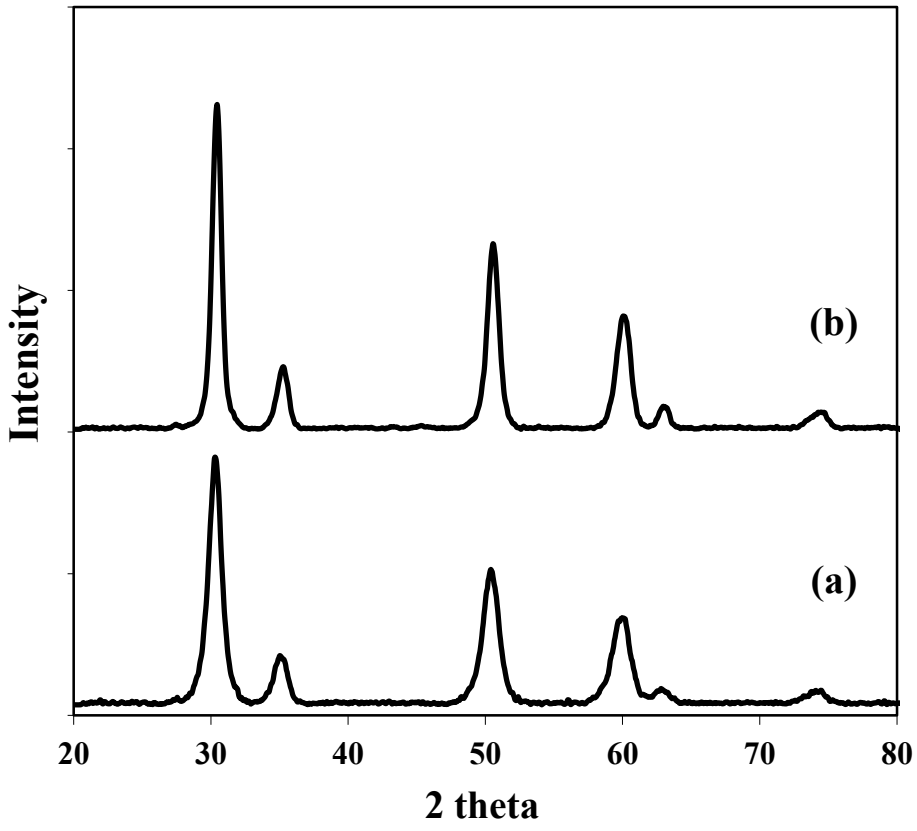

Figure 2.6 XRD patterns of unsupported YSZ mesoporous membrane (a) after calcination at 450°C for 3 h and (b) after further heat treatment at 700°C for 30 h

Supported mesoporous YSZ membranes were first prepared by dip-coating the 0.25 M YSZ sol on supported macroporous YSZ membranes. The dip-coating, drying and calcination steps were repeated several times to ensure the formation of YSZ layers of a proper thickness. There were however many cracks observed on the surface of the as-synthesized mesoporous YSZ membrane after 3 repetitions of the dip-coating, as shown in Figure 2.7. From the figure, it is observed that the cracks are about 5 to 10 μm in length and 1 to 2 μm in width. The cracks form even on one-dip-coating layer. The cracks on the membrane are likely caused by the drying stress (σ_x) developed during the drying process. The larger the stress, the more likely cracks are to form. The drying stress on the membrane could be approximately fitted into equation as follow [Brinker & Scherer, 1990]:

$$\sigma_x \approx L\eta_L \dot{V}_E / 3D \tag{2.5}$$

L is the thickness (m) of the membrane, η_L is the viscosity of the solvent (Pa·s), $\dot{V}_E$ is drying rate (m/s) and D is the permeability of the membrane (m^2).

In this work, the membranes were dried in a humidity-controlled chamber at a relative humidity (RH) of 50%-60% and a temperature of 40°C. A further increase in humidity was not effective to prevent crack formation. The other effective way to reduce the stress is to decrease the membrane thickness and perform multiple dip-coating, drying and calcination processes. The membrane thickness for each dip-coating is proportional to the sol concentration. In this work, the original 0.154 M YSZ sol was

diluted to 0.026 M, 0.013 M, and 0.0087 M. Both PVA and HPC were studied as the DCCA to strengthen the gel structure and reduce the solvent viscosity. For comparison, mesoporous YSZ membranes were also prepared on macroporous alumina support as reported in our previous work [Kim & Lin, 1998]. Table 2.3 summarizes 9 membrane samples prepared and the characteristics of these samples. For each sample the dip-coating, drying and calcination process was repeated by 5 times.

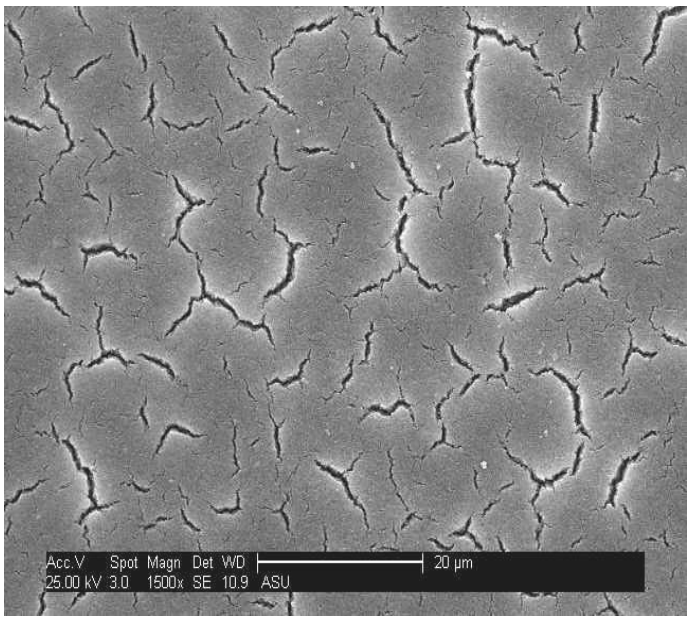

Figure 2.7 SEM images of surface morphology of YSZ mesoporous membrane prepared with original 0.154 M sol on YSZ macroporous membrane after 3 times' dip-coating

Figures 2.8 and 2.9 are surface and cross-section SEM images of mesoporous YSZ membranes on YSZ macroporous membranes prepared from the sol with a concentration of 0.026 M, 0.013 M, and 0.0087 M, respectively with PVA and HPC as DCCA. Comparing the surfaces in Figure 2.8 with that in Figure 2.7, it could be seen that crack formation was improved by virtue of the fact that the cracks decreased in size quite

drastically after using the sol with a lower concentration. Cracks on the membranes prepared from 0.154 M sol were about 5 to 10 μm in length and 1 to 2 μm in width. Here, the cracks are just 1 to 1.7 μm in length and 0.16 to 0.34 μm in width for the membranes prepared from 0.026 M sol and about 0.17-0.3 μm in length and 0.09 to 0.16 μm in width for the membranes from 0.013 M sol. In some ways, it could be inferred that the size of cracks decreased reciprocally to the sol concentration. The membranes made from 0.0087 M sol are crack free. From Figures 2.8 (b), (d) and (e), a clear triple-layer structure of the composite membrane can be observed. The top YSZ layers are about 3.35 μm, 1.35 μm and 1.02 μm thick corresponding to 0.026 M, 0.013 M, and 0.0087 M. The thicknesses of the membranes decrease with a reduction of sol concentration, hence lessening the stresses and preventing crack formation. This is evident when the sol concentration is very low (0.0087 M) which led to the formation of a crack free mesoporous YSZ membrane.

Comparing the cross sections shown in Figure 2.9 (membranes prepared with HPC as DCCA) with those in Figure 8 (PVA as DCCA), it was found that the film formations are very similar regardless of what DCCA is used. The membranes become thinner when the lower concentrations of sol are used. The thicknesses of the YSZ mesoporous membranes prepared with HPC are about 3.37 μm, 1.33 μm and 1 μm, which are almost same as those obtained from the sol with PVA added. However, despite the similarity in thickness, differences in surface morphology can be distinguished from the SEM images. By comparing Figure 2.9 (a) and Figure 2.8 (a), when the 0.026 M sol is used, the cracks

on the sample with HPC are about 2 to 5 μm in length and 0.5 to 1 μm in width which are much larger than those on the membranes with PVA added as DCCA. It looks like the use of PVA is better than HPC in terms of limiting crack formation. When a lower concentration sol is used, crack formation is drastically improved for the sol with HPC and the quality of the membrane is very similar to that from the sol with PVA. When the concentration of the sol with HPC added is 0.013 M, the cracks are about 0.15 to 0.3 μm long and 0.1 to 0.15 μm wide. This size is smaller than those made from 0.026 M sol. Finally, when the concentration is 0.0087 M with HPC, crack free membranes could be obtained, as was also the case when PVA was used.

Figures 2.10 (a) to (f) are SEM images of mesoporous YSZ membranes directly prepared on alumina supports with PVA added. Compared with Figure 2.7, it can be seen that, with the same YSZ sol concentration used, the size of the cracks formed and the film thickness of the mesoporous YSZ membranes on macroporous YSZ membranes or alumina supports are almost same. This indicates that the difference in support properties does not influence the synthesis of mesoporous YSZ membranes, and that sol concentration remains the key factor in film preparation. The membrane prepared from 0.026 M YSZ sol on alumina support after 5 times dip-coating is around 3.5 μm, which is the same as that from our previous work [Kim & Lin, 1998]. However the previous work showed that mesoporous YSZ membrane of this thickness on alumina support was crack-free. Although in both studies drying was conducted in a humidity-controlled chamber, the dip-coating process was conducted in the air. The air humidity in the location of the previous work (Cincinnati, Ohio) is about 50-70%, much higher than that in the location of the present work (Tempe, Arizona) (10-20%). The initial exposure of

the dip-coated YSZ gel to the air of different humidity is the main reason for the different extent of cracks for the mesoporous YSZ membranes prepared in the present and previous work. The results suggest a need to perform dip-coating in a humidity-controlled chamber in a relatively dry location if one wants to obtain crack-free thick membranes.

Table 2.3

Summary of the YSZ mesoporous membranes prepared and result observed and measured from SEM images

Sample No.	YSZ sol concentration (M)	Support	DCCA	Crack width range (μm) L: length W: width	Top layer thickness (μm)
1	0.026	Macroporous YSZ Membrane	PVA	L: 1-1.7 W: 0.16-0.34	3.35
2	0.013	Macroporous YSZ Membrane	PVA	L: 0.17-0.3 W: 0.09-0.16	1.35
3	0.0087	Macroporous YSZ Membrane	PVA	No Cracks	1.02
4	0.026	Macroporous YSZ Membrane	HPC	L: 2-5 W: 0.5-1	3.33
5	0.013	Macroporous YSZ Membrane	HPC	L: 0.15-0.3 W; 0.1-0.15	1.37
6	0.0087	Macroporous YSZ Membrane	HPC	No cracks	1
7	0.026	Alumina Support	PVA	L: 1-1.8 W: 0.15-0.36	3.5
8	0.013	Alumina Support	PVA	L: 0.17-0.3 W: 0.1-0.21	1.4
9	0.0087	Alumina Support	PVA	No Cracks	1.1

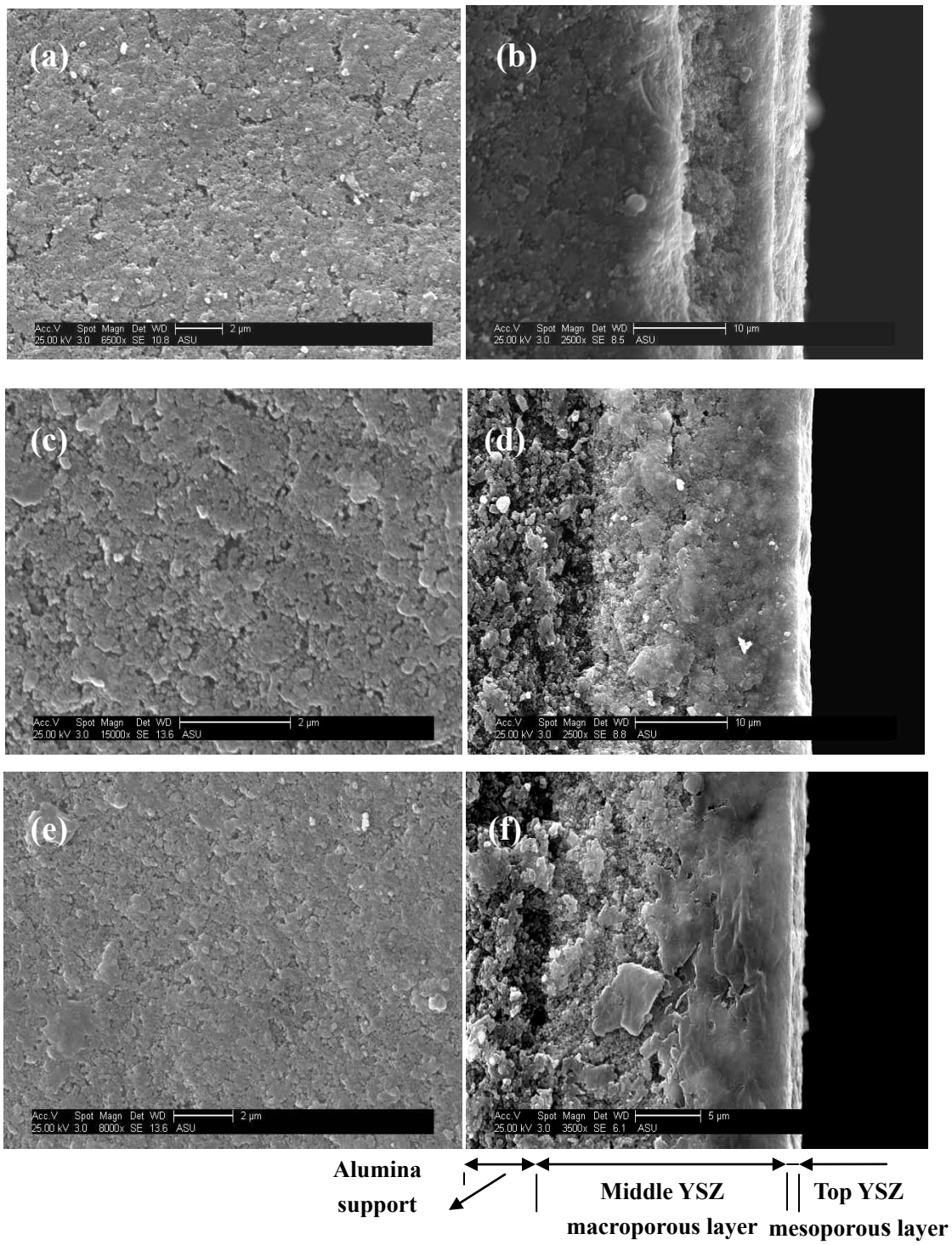

Figure 2.8 SEM images of top surface and cross section of YSZ mesoporous membrane prepared on YSZ macroporous membrane with PVA after 5 times dip-coating by a sol concentration of 0.026 M (a), (b) and a 0.013 M sol (c), (d) and 0.0087 M (e), (f)

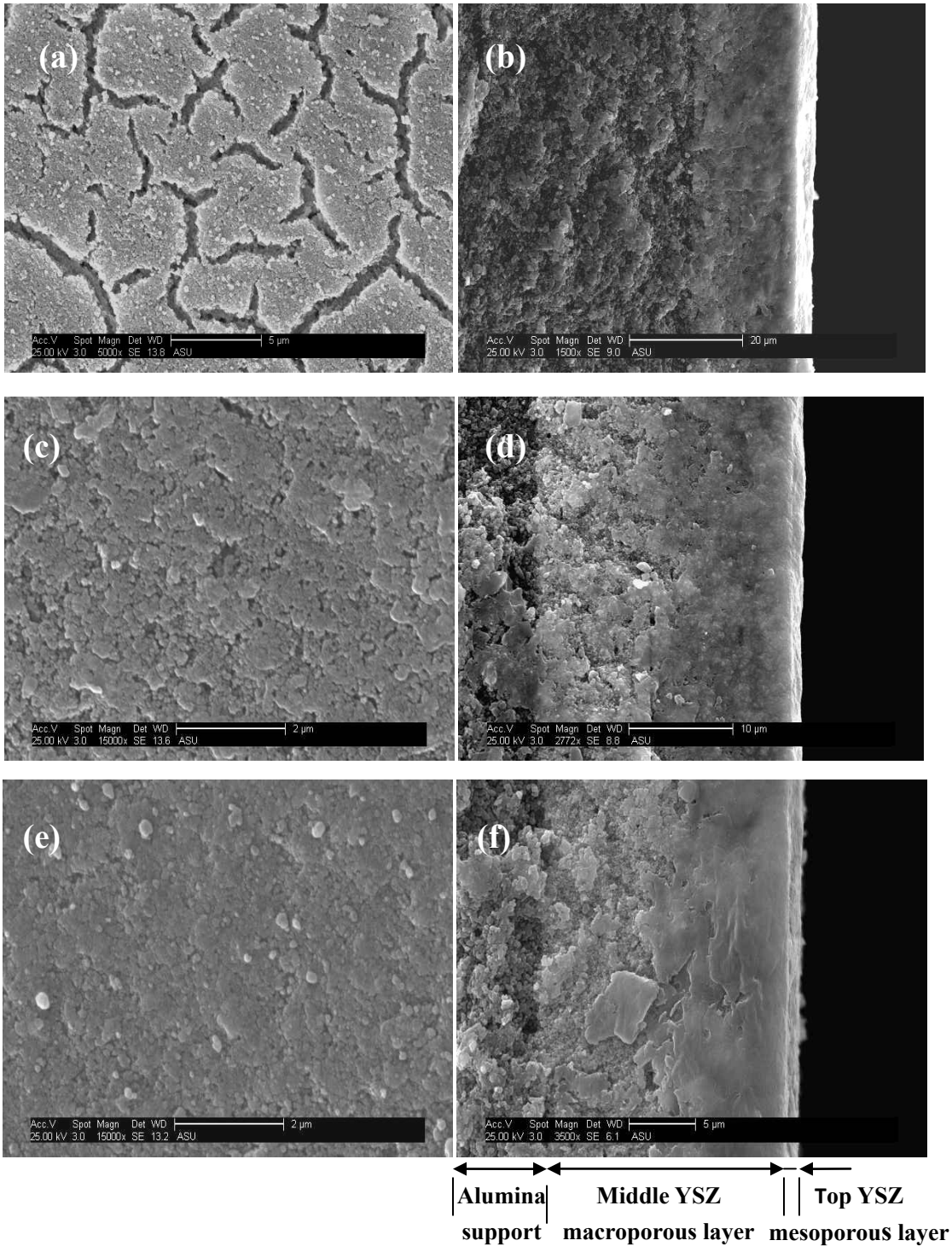

Figure 2.9 SEM images of top surface and cross section of YSZ mesoporous membrane prepared on YSZ macroporous membrane with HPC after 5 times dip-coating by a sol concentration of 0.026 M (a), (b) and a 0.013 M sol (c), (d) and 0.0087 M (e), (f)

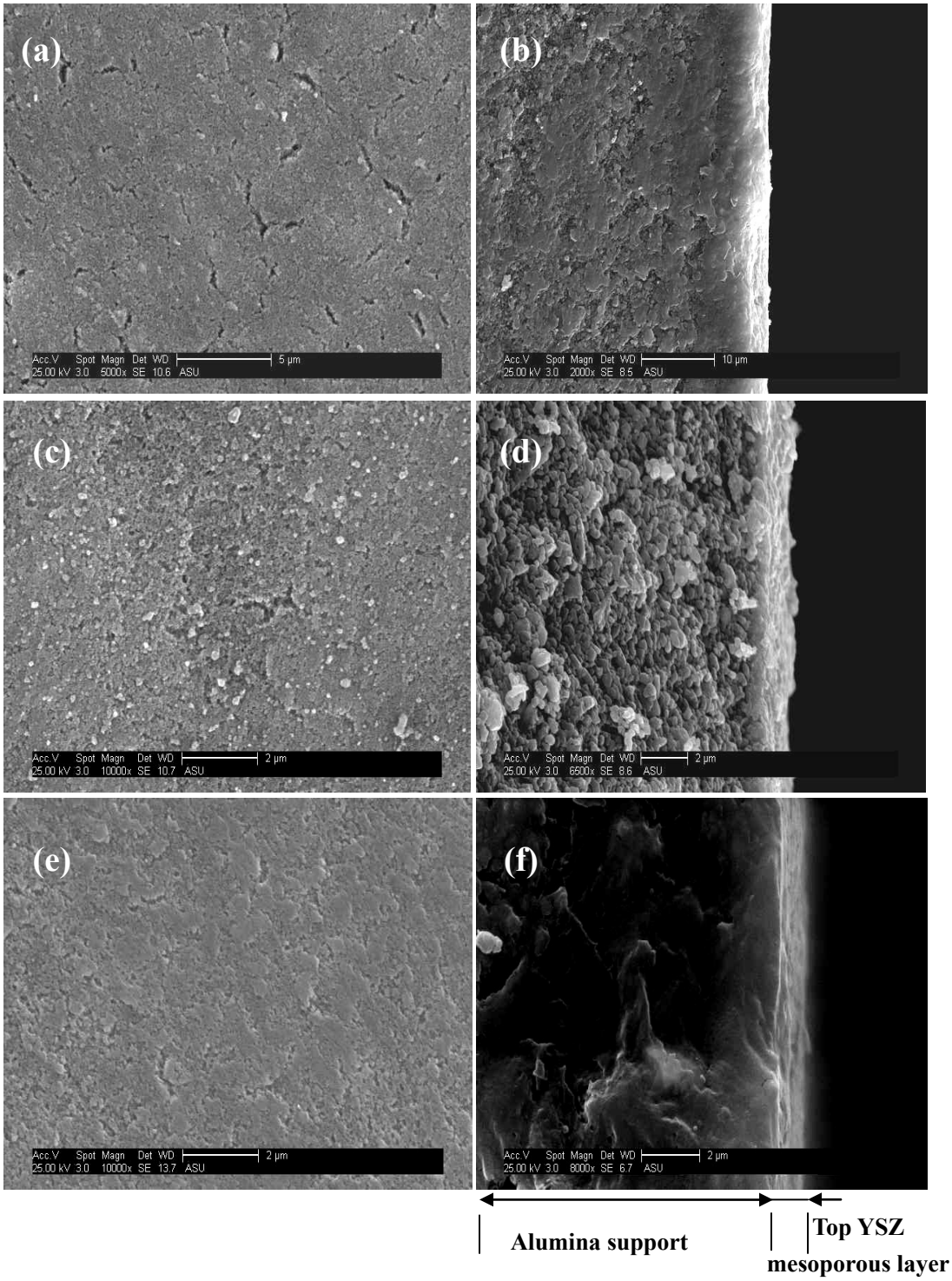

Figure 2.10 SEM images of top surface and cross section of YSZ mesoporous membrane prepared on alumina support with PVA after 5 times dip-coating by a sol concentration of 0.026 M (a), (b) and a 0.013 M sol (c), (d) and 0.0087 M (e), (f)

Gas permeation tests were done to check for the presence of the defects in the mesoporous YSZ membranes. Based on the PSD, the gas permeation mechanism through the mesoporous YSZ membrane should obey the rule of Knudsen flow. Consequently, gas separation factor should be equal to reciprocal of the square root of the molecular weight of the permeating gases. Helium and nitrogen permeation test were done through the crack free mesoporous YSZ membrane prepared on YSZ macroporous membrane and alumina support. Gas permeance data and the calculated separation factors are shown in Table 2.4. The theoretical Knudsen-separation factor of helium and nitrogen is 2.65. From Table 2.4, it is seen that the helium and nitrogen permeance through mesoporous YSZ membrane on alumina support are 1.112 and 0.421 (10^{-6} mol/m^2/s/Pa) with a separation ratio of 2.64. While for mesoporous YSZ membrane prepared on macroporous YSZ membrane, the permeances are 1.085 and 0.408 (10^{-6} mol/m^2/s/Pa) with a separation ratio of 2.66. For both membranes, the He/N2separation factor are approximately equal to the theoretical value, indicating the YSZ mesoporous membranes prepared on both supports are defect and pin-hole free.

Table 2.4

Helium and Nitrogen permeances through YSZ mesoporous membranes and gas separation ratio of the two gases

	He Permeance P_{He} (10^{-6} mol/m^2/s/Pa)	N_2 Permeance P_{N2} (10^{-6} mol/m^2s/Pa)	P_{He}/ P_{N2}
Mesoporous YSZ membrane on alumina support	1.112	0.421	2.64
Mesoporous YSZ membrane on macroporous YSZ membrane	1.085	0.408	2.66

2.4 Conclusions

High-quality, crack-free supported YSZ macroporous membranes were prepared from a stable suspension under optimum condition. The membrane prepared was of a cubic fluorite structure and average pore size was 116 nm measured by helium permeance test. Supported, crack-free, high-quality YSZ mesoporous membranes could be prepared from an YSZ sol with a lower concentration by dip-coating on supported YSZ macroporous membrane. The average pore size of the membrane was found to be about 3 nm, as measured by nitrogen adsorption porosimeter. The optimum concentration of the YSZ sol was determined to be 0.0087 M in this work. Concerning the use of the DCCA, there were no difference between using PVA and HPC on crack improvement and film formation of the YSZ membrane. At a relatively high concentration, PVA had a better effect on minimizing crack formation than HPC. Crack-free YSZ mesoporous membranes were around 1 μm thick after 5 times' dip-coating. Crack-free YSZ mesoporous membranes were also prepared on alumina supports. The membrane properties were similar to those made on YSZ macroporous membranes and the quality of the membranes was not influenced by supports. Helium permeance experiments show Knudsen gas separation factor confirming that the supported YSZ mesoporous membranes are free of defects and pin-holes. Asymmetric supports with multi-layer structure could be successfully prepared. In Chapter 3, the methods developed in this Chapter will be applied to make thin ceramic-carbonate dual-phase membranes.

CHAPTER 3

SYNTHESIS AND CHARACTERIZATION OF THIN CERAMIC-CARBONATE DUAL-PHASE MEMBRANES FOR CARBON DIOXIDE SEPARATION

3.1 Introduction

To develop a high temperature CO_2-permselective membrane, concept of dual-phase membrane consisting of an electronic or ionic conducting solid phase and molten carbonate liquid phase was proposed by Lin's group [Chung et al., 2005]. Metal-carbonate dual-phase membranes using stainless steel [Chung et al., 2005] and metal silver [Xu et al., 2012] were synthesized. The membranes exhibited promising CO_2 permeation flux and selectivity. However, reaction between metal phase and molten carbonate and additional steps to remove O_2 in the permeate stream limited application of the membranes. Improvement was made by replacing metal supports with mixed or ionic conducting ceramics [Anderson & Lin, 2006]. Such membranes could give selective permeation of CO_2 at high temperature due to the transport of carbonate ion in the carbonate phase and oxygen ion in the ceramic phase.

Several groups have reported the synthesis and CO_2 permeation properties of these membranes. Anderson and Lin [Anderson & Lin, 2010] synthesized a dual-phase membrane on porous, ionic-electronic conducting $La_{0.6}Sr_{0.4}Co_{0.8}Fe_{0.2}O_{3-\delta}$ (LSCF) support. At 900 °C, 3.0, 1.5, 0.75 and 0.375 mm thick dual-phase membranes offered CO_2 fluxes of 1.02, 1.89, 2.35 and 2.42×10^{-3} mol/s/m^2, respectively. CO_2/Ar separation factor was

at least 225. The membrane stability could be improved by adding oxygen in the feed gas [Norton et al., 2014]. Wade et al. [Wade et al., 2011] synthesized 200-400 μm thick yttria-stabilized zirconia (YSZ)-carbonate dual-phase membrane with a flux of 1.0×10^{-3} mol/s/m^2 at 750°C and gadolinia doped ceria (GDC)-carbonate membrane reaching 1.5×10^{-3} mol/s/m^2 at 850°C. Rui et al. prepared the membrane with $B_{1.5}Y_{0.3}Sm_{0.2}O_{3-\delta}$ (BYS) modified with γ-alumina [Rui et al., 2012]. CO_2 flux was 0.55×10^{-3} mol/s/m^2 at 650 °C. Recently, Zhang et al. [Zhang et al., 2012] reported synthesis of the dual-phase membranes on porous samarium doped ceria (SDC). The membrane exhibited a CO_2 flux of 1.37×10^{-2} mol/s/m^2 at 700°C. Lin and workers [Dong et al., 2013] achieved tubular SDC-carbonate dual-phase membrane from asymmetric support which was made via a centrifugal slip-casting method. The membrane obtained a CO_2 flux of 1.16×10^{-2} mol/s/m^2 at 900°C. Permeation properties of the membranes were previously summarized in Table 1.1 and Figure 1.2. In summary, ceramic-carbonate dual-phase membranes can be prepared on various oxygen ionic conducting porous supports, and the membranes exhibit high CO_2 flux at high temperatures.

The studies reported were mainly focused on the fabrication of thick membranes (1-2 mm). So far there are no synthesis and performance studies reported on thin ceramic-carbonate dual-phase membranes for CO_2 separation. Transport model demonstrated that CO_2 permeation through the dual-phase membrane was dominated by oxygen ionic transport [Wade et al., 2007, Rui et al., 2009]. As discussed in

Chapter 1, the membrane of this kind will have a higher gas permeation flux with a smaller thickness [Lin et al., 1992, Han et al., 1997].

To increase CO_2 permeation flux of ceramic-carbonate dual-phase membrane, it was proposed to prepare the thin ceramic-carbonate dual-phase membrane as shown in Figure 3.1. The support should consist of a thick (1-2 mm), large pore (0.5-5 μm) base and a thin (5-50 μm), small pore (<100 nm), oxygen ionic conducting or mixed conducting ceramic top-layer. It is desirable to use same materials for top-layer and base to avoid mismatch issue. The molten carbonate fills the pores of the top-layer by a direct infiltration method [Chung et al., 2005]. The key point is to ensure that after infiltration with carbonate the top-layer is gas tight while the base remains porous. The capillary force achieved in the top-layer, for the materials with similar surface tension, can be 50-100 times larger than that in the base due to the smaller pore size. It is expected to be strong enough to hold the molten carbonates leaving the base non-infiltrated and porous. The CO_2 perm-selectivity can be guaranteed by the thin, non-porous dual-phase top-layer.

The asymmetric two layer porous supports shown in Figure 3.1 can be prepared by the suspension coating method reported in Chapter 2. The objective of Chapter 3 is to report synthesis and characterization of the thin ceramic-carbonate dual-phase membranes. $B_{1.5}Y_{0.3}Sm_{0.2}O_{3-\delta}$ (BYS), $Y_{0.16}Zr_{0.84}O_{2-\delta}$ (YSZ) and α-alumina were selected as the materials for the base support in this work. Porous or dense supports

of these materials have demonstrated good mechanical and chemical stability in previous research [Kim & Lin, 1999, Rui et al., 2012]. $Y_{0.16}Zr_{0.84}O_{2-\delta}$ (YSZ) and $La_{0.6}Sr_{0.4}Co_{0.8}Fe_{0.2}O_{3-\delta}$ (LSCF) were selected as the ionic conducting materials for the thin top layer. Synthesis of thick dual-phase membranes [Anderson & Lin, 2010, Wade et al., 2011, Ortiz-Landeros et al., 2013] could give guidance for thin membrane preparation. CO_2 permeation and separation properties of thin dual-phase membranes at high temperatures were studied as well.

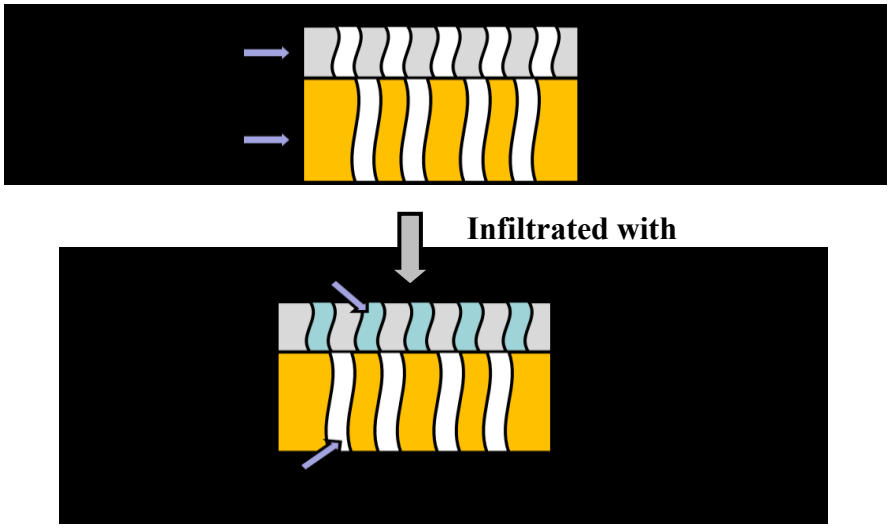

Figure 3.1 Schematic configuration of asymmetric thin dual-phase membrane

3.2 Experimental

3.2.1 Preparation of asymmetric porous supports

Powders of $Bi_{1.5}Y_{0.3}Sm_{0.2}O_{3-\delta}$ (BYS), $Y_{0.16}Zr_{0.84}O_{2-\delta}$ (YSZ) and α-alumina were prepared to make the base supports. BYS powders were prepared by the citrate method [Rui et al., 2012]. Stoichiometric amounts of the corresponding metal nitrates, i.e., $Bi(NO_3)_3{\cdot}5H_2O$ (98%, Sigma-Aldrich), $Y(NO_3)_3{\cdot}6H_2O$ (99.9%, Sigma-Aldrich) and

$Sm(NO_3)_3 \cdot 6H_2O$ (99.9%, Sigma-Aldrich), were fully dissolved in a dilute nitric acid solution (10 vol% of concentrated HNO_3), followed by addition of anhydrous citric acid (99.5%, Alfa Aesar). The solution was heated to 90–110°C forming sticky gel-like solid and performed a fast and uniform self-ignition of the organics at 400°C. After self-ignition, the powders were further calcined at 900°C for 6 hours. $Y_{0.16}Zr_{0.84}O_{2-\delta}$ (YSZ) powders (8-mol% Y_2O_3-stabilized ZrO_2) (TZ-8Y, Tosoh Co., Tokyo, Japan) and α-alumina powders (A13, Alcoa) were from commercial sources.

The large pore base supports were prepared by the ceramic powders (BYS, YSZ and α-alumina) as described above. The weight of powders used was 4 g for BYS disk and 2 g for both YSZ and α-alumina disks. Polyvinyl alcohol (PVA) (3 wt%, Fluka, MW=72000) was applied as the binder. The amount of PVA added was 10 wt% of the dry green powders. The powder mixtures were packed into a stainless steel mold (22 mm in diameter) and uniaxially pressed into disk shape under a hydraulic pressure of 100 MP for BYS [Rui et al., 2012] while 150 MP for YSZ and α-alumina [Kim & Lin, 1999]. The pellets prepared were around 1.5 mm thick. The sintering temperatures for the disks were 750°C for BYS [Rui et al., 2012], 1100°C for YSZ [Kim & Lin, 1999] and 1260°C for α-alumina with a heating and cooling rate of 60°C per hour. The sintering time for all three disks was selected as 24 h. The symbols of BYS, YSZ and ALU are used to denote three base supports prepared by BYS, YSZ and α-alumina powders, respectively. The characteristics of the base supports are summarized in Table 3.1.

Asymmetric porous supports consisting of a small pore top-layer on the large pore base support were prepared by dip-coating the suspension of $Y_{0.16}Zr_{0.84}O_{2-\delta}$ (YSZ) and $La_{0.6}Sr_{0.4}Co_{0.8}Fe_{0.2}O_{3-\delta}$ (LSCF) on the base supports. YSZ suspension was made according to the procedures described in Chapter 2. YSZ powders (8-mol% Y_2O_3-stabilized ZrO_2) (TZ-8Y, Tosoh Co., Tokyo, Japan), mixed with dilute nitric acid (pH= 3-4) at a weight ratio of 1:2, were ball milled in polyethylene (PE) pots with ZrO_2 balls for 5-7 days. After the ball-milling process, the YSZ suspension was diluted to 10 wt% by adding more nitric acid. LSCF powder was synthesized by the liquid citrate method (Yin & Lin, 2007, Anderson & Lin, 2010). Corresponding amounts of the metal nitrates $La(NO_3)_3.6H_2O$, $Sr(NO_3)_2$, $Co(NO_3)_3$ and $Fe(NO_3)_3$ were mixed and dissolved in water and heated to 110°C. After self-ignition, dried gel was finally calcined at 600°C to achieve the powder. LSCF suspension was synthesized with similar step as that of YSZ. The pH of the suspension was 1-2 and concentration was set to be 7.5 wt %.

Ceramic suspensions (YSZ and LSCF) were separately dip-coated on large pore base supports. PVA was used as drying control chemical additive (DCCA) to prevent crack formation on the membranes during the drying step. The optimum amount of PVA solution to be added into the suspension was determined to be at a volume ratio of 1:4 for YSZ suspension and 1:5 for LSCF suspension. The dip-coated disks were dried in air at a relative humidity (RH) of 50%-60% and a temperature of 40°C for 24 hrs. After drying, the membranes were sintered in air at 750°C for 6 h with a heating and

cooling rate of 1°C/min. The coating, drying and sintering processes were repeated to ensure the formation of crack-free top-layers. Six porous asymmetric supports were prepared and are summarized in Table 3.2.

3.2.2 Preparation of thin film ceramic-carbonate dual-phase membranes

Thin dual-phase membrane was obtained via a direct infiltration of molten carbonates into the top-layer of asymmetric porous support [Chung et al., 2005]. Lithium (Li), sodium (Na), and potassium (K) carbonates from Fisher Scientific (Li_2CO_3, 99.2%; Na_2CO_3, 99.9%; K_2CO_3, 99.8%) were mixed in 42.5/32.5/25 mole percent ratio and heated to 580°C in a box furnace. The asymmetric support, with macroporous membrane facing down, was preheated in the furnace for 20 minutes. Then the membrane was dipped into molten carbonate. The support was held for 10 minutes to allow the molten carbonates infiltrating into the thin top-layer via capillary action. The membrane was cooled down to room temperature with a rate of 1°C/min. Thin dual-phase membranes of d-YSZ/BYS, d-YSZ/YSZ, d-YSZ/ALU, d-LSCF/BYS, d-LSCF/YSZ and d-LSCF/ALU were synthesized, as summarized in Table 3.3.

3.2.3 Membrane characterization and high temperature CO_2 permeation measurements

The average pore size of porous base supports (BYS, YSZ and α-alumina) and supported macroporous ceramic membranes (YSZ and LSCF) were separately measured by the steady state helium permeation method. Porosity of porous base supports was examined by the liquid nitrogen method. Molten carbonate wettability on the metal

oxide supports was checked by observing the contact angles of the molten carbonate drop on the supports at 550°C. Phase structure of porous supports and dual-phase membranes were determined by X-ray diffraction (XRD) (Bruker AXS, D8 Focus Diffractometer, CuKα). The morphology of the membranes was examined by scanning electron microscopy (SEM, Phillips, FEI XL-30). Composition of thin dual-phase membrane was checked by an energy dispersive spectrometer (EDS).

High temperature CO_2 permeation tests were carried out in a home-made permeation set-up as described in our previous publication [Rui et al., 2012] as shown in Figure 3.2. The thin dual-phase membrane was sealed with graphite seals in the middle of a high temperature cell. CO_2 (25 ml/min, STP) and N_2 (75 ml/min, STP) were introduced to the feed side, and He (100 ml/min, STP) to the downstream as sweep gas during the heating and permeation measurements. Before heating the system, inert gases of N_2 (50 ml/min, STP) to the feed side and He (50 ml/min, STP) to the sweep side were introduced for 10 min to eliminate oxygen in the membrane cell and protect the graphite seals from decomposition. The system was heated at a rate of 1 °C/min to 500°C. After allowing the system to remain at 500°C for one hour reaching steady state, data collection began. Measurements were taken in 25°C (1°C/min ramp) increments, starting at 500°C and working upward to 650°C. Once reaching the desired temperature, the system was kept at that temperature for one hour before data collection.

The gas composition in the sweep gas was measured by a HP 5890 Series II gas chromatograph with a TCD detector, an Alltech's Hayesep DB 100/120 column (30'× 1/8"×0.85" SS), and argon as the carrier gas. The amount of N_2 detected in the sweep gas during permeation experiments allowed determination of CO_2 leak through the seal. Corrected CO_2 flux was made by subtracting the CO_2 associated with the leak. Gas leakage through the membrane or the seal is assumed to follow the Knudsen diffusion mechanism. Leaking nitrogen flux was around 5-8 % of that total amount of CO_2 measured. For each condition, we measured 2 to 3 data in around 30 min intervals. The errors of the data are within 10%.

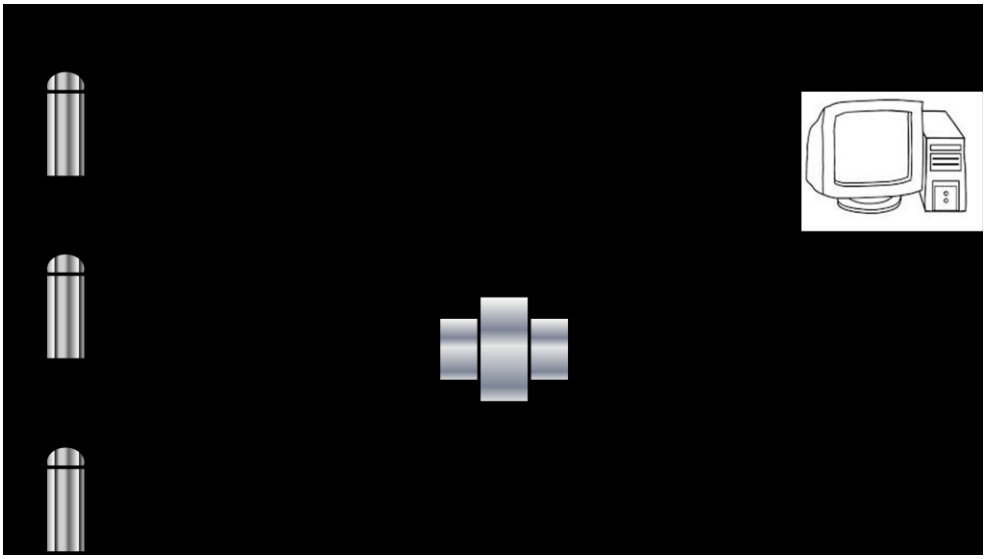

(1-3) Gas cylinders; (4) Mass flow controller; (5) Valve; (6) Box furnace; (7) High temperature permeation cell; (8) Gas chromatograph and data collection; (9) Pressure gauge; (10) Needle valve.

Figure 3.2 Schematic drawing of high temperature permeation setup

3.3 Results and discussion

3.3.1 Membrane synthesis

3.3.1.1. Characteristics of the supports

Phase structure of ceramic powders of BYS, YSZ and α-alumina (ALU) was examined by XRD. XRD patterns of the powders are consistent with previous research [Wade et al., 2011, Rui et al., 2012] that were ready for synthesis of porous asymmetric supports. Porosities of the base supports are 30-40% for BYS, 40% for YSZ and 50-55% for ALU measured by the liquid nitrogen method.

Figure 3.3 shows steady state helium permeance through the YSZ, BYS and ALU supports. As shown, in the pressure range reported, the He permeances of the BYS, YSZ and ALU supports are separately on the order of 10^{-6}, 10^{-6} and 10^{-5} mol/s/m^2/Pa.

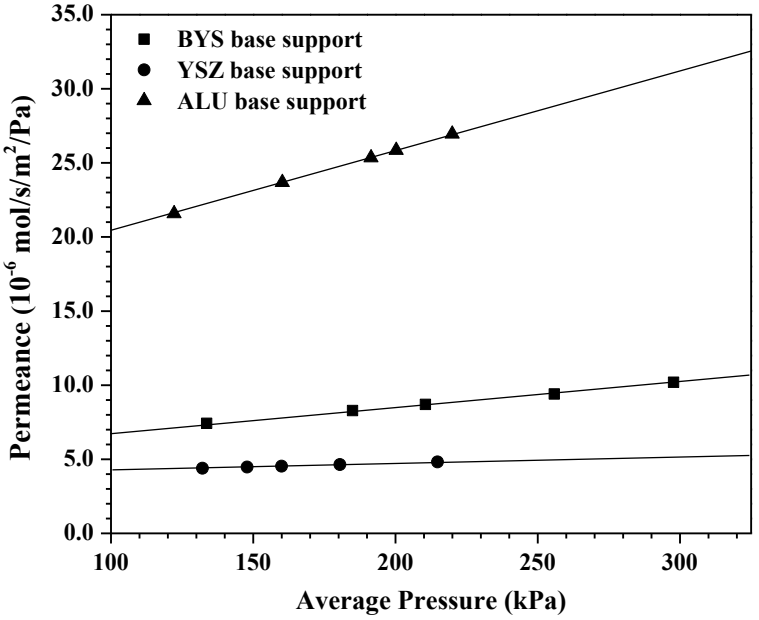

Figure 3.3 Helium permeance of BYS, YSZ and ALU base supports vs. average pressure

The permeance versus average pressure data for each support can be correlated by a straight line, with the intercept and slope correlated to the pore structure and permeating gas properties as [Leenaars et al., 1984, Kanezashi et al., 2007].

$$\alpha = 1.06\left(\frac{\epsilon}{\tau}\right)\frac{r_p}{L\sqrt{RTM_w}} \tag{3.1}$$

$$\beta = 0.125\left(\frac{\epsilon}{\tau}\right)\frac{r_P^2}{L\mu RT} \tag{3.2}$$

where L is the thickness of the membrane (m), μ is the viscosity (cp) of helium at room temperature, ε and τ represent the porosity and tortuosity of the membrane, R is the gas constant (8.314 m^3·Pa/mol/K), T is the temperature (K), M_w is the molecular (g/mol) weight of helium and r_p is the average pore radius (m). The values for the intercept and slope were obtained by regression of the straight line shown in Figure 3.2. The average pore radius of the base support can be obtained from the ratio of the slope to intercept (β/α) by:

$$r_p = 8.48\,(\frac{\beta}{\alpha})\sqrt{\frac{\mu^2 RT}{M_w}} \tag{3.3}$$

The measured pore radius for BYS, YSZ and ALU base supports are 470 nm, 202 nm and 550 nm respectively. Characteristics of the base supports were listed in Table 3.1.

The results of checking molten carbonate wettability to the supports are shown in Figure 3.4. Figure 3.4a shows dry carbonate mixtures (Li/Na K) on top of each support at room temperature. The supports were then heated to 550°C and carbonates melted. Figure 3.4b shows the same supports staying at 550°C. Compared with Figure 3.4a, no carbonate residuals are observed on top of YSZ and ALU showing that molten carbonates

infiltrating into the pores of the supports. However, clear liquid drop of melting carbonates can be observed on the surface of BYS support. It can be concluded that molten carbonates are wettable to YSZ and ALU but non-wettable to BYS.

Table 3.1

Characteristics of base supports

Ceramic powder	Denotation	Pore radius	He Permeance (10^{-6} mol/s/m^2/Pa)	Porosity	Carbonate wettability
$Bi_{1.5}Y_{0.3}Sm_{0.2}O_{3-\delta}$	BYS	470	8.78	30-40%	Non-wettable
$Y_{0.16}Zr_{0.84}O_{2-\delta}$	YSZ	202	4.53	40%	Wettable
α-alumina	ALU	550	24.55	50-55%	Wettable

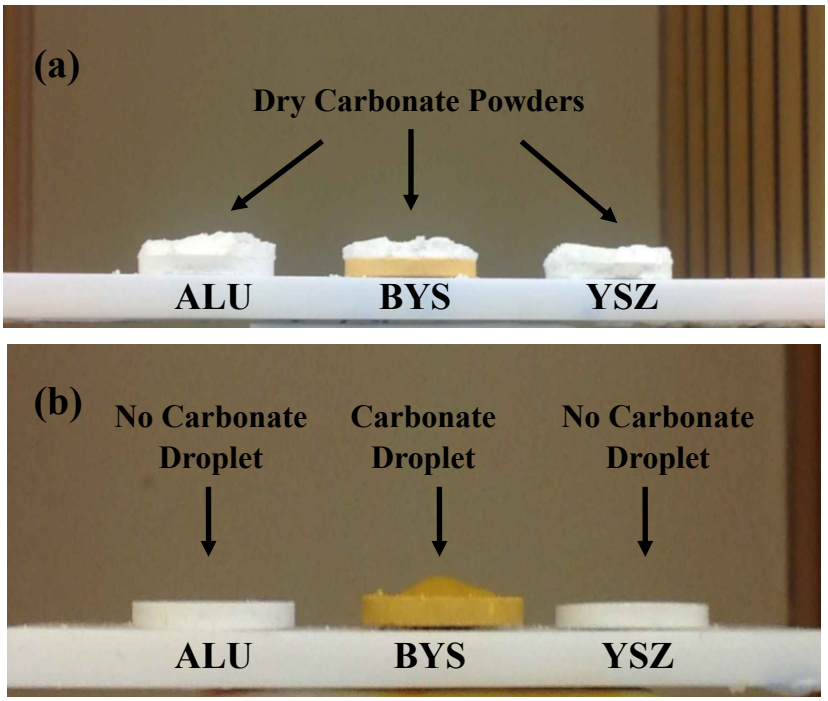

Figure 3.4 Examination of molten carbonates wettability on the metal oxide supports (a) dry carbonate powders on top of the supports at room temperature and (b) same supports heated and stayed at 550℃.

Asymmetric porous supports consisting of thin porous top-layer of YSZ and LSCF, coded as t-YSZ/BYS, t-YSZ/YSZ, t-YSZ/ALU, t-LSCF/BYS, t-LSCF/YSZ and t-LSCF/ALU, were prepared. Properties of the supports are shown in Table 3.2. A great disparity exists in sintering behavior between YSZ/LSCF and BYS. It was found that sintering of BYS support affected preparation of the supports. When sintering temperature was lower than 750^{o}C, BYS support could not provide enough mechanical strength for synthesis of thin dual-phase membrane in the following steps. When sintering temperature is higher than 750^{o}C, the support could not provide enough porosity with a strong capillary force. YSZ or LSCF suspension could not be dip-coated on the surface forming a layer. Hence optimum sintering temperature for BYS support was set at 750^{o}C. Sintering of YSZ or LSCF at this temperature did not influence the fabrication of the membrane. Helium permeance of the base supports, after coated with the top-layer, decreased by 5-10% due to resistance offered by the top-layer.

Table 3.2

Composition and characteristics of porous asymmetric supports

Base support	Top layer	Denotation	Top-layer thickness (μm)	Radius (nm)	Top-layer porosity	He Permeance (10^{-6} mol/s/m^2/Pa)
BYS	YSZ	t-YSZ/BYS				7.89
YSZ	YSZ	t-YSZ/YSZ	～10	50	46%	4.11
ALU	YSZ	t-YSZ/ALU				22.55
BYS	LSCF	t-LSCF/BYS				8.12
YSZ	LSCF	t-LSCF/YSZ	～10	120	57%	4.23
ALU	LSCF	t-LSCF/ALU				23.87

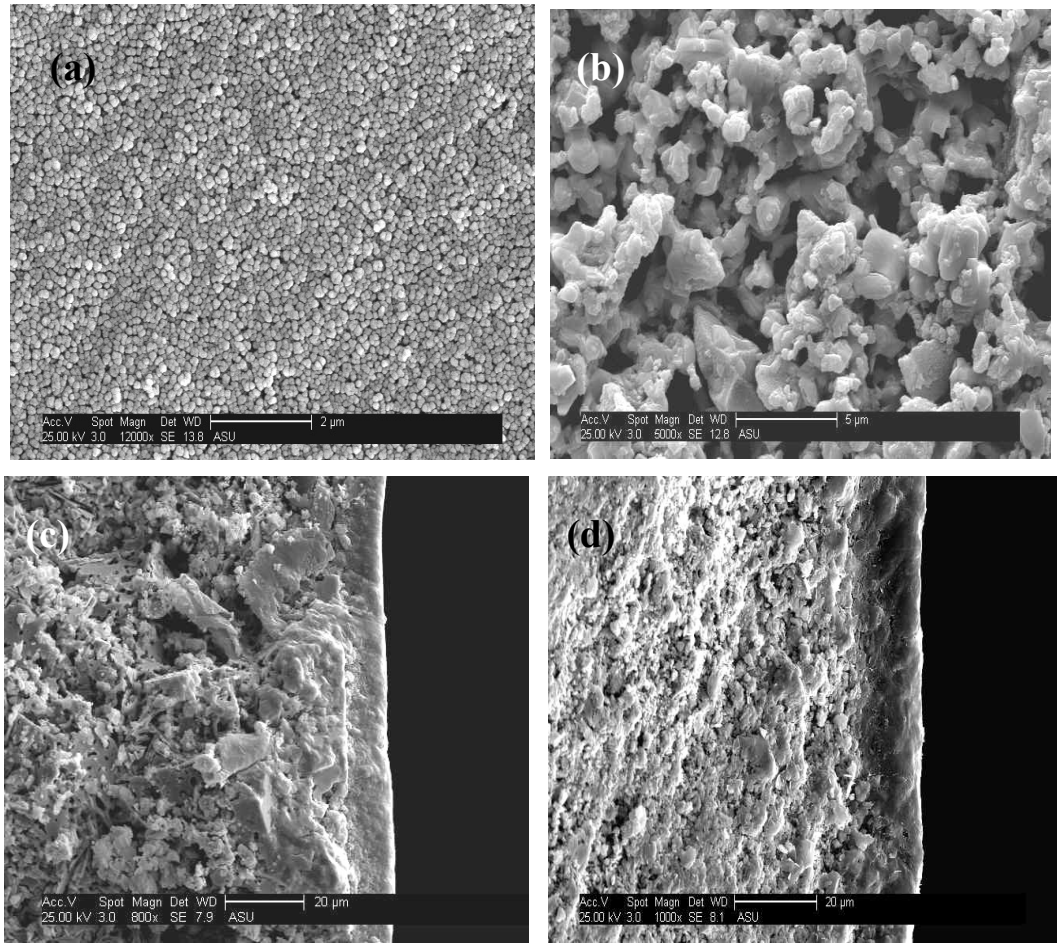

Figure 3.5 Scanning electron microscopy (SEM) images of macroporous membranes on BYS supports: surface morphology of (a) YSZ, (b) LSCF, and cross section of the membrane (c) YSZ, (d) LSCF

Figure 3.5a and 3.5b respectively shows the SEM images of surface morphology of macroporous YSZ and LSCF membranes on BYS base supports. It is seen that both membranes are homogeneous and defect free. Figure 3.5c and 3.5d present cross section of thin YSZ and LSCF membrane on BYS base supports. The thicknesses of both membranes are around 10 µm. Same SEM images were also observed for the thin YSZ and LSCF membranes on YSZ and ALU base supports. Thin LSCF membrane

exhibits a larger porosity and pore radius than those of YSZ layer. Average pore radius measured by the steady state method is around 50 nm for YSZ layer and 120 nm for LSCF membrane.

3.3.1.2 Thin ceramic-carbonate dual-phase membranes

The thin ceramic-carbonate dual-phase membranes were prepared by directly infiltrating the molten carbonate into the asymmetric supports. After infiltration with carbonate, LSCF top layer peeled off from d-LSCF/BYS, but all other thin dual-phase membranes were of good quality. As listed in Table 3.3, thin dual-phase membranes derived from BYS, YSZ and ALU supports separately exhibited 2, 4 and 5 orders of magnitude reduction in helium permeance compared to the supports before the infiltration. It was hoped that only the top layer was infiltrated with the carbonate because of the larger capillary pressure in the top-layer due to its smaller pore size as compared to the base support. However, the asymmetric supports of BYS, YSZ and ALU respectively exhibited 2 wt%, 25 wt% and 35 wt% weight gain after infiltration with carbonate. Based on the pore volume and thickness of the top-layer, the carbonate infiltration into the top-layer should only result in about 1 wt% weight gain for YSZ and ALU supports and 2 wt% for BYS support. The much larger weight gain after infiltration for the YSZ and ALU base supports suggests that carbonate not only fills the pores in the top-layer but also penetrates into the base support. Figure 3.6 shows morphology of cross section of the asymmetric porous supports before and after

infiltration with molten carbonate. It is clear that only BYS base support maintains its porous structure after the infiltration. Both YSZ and ALU base supports are filled with carbonate, which are highly undesirable as membranes.

Figure 3.7 shows the percent of weight gain for the three asymmetric supports after infiltration with carbonate with different contact time at 580^{o}C. For d-YSZ/BYS, a 2 wt% weight gain is quickly achieved and stays the same with longer contact time. For d-YSZ/YSZ and d-YSZ/ALU, the weight gain increases with increasing contact time. Even at a contact time of 5 s, a 7-8 wt% weight gain is observed, larger than theoretical value for infiltration into the top-layer only. These data confirm that for d-YSZ/YSZ and d-YSZ/ALU the carbonate fills the top-layer and then infiltrate into the base during infiltration. Capillary pressure P_c produced during infiltration could be expressed [Chung et al., 2005]

$$P_c = -\gamma_{lv} \cos\theta \frac{1}{r} \tag{3.4}$$

where γ_{lv} is the carbonate liquid-vapor surface tension, θ is contact angle of molten carbonate on the solid surface and r is the radius of the pore. The capillary pressure in the base can be significant with good carbonate wettability (smaller contact angle). Results in Figure 3.4 clearly show that carbonate can easily wet the base support of YSZ and ALU but not wet the BYS. It is the non-wettability of molten carbonate to BYS that results in the infiltration of the carbonate in the top YSZ layer only.

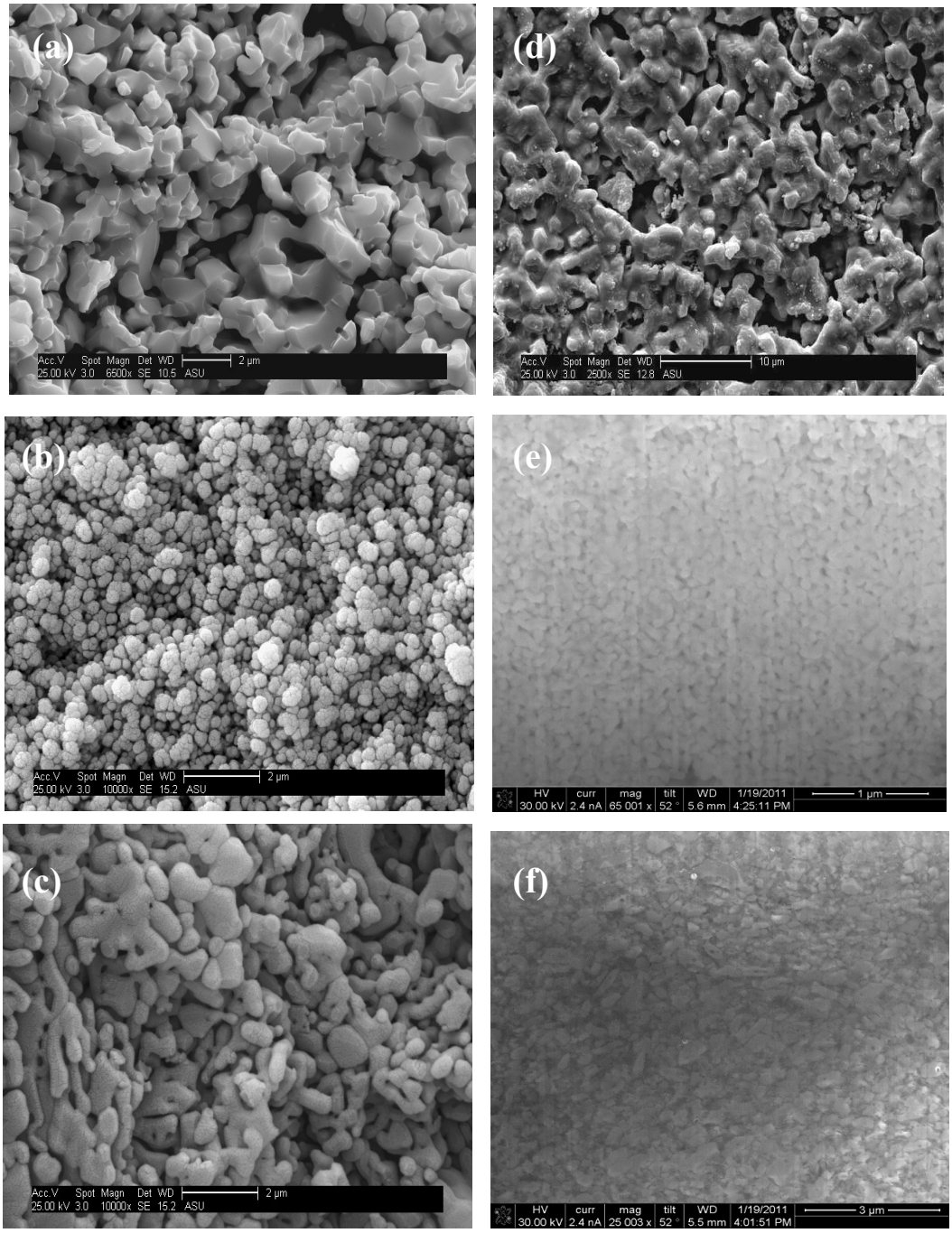

Figure 3.6 Scanning electron microscopy (SEM) images of cross section of asymmetric porous supports before infiltration-(a) BYS base support, (b) YSZ base support, (c) α-alumina (ALU) base support and morphologies after infiltration with carbonate-(d) BYS base support, (e) YSZ base support, (f) α-alumina (ALU) base support

Table 3.3

Characteristics of thin dual-phase membranes

Supports	Peeling of top layer	Infiltration of base support	He Permeance after infiltration (10^{-10} mol/s/m^2/ Pa)	Order magnitude reduction in permeance after infiltration
d-YSZ/BYS	No Peeling	No	500	2
d-YSZ/YSZ	No Peeling	Yes	4.58	4
d-YSZ/ALU	No Peeling	Yes	1.89	5
d-LSCF/BYS*	Peeling off	No	N/A	N/A
d-LSCF/YSZ	No Peeling	Yes	4.88	4
d-LSCF/ALU	No Peeling	Yes	1.93	5

**LSCF top layer peeled off after infiltration with carbonate and helium permeance could not be measured.*

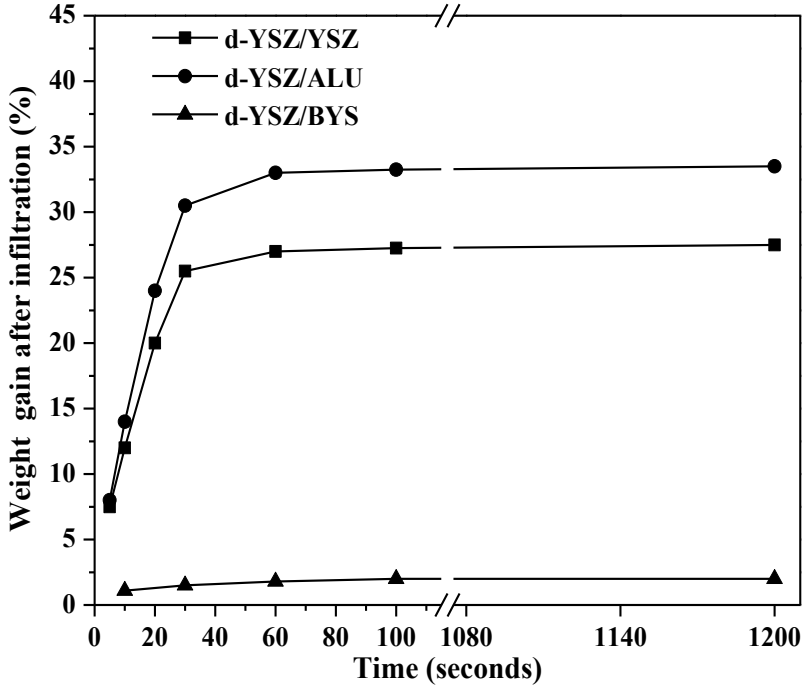

Figure 3.7 Weight gain of asymmetric supports after infiltration with molten carbonate versus different dipping contact time

The asymmetric porous support should be prepared with a thin porous top-layer derived from oxygen ionic-conducting or mixed-conducting ceramic phase on a porous base made of molten carbonate non-wettable material. During infiltration, carbonate should fill the top-layer, but not the non-wettable base support. This will result in formation of a thin and dense supported ceramic-carbonate dual-phase membrane and base support remains porous. D-YSZ/YSZ, d-YSZ/ALU, d-LSCF/YSZ and d-LSCF/ALU do not form thin dual-phase membranes due to infiltration of carbonate into bases. D-LSCF/BYS does not work either because the LSCF top layer peeled off. A stress is developed during the cooling of molten carbonate after infiltration because of the phase change [Mamantov et al., 1981]. It is possible that the adhesion between LSCF layer and BYS support is not strong enough to resist the stress resulting in peeling off of the LSCF-carbonate layer upon cooling process. Thus the only good thin dual-phase membrane on porous base support prepared in this work is d-YSZ/BYS.

Figure 3.8a shows the morphology of the cross-section of the as-synthesized d-YSZ/BYS. The membrane consists of three layers. The porous part is the BYS base support. The results of the EDS analysis show Y/K and Zr/K ratios are 0.009 and 0.018 for the top layer, and 0.86 and 1.64 for the middle layer. This means that the middle layer contains about 90 times more Y and Zr than those in the top layer. The results indicate that supported top YSZ layer has been infiltrated generating a dense membrane. However, there is a carbonate layer covering the YSZ-carbonate top-layer.

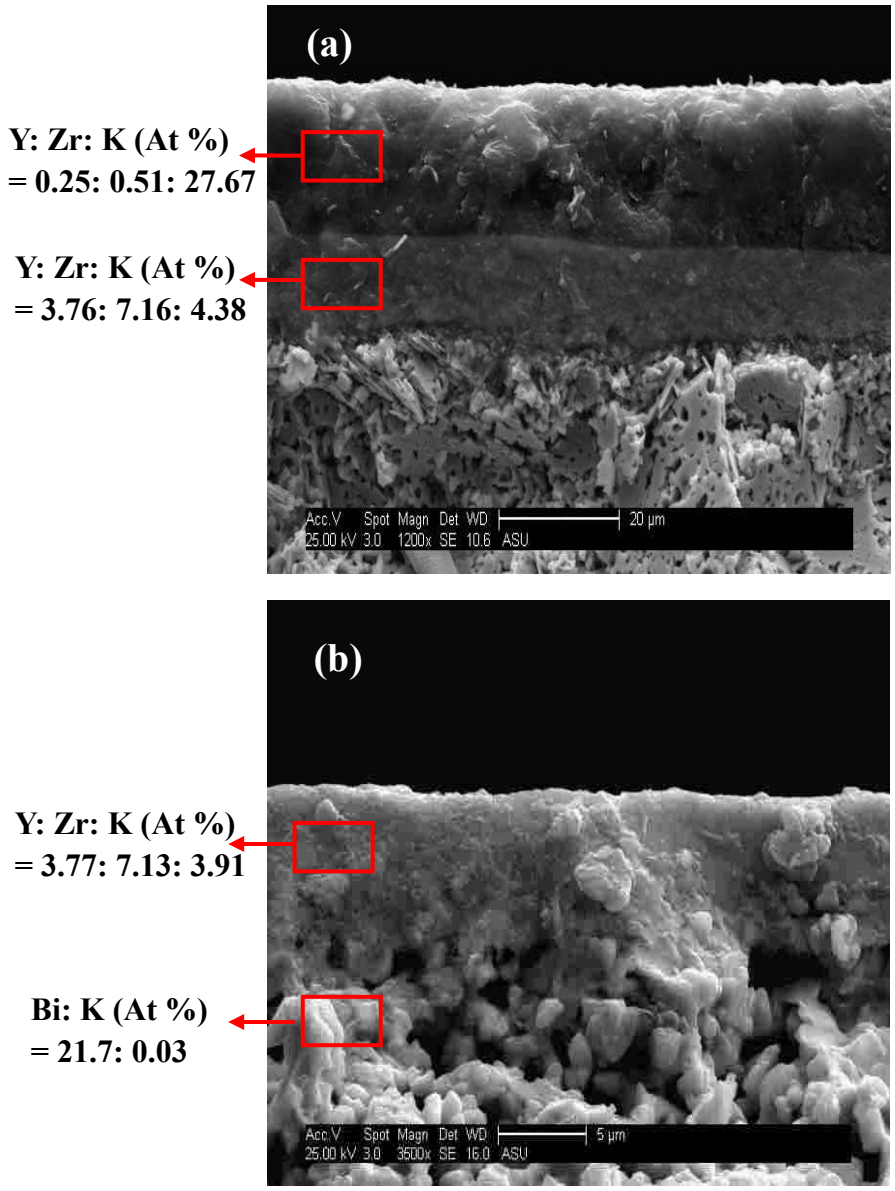

Figure 3.8 Scanning electron microscopy (SEM) images of morphology of (a) cross section of thin dual-phase membrane after infiltration and (b) cross section of thin dual-phase membrane after removal of residual carbonate

Residual carbonate layer could often be found on the contact surface between the support and molten carbonate after infiltration [Anderson & Lin, 2010, Wade et al., 2011, Rui et al., 2012]. Since this is a pure carbonate layer transporting carbonate ions only, it

could not permeate neutral CO_2. Therefore, the residual carbonate layer should be removed. For thick dual-phase membrane, the residual carbonates could be physically removed by light polishing with a SiC polishing paper [Anderson & Lin, 2010, Rui et al., 2012]. Such polishing can easily damage the thin dual-phase membrane. In this work, we used a new method, as schematically showed in Figure 3.9 to remove the residual carbonate layer on the thin dual-phase membrane.

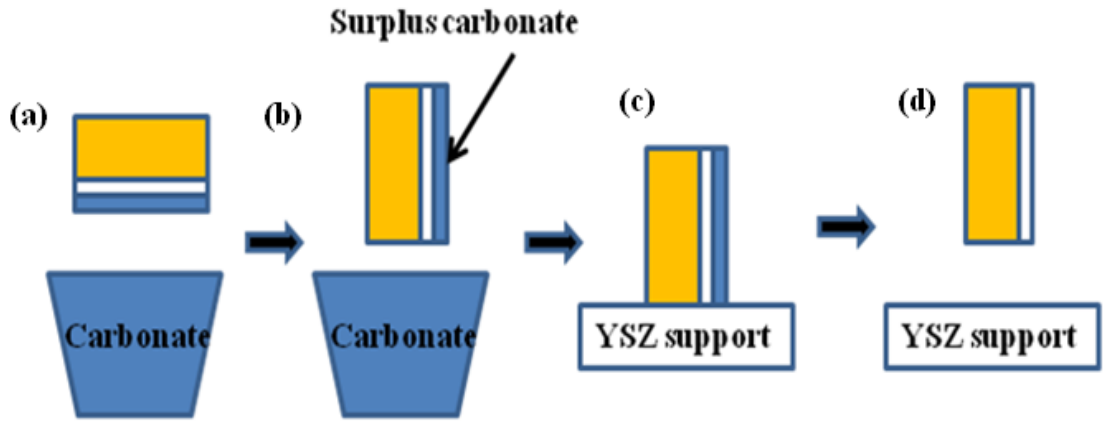

Figure 3.9 Schematic drawing of procedure for residual carbonate layer removal: (a) infiltration, (b) composite membrane was vertically placed; (c) the membrane is vertically lowered to contact YSZ absorbent and (d) the excess of molten carbonate is sucked with the consequent removal of cover layer

After infiltration, without cooling down, the membrane was placed in a vertical position. A porous YSZ base support was also preheated in the furnace. The membrane was then vertically lowered down to contact the surface of YSZ support. Most residual carbonate would be absorbed by YSZ base support due to its carbonate

wettablity. As shown in Equation 3.4, for material with the same contact angle, the smaller the pore size, the larger the capillary pressure it has. The YSZ top layer has a smaller pore size (r_p=50 nm) than the YSZ support (r_p=202 nm) used to remove carbonate residual layer, it has a stronger capillary force which prevents the carbonate in its pores to be absorbed by the YSZ base support. Figure 3.8b shows the morphology of the cross section of thin dual-phase membrane after removal of the carbonate residual layer by this method. A desirable two-layer asymmetric support is observed. The result of the EDS analysis result in top-layer shows Y/K and Zr/K ratios are 0.96 and 1.82 confirming removal of carbonate residuals leaving a dual-phase membrane. EDS result of bottom porous support demonstrates carbonate only staying in top-layer not penetrating into the base. The membrane has a dense dual-phase layer of about 10 μm thick.

Figure 3.10 compares XRD patterns of thin YSZ dual-phase membrane with that of t-YSZ/BYS support before infiltration with carbonate. In Figure 3.10a, designated peaks are in agreement with cubic fluorite YSZ [Kim & Lin, 1999]. In Figure 3.10b, except for characteristic YSZ peaks, the small peaks around 21.6^o (2θ) and 38^o (2θ) are consistent with the most intensive XRD peaks of $LiNaCO_3$ (Anorthic, JCPDS File Card No. 01-084-2168). The XRD results confirm the infiltration of molten carbonate into the pores of top macroporous YSZ membrane. No other new peaks are found in Figure 3.10b and the asymmetric support is chemically stable after infiltration with carbonate.

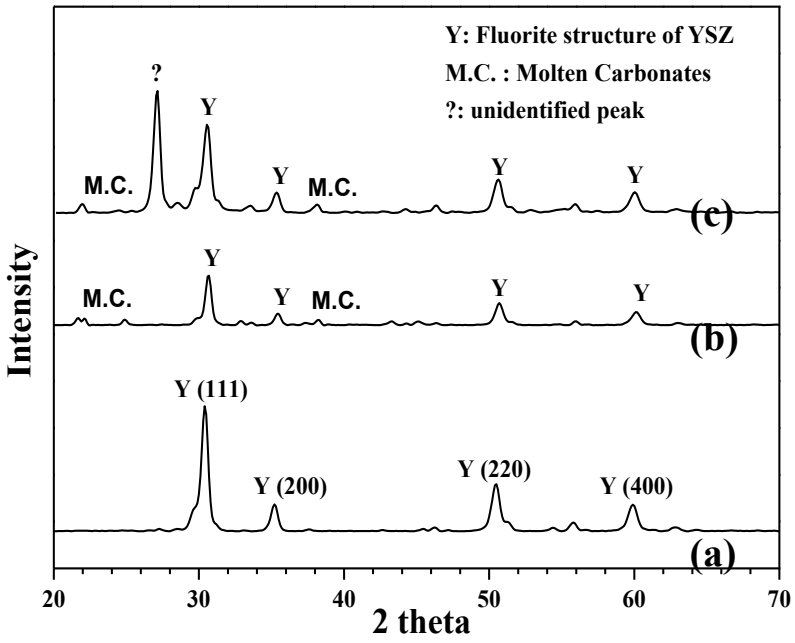

Figure 3.10 X-ray diffraction patterns of (a) macroporous YSZ membrane on BYS support; (b) thin YSZ-carbonate dual-phase membrane before high temperature CO_2 permeation test; (c) thin YSZ-carbonate dual-phase membrane after high temperature CO_2 permeation test.

3.3.2 High temperature CO_2 permeation test

CO_2 flux for the thin dual-phase YSZ/BYS membrane is shown in Figure 3.11a as a function of temperature. Arrhenius plot of the permeance data are given in Figure 3.11b to estimate the apparent activation energy (Ea) for CO_2 permeation through the thin YSZ-carbonate dual-phase membrane, which is 106 kJ/mol. The value is larger than that of thick YSZ-carbonate dual-phase membrane of 84 kJ/mol [Wade et al., 2011] and that for oxide-ion conduction in YSZ electrolytes reported in literature.

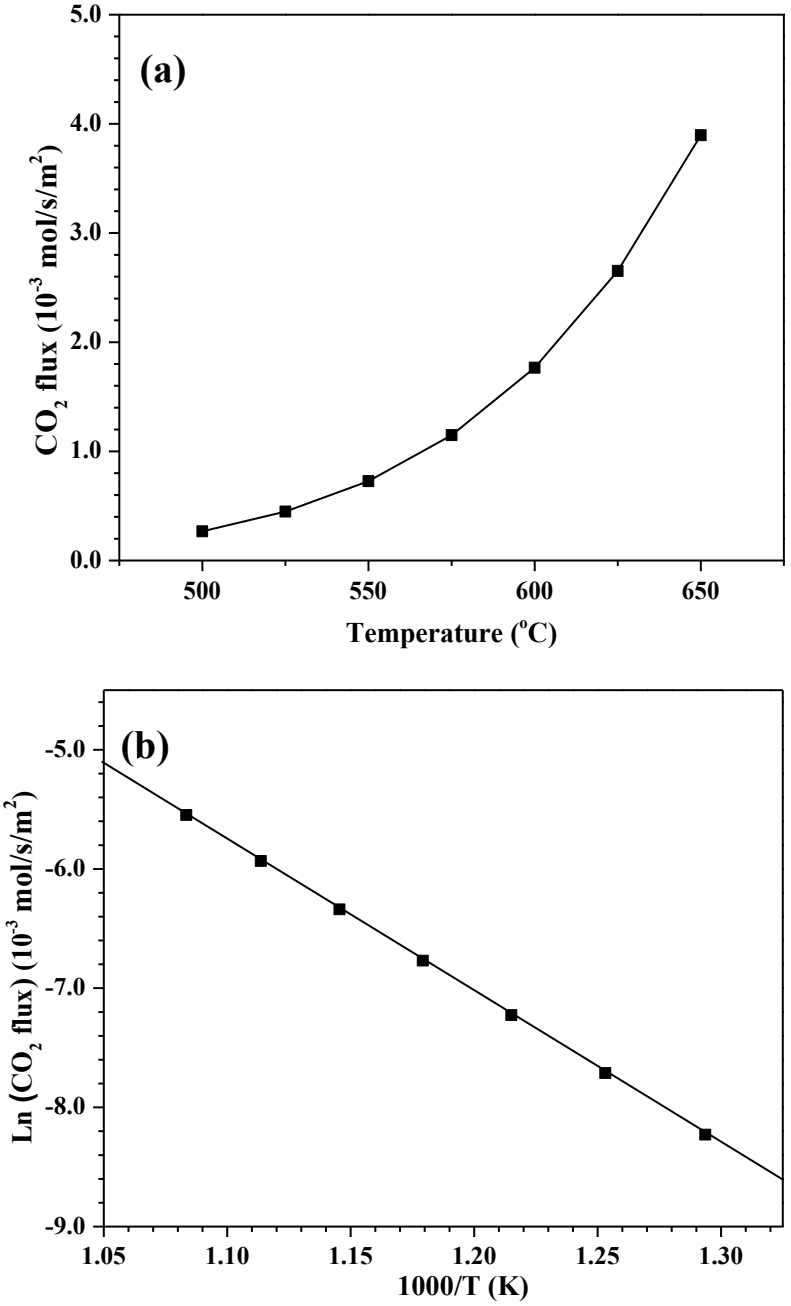

Figure 3.11 (a) Temperature dependence of CO_2 flux through thin YSZ-carbonate dual-phase membrane and (b) Arrhenius plot of the thin YSZ-carbonate membrane

The measured CO_2 flux of thin YSZ-carbonate dual-phase membrane is compared with other membranes reported in literature as shown in Figure 3.12. It is seen that the

CO_2 flux of thin dual-phase membrane developed in this work is at least 10 times higher than those reported for the thick LSCF-carbonate membrane at 700°C [Anderson & Lin, 2010] and YSZ-carbonate and GDC-carbonate membranes at 650°C [Wade et al., 2011] and over 5 times higher than that of BYS-carbonate [Rui et al., 2012] and SDC-carbonate membrane (70 vol% SDC) [Zhang et al., 2012] at 650°C. It is only a little bit smaller than SDC-carbonate dual-phase membrane containing 50 vol% SDC which has a very different microstructure of the solid phase [Zhang et al., 2012]. It is also observed that CO_2 permeances for the LSCF, YSZ and CGO membranes at 900°C could still not match that of thin dual-phase membrane.

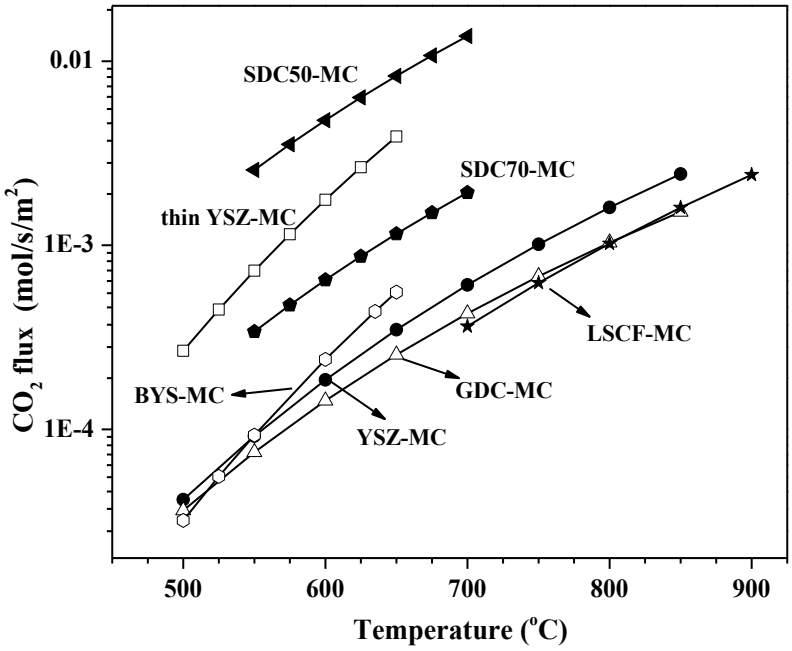

Figure 3.12 Comparison of CO_2 flux for thin YSZ-carbonate dual-phase membrane developed in this study with those for thick dual-phase membranes in the literature (The tests were performed with CO_2: N_2 feed and He sweep, P'_{CO_2}=0.5 atm, F_{He}=100ml/min)

Table 3.4 compares permeation properties of the membranes. A higher oxygen ionic conductivity of solid phase will lead to a larger CO_2 permeance. YSZ has the lowest oxygen ionic conductivity among all the materials, thin YSZ-carbonate dual-phase membrane however shows a second high permeance. The significant improvement is attributed to the reduction of membrane thickness. CO_2 permeation through dual-phase membranes was controlled by oxygen ionic transport [Rui et al., 2012]. Thin membrane shortens the path and reduces the resistance of ion transport. An enhanced ionic transport is allowed in the membrane and accelerates uptake and release of CO_2 at upstream and downstream. Therefore a higher CO_2 flux will be achieved.

Based on transport mechanism, gas permeation through the membrane should be reciprocally proportional to membrane thickness. The 10 μm YSZ-carbonate dual-phase membrane should have a CO_2 flux up to 1×10^{-2} mol/s/m^2, about 30 times larger than the flux for the thicker (200-400 μm) dual-phase membranes. However, as shown in Table 3.4, the measured flux for the 10 μm membrane is only about 10 times larger than that for the 200-400 μm thick membrane. Activation energy of thin YSZ-carbonate dual-phase membrane is 106 kJ/mol that is larger than 84 kJ/mol of thick membrane. Similar phenomenon was also reported by Anderson and Lin [Anderson & Lin, 2010]. For thin dual-phase membranes, improved permeance is not reciprocally proportional to reduced thickness and activation energy is larger than that of thick membrane. Both imply that the surface reaction becomes a factor as thickness decreases. CO_2 permeability of thin

YSZ-carbonate dual-phase membrane is also compared with other membranes as shown in Figure 3.13.

The permeability for thin YSZ-carbonate dual-phase membrane however is around 10-100 times lower than that for thicker membranes. The permeability of the thin membrane should be similar with that of thick membranes if gas permeation through the membrane is majorly driven by bulk diffusion. Comparison of permeability further confirms that surface reaction also affects gas permeation through dual-phase membrane when thickness reduces.

Table 3.4

Comparison of CO_2 flux through dual-phase membranes

Ceramic phase	Membrane thickness (μm)	T (°C)	CO_2 flux (10^{-3} mol/s/m^2)	Ea (kJ/mol)	σ_v (S/cm)	Ref.
$La_{0.6}Sr_{0.4}Co_{0.8}Fe_{0.2}O_{3-\delta}$	375	700	0.37	89.9	0.024	Anderson & Lin, 2010
$Bi_{1.5}Y_{0.3}Sm_{0.2}O_{3-\delta}$	~ 50	650	0.55	113	0.137	Rui et al., 2012
$Ce_{0.8}Sm_{0.2}O_{1.9}$[1]	1200	650	1.94	74.3	0.5	Zhang et al., 2012
$Ce_{0.8}Sm_{0.2}O_{1.9}$[2]	1200	650	13.7	77.2	0.5	Zhang et al., 2012
$Ce_{0.9}Sm_{0.1}O_{1.9}$	200-400	650	0.25	77±6	0.029	Wade et al., 2011
$Y_{0.16}Zr_{0.84}O_{2-\delta}$	200-400	650	0.35	84±14	0.01	Wade et al., 2011
$Y_{0.16}Zr_{0.84}O_{2-\delta}$	~ 10	650	3.9	106	0.011	This work

$Ce_{0.8}Sm_{0.2}O_{1.9}$[1], 70 vol% SDC is contained in dual-phase membrane

$Ce_{0.8}Sm_{0.2}O_{1.9}$[2], 50 vol% SDC is contained in dual-phase membrane

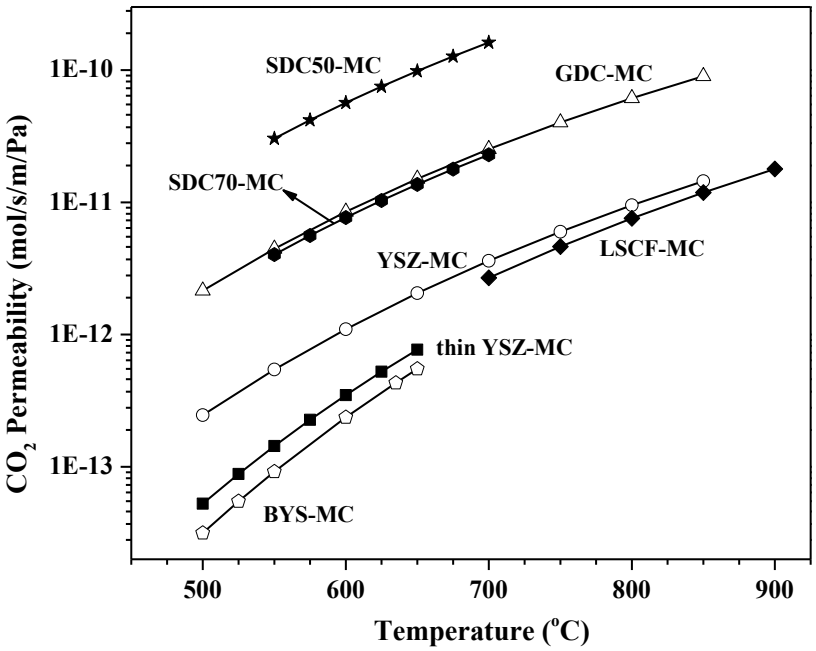

Figure 3.13 Comparison of CO_2 permeability for thin YSZ-carbonate dual-phase membrane developed in this study with those for thick dual-phase membranes made of LSCF, YSZ, CGO, BYS and SDC available in the literature (The tests were performed with CO_2: N_2 feed and He sweep, P'_{CO_2}=0.5 atm, F_{He}=100ml/min)

Selectivity of the membrane was determine by ratio of corrected CO_2 flux to measured N_2 flux in the permeate side. For the particular membrane studied here, the selectivity of CO_2 to N_2 is 20. Theoretically, the dense dual-phase membrane should be perm-selective to CO_2 only and have an infinite selectivity. The N_2 detected in the permeate side should be leaking from the gaps between graphite seals and the thin dual-phase membrane. The membrane itself is still un-permeable to other gases. If the proper sealing material and method was applied, CO_2 selectivity of the membrane could be improved over 1000 [Norton et al., 2014].

Figure 3.14 shows the CO_2 permeation flux through the thin YSZ-carbonate dual-phase membrane as function of time. It is seen that CO_2 flux of the membrane is stable during the operation period. Figure 3.10c shows the XRD pattern of thin YSZ-carbonate dual-phase membrane after the high temperature CO_2 permeation test. All are consistent with YSZ and carbonate characteristic peaks as shown in Figure 3.8b indicating good stability of the thin dual-phase membrane operated at high temperatures. However, one peak around 28^o (2θ) is found unidentified. Wade et al. reported similar phenomenon when they studied the chemical stability of YSZ and $Li/Na/KCO_3$ [Wade et al., 2011]. It is possible that the unidentified peak might correspond to tertiary phase zirconate material.

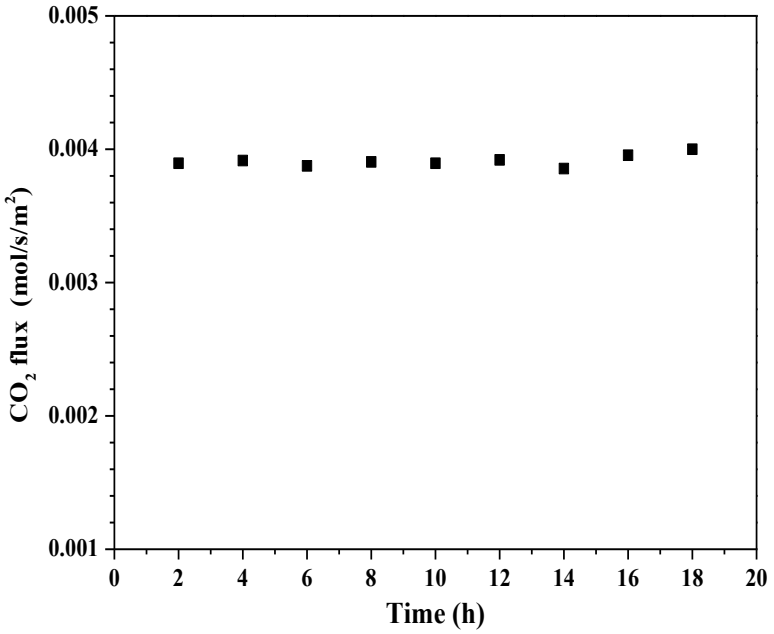

Figure 3.14 Time dependence of CO_2 permeation flux through the thin YSZ-carbonate dual-phase membrane at 650^oC

3.4 Conclusions

Thin ceramic-carbonate dual-phase membrane is synthesized on a two-layer asymmetric support. The support should consist of an oxygen ionic-conducting thin layer supported by a porous base made of molten carbonate non-wettable and ionic conductive material. During infiltration, carbonates fill the top-layer but not infiltrate into the non-wettable base support. Ionic conducting property of the support will ensure ion transport even limited molten carbonates penetrating into the support. YSZ and α-alumina (ALU) are carbonate wettable and could not be applied as base supports. A thin dual-phase membrane of d-YSZ/BYS is successfully prepared by infiltration carbonate into macroporous YSZ layer supported by porous BYS base support which is carbonate non-wettable. The membrane is around 10 μm thick and hermetic. A carbonate cover layer is found on the surface of thin dual-phase membrane after infiltration. The layer prevents transport of neutral CO_2 and a new particular method is applied to remove the layer. Gas permeation through the membrane is measured at high temperature (500°C to 650°C). The membrane has a maximum CO_2 flux of 3.9×10^{-3} mol/s/m^2 at 650°C which is 5-10 times larger than other thick (200-400 μm) dual-phase membranes. Activation energy for carbon dioxide permeation of the membrane is 106 kJ/mol. The membrane is chemically stable during the permeation test. The thin membrane has a lower flux than estimated value based on bulk diffusion transport and larger activation energy for permeation than thicker membranes. CO_2 permeability of

the thin membrane is lower than those of thicker membranes. All above indicate effects of the surface reaction on CO_2 permeation for the thin dual-phase membrane. The thin ceramic-carbonate dual-phase membrane was successfully prepared. Synthesis conditions were also identified. In the next chapters, efforts would be made on performance optimization-flux and permeation stability-of the thin ceramic-carbonate dual-phase membranes.

CHAPTER 4

CARBON DIOXIDE PERMEATION PROPERTIES AND STABILITY OF SAMARIUM DOPED CERIA-CARBONATE DUAL-PHASE MEMBRANE

4.1 Introduction

The development of CO_2 selective membranes for pre-combustion capture is a considerable challenge, as it requires the separation of larger CO_2 from smaller H_2. In addition, polymeric and inorganic membranes are both limited in their separation performance at high temperatures. To improve upon these limitations, adapting from the concept of a molten carbonate fuel cell, the concept of a CO_2-selective dual-phase dense membrane consisting of metallic phase and molten carbonate phase was proposed [Chung et al., 2005]. By taking advantage of the conducting properties of both the metal support and infiltrated molten carbonate, CO_2 could be selectively separated from a gas mixture by reacting with oxygen on the membrane surface, resulting in a permeable carbonate ion. Metal-carbonate dual-phase membranes were synthesized with stainless steel [Chung et al., 2005] and silver [Xu et al., 2012]. However, stability concerns at high temperature and existence of O_2 in the permeate products limited membrane application.

Improvement was made by using an oxygen ion conducting ceramics [Anderson & Lin, 2006]. The use of an ionic conducting support allows for the formation of a carbonate ion on the membrane surface by the reaction of CO_2 with lattice oxygen ions in

the ceramic phase, rather than gaseous O_2. The CO_2 partial pressure difference across the membrane provides the driving force for carbonate ion permeation, and on the permeate membrane surface, CO_2 is released from the carbonate phase and oxygen ions return to the ceramic phase. The first ceramic support used to report experimental CO_2 permeation in the dual-phase membrane was the oxygen ionic-electronic mixed-conducting perovskite-type material $La_{0.6}Sr_{0.4}Co_{0.8}Fe_{0.2}O_{3-\delta}$ (LSCF) [Anderson & Lin, 2010]. Since then several groups have reported on synthesis of ceramic-carbonate dual-phase membranes using various ionic-conducting metal oxides as the support [Wade et al., 2011, Rui et al., 2012, Zhang et al., 2012]. The work has been summarized in Chapter 1.

In Chapter 2 and 3, efforts were also made to synthesize ceramic-carbonate dual-phase membranes with smaller thickness. A 10 μm YSZ-carbonate membrane has shown a CO_2 flux of 3.9×10^{-3} mol/s/m^2 at 650^{o}C around 10 times higher than bulk membrane. Reducing thickness could effectively increase CO_2 flux. All the studies were focused on synthesis and initial CO_2 permeation properties of ceramic-carbonate membranes at high temperatures and atmospheric pressure. Little was done to examine the long term stability or the effect of increased system pressure on the permeation performance of the ceramic-carbonate membrane. For industrial applications, especially for pre-combustion processes, long term stability and an ability to withstand large system pressures will be necessary.

Recently, stability studies have been examined on LSCF-carbonate [Norton et al., 2014] and $La_{0.85}Ce_{0.1}Ga_{0.3}Fe_{0.65}Al_{0.05}O_{3-\delta}$ (LCGFA)-carbonate [Norton et al., 2014] membranes under the conditions of CO_2 permeation and separation. LSCF-carbonate membranes have shown poor stability in the absence of O_2, as the membrane surface reacts with CO_2, resulting in a carbonate surface layer that limits the surface exchange reaction between CO_2 and lattice oxygen. LCGFA-carbonate membranes have shown high chemical stability in the presence of simulated syngas conditions, as well as stable CO_2 permeation for one month at high 900^oC. However, limited ionic conductivity of the ceramic phase results in a relatively low CO_2 permeance relative to other materials previously studied.

To improve the performance of thin ceramic-carbonate dual-phase membranes, candidate ceramic support should not only exhibit high CO_2 permeation flux but also maintain long-term stability in harsh experimental conditions. The fluorite-type ceramic material samarium doped ceria (SDC) with composition $Ce_{0.8}Sm_{0.2}O_{1.9}$ was chosen as the ceramic support for the dual-phase membrane. This material has been extensively studied as electrolyte for solid oxide fuel cells [16]. It has also been shown to have high CO_2 permeance in the presence of molten carbonate at intermediate temperatures at high temperatures [Zhang et al., 2012]. The objective of Chapter 4 is to study the chemical and CO_2 permeation stability of the membrane under inert and simulated syngas conditions at high temperature and high pressure.

4.2 Experimental

4.2.1 Synthesis and characterization of ceramic-carbonate dual phase membranes

Samarium doped ceria (SDC) powder of composition $Ce_{0.8}Sm_{0.2}O_{2-x}$ was prepared by the citrate method previously described by Yin and Lin [Yin & Lin, 2007]. Stoichiometric amounts of metal nitrate precursors $Ce(NO_3)_3 \cdot 6H_2O$ (99.5%, Alfa Aesar) and $Sm(NO_3)_3 \cdot 6H_2O$ (99.9%, Alfa Aesar) were weighed out in a 0.05 mole basis and mixed with a 100 percent excess of citric acid (99.5%, Alfa Aesar). The precursors were dissolved in 1000 ml of de-ionized water and heated to 105 ^oC and covered for four hours to prevent evaporation and promote polymerization. Evaporation was then implemented by uncovering and heating the solution at 110^oC for 3-4 hours. The resulting viscous solution was dried in a furnace (Thermolyne, 46100) at 110^oC for 24 hours. Self-ignition of the dried gel was then performed at 400^oC to burn out the organic compounds. The resulting powder was then ground with a mortar and pestle to reduce the particle size. The powder was then calcined at 550^oC in air for 10 hrs with heating and cooling ramping rates of 10^oC/min. The calcined powder was again ground using a mortar and pestle. Approximately 3 grams of powder was placed in a 30 mm stainless steel mold and pressed to 160 MPa for 5 minutes using a hydraulic press (Carver, Model #3853). The green disks were then sintered at 1100^oC for about 20 hours with heating and cooling ramping rates of 2^oC/min resulting in porous SDC disk supports.

Synthesis of SDC-carbonate dual-phase membranes was achieved by direct infiltration of molten carbonate into the pores of sintered SDC support via the direct infiltration technique [Chung et al., 2005]. The carbonate powders Li_2CO_3 (99.2%, Fischer Scientific), Na_2CO_3 (99.9%, Fischer Scientific), and K_2CO_3 (99.8%, Fischer Scientific) were weighed out in a 42.5/32.5/25 mol% ratio, respectively, and heated to 550^oC in a furnace. Porous ceramic supports were preheated above the molten carbonate mixture to prevent thermal shock prior to being lowered into contact with carbonate. Supports were left in contact with molten carbonate for 5-10 minutes to ensure complete infiltration via capillary force. The membrane was then lifted and slowly removed from the furnace and cooled. Residual carbonate on the membrane surface was removed using SiC polishing paper.

The porosity of the porous ceramic supports was measured by the Archimedean method using liquid nitrogen. Room temperature helium permeation was used to determine the average pore size of porous supports as well as verifying the gas tightness of dense ceramic and ceramic-carbonate dual-phase membranes. The phase structure of the SDC powder and membranes were characterized using X-ray diffraction (XRD) (Bruker, $CuK_{\alpha 1}$) evaluated in the 2θ range of 20^o to 80^o. Scanning electron microscopy (SEM, Phillips, FEI XL-30) imaging was performed to confirm the porous nature of ceramic supports.

4.2.2 Carbon dioxide permeation measurements

For high temperature permeation experiments, two different permeation systems were used to measure CO_2 permeation fluxes at different system pressures. For atmospheric pressure permeation tests, a Probostat high temperature permeation system (Probostat, Norwegian Electro Ceramics AS) was used as previously described in recent published work [14]. The central part of this setup is shown in Figure 4.1. Using this system, a dense SDC-carbonate disk membrane and silver seal were placed on top of a 20 mm alumina tube, which was then enclosed by a 40 mm diameter alumina tube. The assembled system was placed in a vertical tube furnace and was heated in CO_2 and N_2 to approximately 950^oC to reach the softening temperature of silver at a ramping rate of 1^oC/min. Once the softening point of silver was reached, a spring assembly attached to an alumina spacer above the membrane forced the membrane into the silver ring, forming a seal between the membrane and the 20 mm alumina tube. Upon lowering the system temperature, a gas-tight seal formed from the hardened silver.

The feed and sweep gas flow rates were controlled by MKS mass flow meters. This setup with silver seals can be used to measure CO_2 permeation flux in a wide temperature range (500-950^oC) but the feed gas has to be maintained at atmospheric pressure. Measurements for CO_2 permeation with feed pressures higher than 1 atm were done in permeation setup as shown in Figure 3.2 of Chapter 3. In this setup, a needle valve was installed to regulate total feed pressure. The SDC-carbonate membrane was sealed with

graphite seals in the middle of a high temperature cell. The permeation cell was purged with N_2 (feed side) and He (sweep side) for 20 min prior to heating up. It was then heated to 700^{o}C a rate of 1^{o}C/min under the flow of N_2 and He in the feed and sweep sides, respectively. Feed gas of desired composition was introduced to the feed side at total flow rate of 50 ml/min and the pressure was increased to a value between 1-5 atm by adjusting the needle valve. Due to the limit of graphite seals, this setup cannot be used to measure CO_2 permeation flux at temperatures above 700^{o}C.

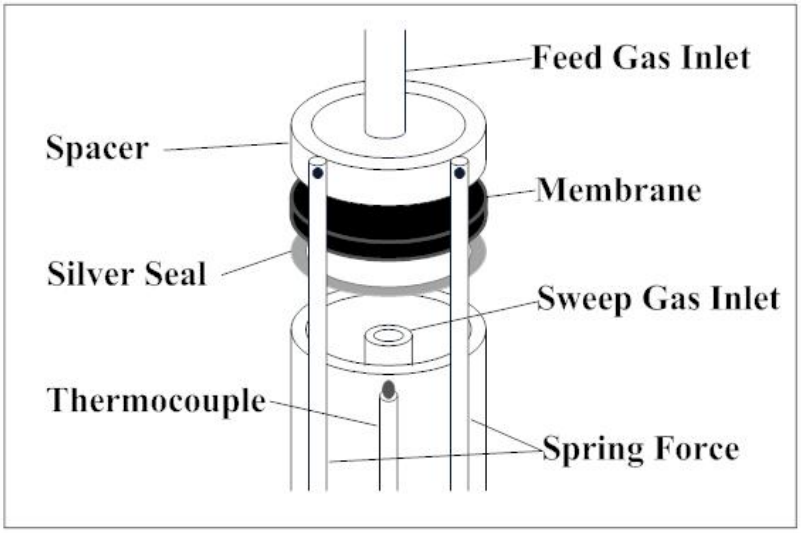

Figure 4.1 Schematic of central part of the module housing membrane for atmospheric feed pressure high temperature CO_2 permeation setup

Both atmospheric and high pressure permeation tests were performed with the feed gas of either CO_2: N_2 mixture or simulated syngas with a composition of 50% CO, 35% CO_2, 10% H_2, 5% N_2. Inert gas of either argon or helium was used as the sweep gas. The composition of the effluent of the sweep gas was by measured by gas chromatography (Agilent Technologies 6890N chromatograph for the atmospheric

pressure permeation setup and HP 5890 Series II gas chromatograph for the high pressure permeation setup, each with a TCD detector and a Alltech Hayesep DB 100/120 column of 30'×1/8"×0.85" SS, using argon carrier gas). Samples were taken two hours after a change in gas composition and one hour after a temperature change to allow the system to reach steady state.

A mass balance on the measured sweep gas was used to calculate the carbon dioxide permeation flux through each membrane. The carbon dioxide permeation error in the permeate gas caused by seal leaks were corrected by measuring the presence of nitrogen in the sweep gas and subtracting the corresponding carbon dioxide from the calculated carbon dioxide permeation flux. The error in determining the carbon dioxide permeation flux using this procedure is approximately ±10%. Table 4.1 summarizes the feed and sweep gas streams and experimental conditions for the atmospheric and high pressure permeation experiments. The flow rates of the feed and sweep were somewhat different for the atmospheric and high pressure permeation tests due to the use of different permeation setups.

Table 4.1

Conditions for atmospheric pressure and high pressure permeation experiments

Tests	Feed side pressure	CO_2% of CO_2:N_2 feed	CO_2% of sygas[1] feed	Permeation Temperature	Feed gas flow rate	Sweep Gas (1 atm)
Atmospheric pressure	Fixed at 1 atm	10-90%	Fixed at 35%	500-900°C	100 ml/min	Ar, 100 ml/min
High Pressure	1-5 atm	Fixed at 50%	Fixed at 35%	Fixed at 700°C	50 ml/min	He, 50 ml/min

Syngas: composition of 50% CO, 35% CO_2, 10% H_2, 5% N_2

4.3 Results and Discussion

4.3.1 Membrane synthesis and permeation properties

Figure 4.2 shows the XRD patterns of SDC powder after calcination, fresh SDC supports, and the feed and sweep sides of a SDC-carbonate membrane after high pressure testing. The XRD patterns of each support tested show the presence of a fully developed fluorite phase without the presence of secondary phases. It is found that the minimum sintering temperature of 950^{o}C is sufficient to achieve the desired structure. The porous SDC supports sintered at 1100^{o}C are of 20 mm in diameter and 1.5 mm in thickness, and have a helium permeance of 10^{-6} mol/m^2/s/Pa at room temperature. The porosity and average pore diameter of the SDC supports are 36% and around 400 nm as measured by the liquid nitrogen and steady state helium permeation method, respectively.

The supports were infiltrated with molten carbonate at 550^{o}C. Figure 4.3 shows SEM images of a SDC support before and after infiltration with molten carbonate. Open pores observed in Figure 4.3a are no longer visible in Figure 4.3b. Infiltrated SDC-carbonate membranes show a dense structure with no visible void space. As shown in Figure 4.2, XRD peaks of dual-phase membranes are consistent with SDC, indicating that it is chemically compatible with molten carbonate during infiltration and after high temperature exposure. Molten carbonate peaks are not prominent due to its lower relative intensity when compared to the ceramic phase.

After cooling the membranes to room temperature, helium permeance testing was used to confirm the dense nature of the membranes. SDC-carbonate dual-phase

membranes show a decrease in helium permeance by four orders of magnitude from 10^{-6} to 10^{-10} mol/m^2/s/Pa when compared to porous supports, confirming complete infiltration of the support pores. EDX analysis of infiltrated supports also indicates the presence of molten carbonate throughout the entire membrane cross-section. The low helium permeance beyond that equipment detection limit (10^{-10} mol/m^2/s/Pa) for the SDC-carbonate membrane indicates the hermetic nature of the dual-phase SDC-carbonate membranes. Thus, gases other than CO_2 have negligible permeance for the dual-phase membranes.

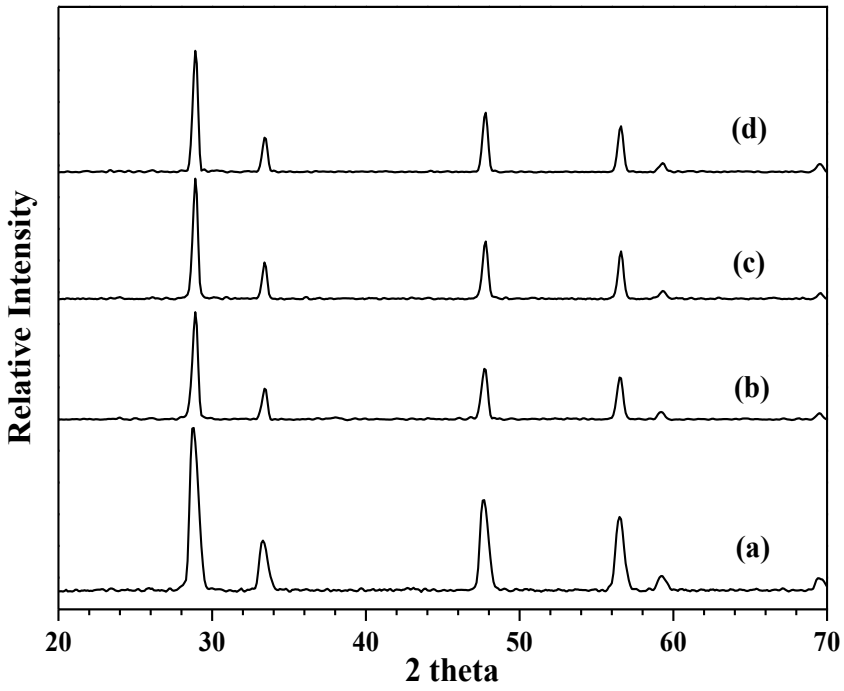

Figure 4.2 XRD patterns of (a) SDC powders and porous SDC support; (b) fresh SDC-MC membrane; (c) feed and (d) sweep sides of SDC-MC membrane after high pressure permeation test at 5 atm and exposure to 50:50 CO_2:N_2 feed at 700^{o}C

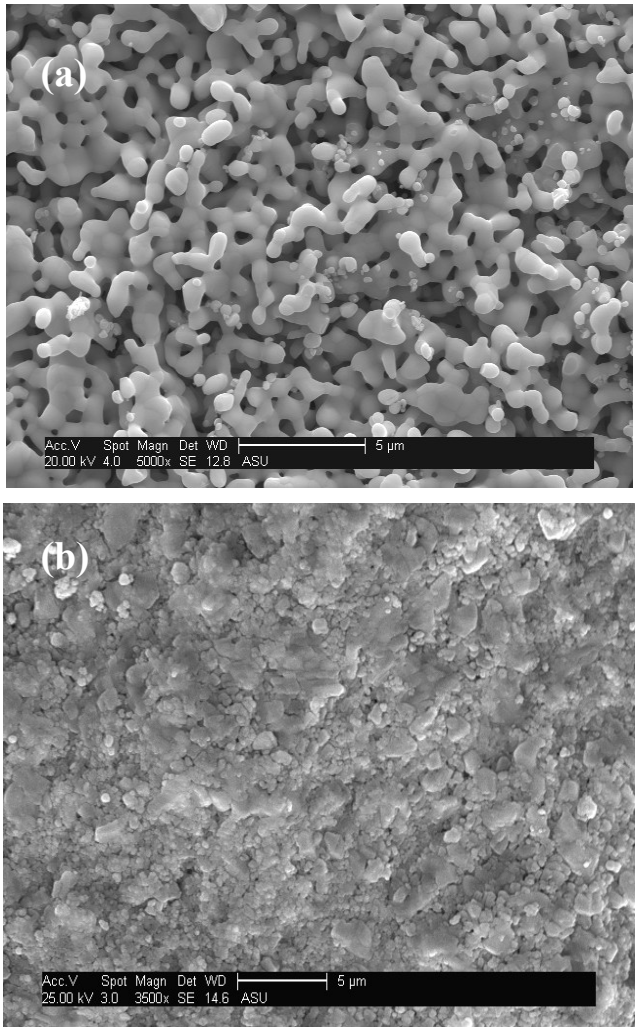

Figure 4.3 SEM images of cross section of SDC support (a) before infiltration and (b) after infiltration with molten carbonate

4.3.2 Carbon dioxide permeation and stability with CO_2:N_2 feed

Figure 4.4 shows temperature dependence on CO_2 permeation flux through SDC-carbonate membranes. The original data includes CO_2 partial pressure measured in the sweep gas, and is tabulated in Tables 4.2. At 900^oC the CO_2 permeation flux is about 5.9×10^{-3} mol/s/m^2 at the feed CO_2 partial pressure of 1 atm. The CO_2 permeation flux shows exponential dependence to increasing temperature, as shown by the linear

behavior of the Arrhenius plot in Figure 4a, resulting in an apparent activation energy of 63 kJ/mol.

Table 4.2

CO_2 permeation data for SDC-carbonate membrane at different permeation temperatures with atmospheric pressure equal molar CO_2:N_2 feed (P_{CO2}'=0.5 atm)

Temp. (^oC)	P_{CO2}"(atm)	J_{CO2} (10^{-3} mol/s/m^2)	σ_c (S/cm)	σ_i (S/cm)
700	0.0036	1.26	1.83	0.017
750	0.0054	2.01	2.21	0.028
800	0.0077	2.98	2.62	0.046
850	0.0099	3.87	3.06	0.071
900	0.0127	5.06	3.52	0.107
950	0.0160	6.40	4.01	0.155

σ_c, Carbonate conductivity, from [Janz et al., 1979]

σ_i, Oxygen ionic conductivity for SDC, from [Mori et al., 2004]

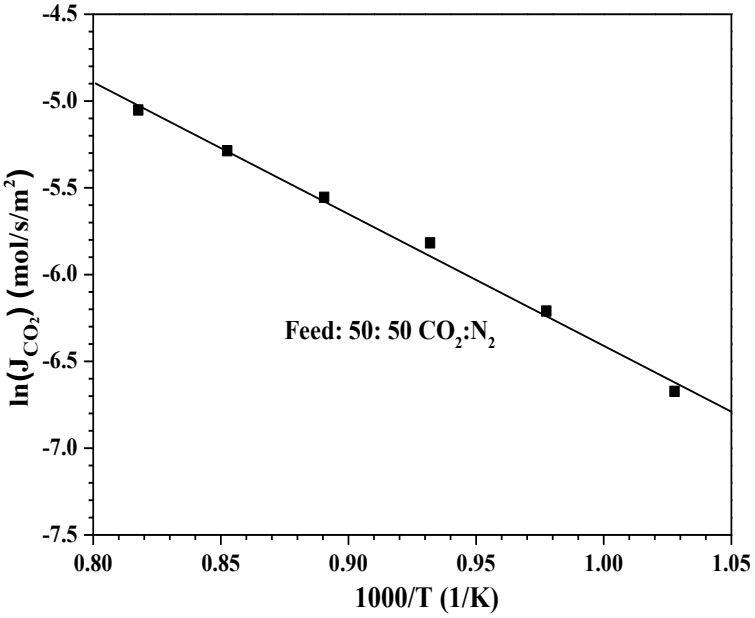

Figure 4.4 Temperature dependence on CO_2 permeation flux through SDC-carbonate dual-phase membrane

Previous experimental studies have demonstrated a CO_2 permeance that is at least two orders of magnitude greater than other gases present in the feed gas [Anderson & Lin, 2010, Norton et al., 2014]. Based on the transport mechanism in the ceramic-carbonate membranes [Anderson & Lin, 2010, Rui et al., 2012], the dense dual-phase membrane is only permeable to CO_2. Any detectible feed gas in the permeate stream, other than CO_2, results from a membrane defect or seal leak. The concentration of N_2 in the permeate stream is roughly 50-65 ppm in the entire temperature range tested resulted in a very similar CO_2:N_2 selectivity on the order of 100. During one particular experiment with a 50: 50 CO_2: N_2 feed at atmospheric feed pressure, the CO_2/N_2 separate factor was determined to be more than 1000. Therefore, it is assumed that a defect or imperfect sealing is the limiting factor in maximizing the measured CO_2 selectivity over other feed gases.

Rui et al. [Rui et al., 2009] reported the following flux equation for CO_2 permeation through ceramic-carbonate membranes at high temperature based on driving forces provided by the oxygen ion conducting phase of the ceramic support as well as the carbonate ion conducting phase of the molten carbonate phase:

$$J_{CO_2} = \int_{P"_{CO_2}}^{P'_{CO_2}} \frac{kRT}{4F^2L} dlnP_{CO2} \tag{4.1}$$

where k is a permeance coefficient (or referred to as total conductance) defined by [Ortiz-Landeros et al., 2013]:

$$k = \frac{\left(\frac{\varepsilon}{\tau}\right)_p \sigma_c \left(\frac{\varepsilon}{\tau}\right)_s \sigma_i}{\left(\frac{\varepsilon}{\tau}\right)_p \sigma_c + \left(\frac{\varepsilon}{\tau}\right)_s \sigma_i} \quad (4.2)$$

and R is the ideal gas constant, T is the system temperature, F is Faraday's constant, L is the membrane thickness, P'_{CO2} and P''_{CO2} are the feed and sweep CO_2 partial pressures, respectively, ε and τ denote the porosity and tortuosity of either the molten carbonate phase which occupies the ceramic support pore (p) or the solid ceramic phase (s). Under most conditions, $\sigma_c >> \sigma_i$, then $k \sim \left(\frac{\varepsilon}{\tau}\right)_s \sigma_i$ and the total conductance is equal to the effective oxygen ionic conductivity of the ceramic phase. Assuming k is independent of P_{CO2}, integration of Equation 4.1 gives to [Dong et al., 2013, Norton et al., 2014]:

$$J_{CO_2} = \frac{kRT}{4F^2L} ln\left(\frac{P'_{CO_2}}{P''_{CO_2}}\right) \quad (4.3)$$

Figure 4.5a plots CO_2 flux data for 700°C or 900°C as J_{CO2} versus $ln\left(\frac{P''_{CO_2}}{P'_{CO_2}}\right)$ and gives two straight lines. The original data for plot is tabulated in Table 4.3. However, both straight lines deviate far from origin of the J_{CO2} versus $ln\left(\frac{P''_{CO_2}}{P'_{CO_2}}\right)$ coordinate. Similar results were obtained for CO_2 permeation data of $La_{0.6}Sr_{0.4}Co_{0.8}Fe_{0.2}O_{3-\delta}$ (LSCF)-carbonate membrane [Norton et al., 2014]. These suggest that Equation 4.3 does not describe pressure dependence of CO_2 permeation flux for the ceramic-carbonate membranes.

Oxygen ionic conductivity of an ionic or mixed-conducting ceramic is known to depend on oxygen partial pressure and the dependence can be approximated by a power function [Bouwmeester & Burggraaf, 1996, Yang & Lin, 2003]. Assuming such power function also applies to the total conductance, one has:

$$k = k^0(P_{O_2})^m \tag{4.4}$$

where k^o is the total conductance at 1 atm oxygen pressure and m is a constant which may depend on temperature. The oxygen partial can be correlated to CO_2 partial pressure by either a mass balance on impurity oxygen in CO_2 and N_2 feeds for the CO_2 and N_2 mixture or a thermodynamic equilibrium relation for the reaction CO_2=CO+1/2O_2. The relationship can be approximated by:

$$P_{O_2} = \emptyset {P_{CO_2}}^q \tag{4.5}$$

where φ and q are constants for Equation 4.5. Inserting Equations 4.4 and 4.5 into Equation 4.1 and integrating with respect to P_{O_2} and then changing P_{O_2} to P_{CO_2} using Equation 4.5 yields:

$$J_{CO_2} = \frac{k'RT}{4F^2L}[{P'_{CO_2}}^n - {P''_{CO_2}}^n] \tag{4.6}$$

where n=m·q, and k' is modified total conductance at 1 atm oxygen partial pressure, i.e., $k'=k^o\varphi^m/n$. Plots of the J_{CO2} versus $(P'_{CO2}{}^n - P''_{CO2}{}^n)$ are given in in Figure 4.6b, and as shown, they exhibit two straight lines going through the origin of the coordinate, confirming that Equation 4.6 describes well the CO_2 pressure dependence of the CO_2 permeation flux through the SDC-carbonate membrane. The value of n is 0.125 and 0.5 for flux versus CO_2 pressure data at 900°C and 700°C respectively. The slope of the corresponding straight lines in Figure 4.6b at 900°C and 700°C is 0.0147 and 0.002 $mol/s/m^2/atm^n$, respectively. According to Equation 4.6, the slope is proportional to (k^oT), which increases with temperature.

The CO_2 permeation flux shows exponential dependence to increasing temperature, as shown by the linear behavior of the Arrhenius plot in Figure 4.5b, resulting in an apparent activation energy of 63 kJ/mol. At 700-950^oC the carbon dioxide ionic conductivity in the molten carbonate phase ranges from 1.83 to 4.01 S/cm (see Table 4.2) [Janz et al., 1979], much larger than the oxygen ionic conductivity for SDC (0.017-0.155 S/cm). With SDC porosity of about 0.36, the much larger carbonate conductivity than the oxygen ionic conductivity would result in the rate-limiting step of CO_2 permeation through the SDC-carbonate membrane by oxygen ionic conduction in the SDC phase, as shown by Equation 4.2. The activation energy for oxygen ionic conduction for SDC ranges from 60 to 74 kJ/mol, depending on the particle morphology [Mori et al., 2004]. The activation energy for CO_2 permeation flux of the SDC-carbonate membrane (kJ/mol) is within this range. Furthermore, the ratio of the slope of the straight line in Figure 4b at 900^oC to that at 700^oC is about 7.3, similar to the ratio of the oxygen ionic conductivity for SDC times temperature ($\sigma_i \cdot T$) at these two temperatures (7.6). These results confirm that CO_2 permeation is mostly controlled by the oxygen conductivity of the ceramic phase of the dual-phase membrane.

The CO_2 permeation data for our SDC-carbonate membranes is about 50% of that of the SDC-carbonate membrane made on SDC of similar porosity reported [Zhang et al., 2012] (~3×10^{-3} mol/s/m^2 at 700^oC for membrane B in that work). The activation energy of our membrane is also slightly lower than that of Zhang et al. (74-80 kJ/mol).

Considering that the SDC-carbonate membrane prepared by Zhang et al. by a different method has very different microstructure and their permeation experiments were run under different conditions (feed gas, etc.) from membranes reported here, one can conclude the SDC-carbonate membranes prepared by these two research groups have similar CO_2 permeation characteristics.

Table 4.3

CO_2 permeation data for SDC-carbonate membrane at different CO_2 pressure gradients

Atmospheric Pressure Feed at 900°C			High Pressure Feed at 700°C		
P_{CO_2}' (atm)	P_{CO_2}" (atm)	CO_2 flux (10^{-3} mol/s/m^2)	P_{CO_2}' (atm)	P_{CO_2}" (atm)	CO_2 Flux (10^{-3} mol/s/m^2)
0.1	0.007	2.90	0.5	0.0024	1.26
0.25	0.010	4.09	1.0	0.0037	1.93
0.5	0.012	5.13	1.5	0.0046	2.53
0.75	0.014	5.65	2.0	0.0054	2.90
0.9	0.014	5.88	2.5	0.0058	3.21

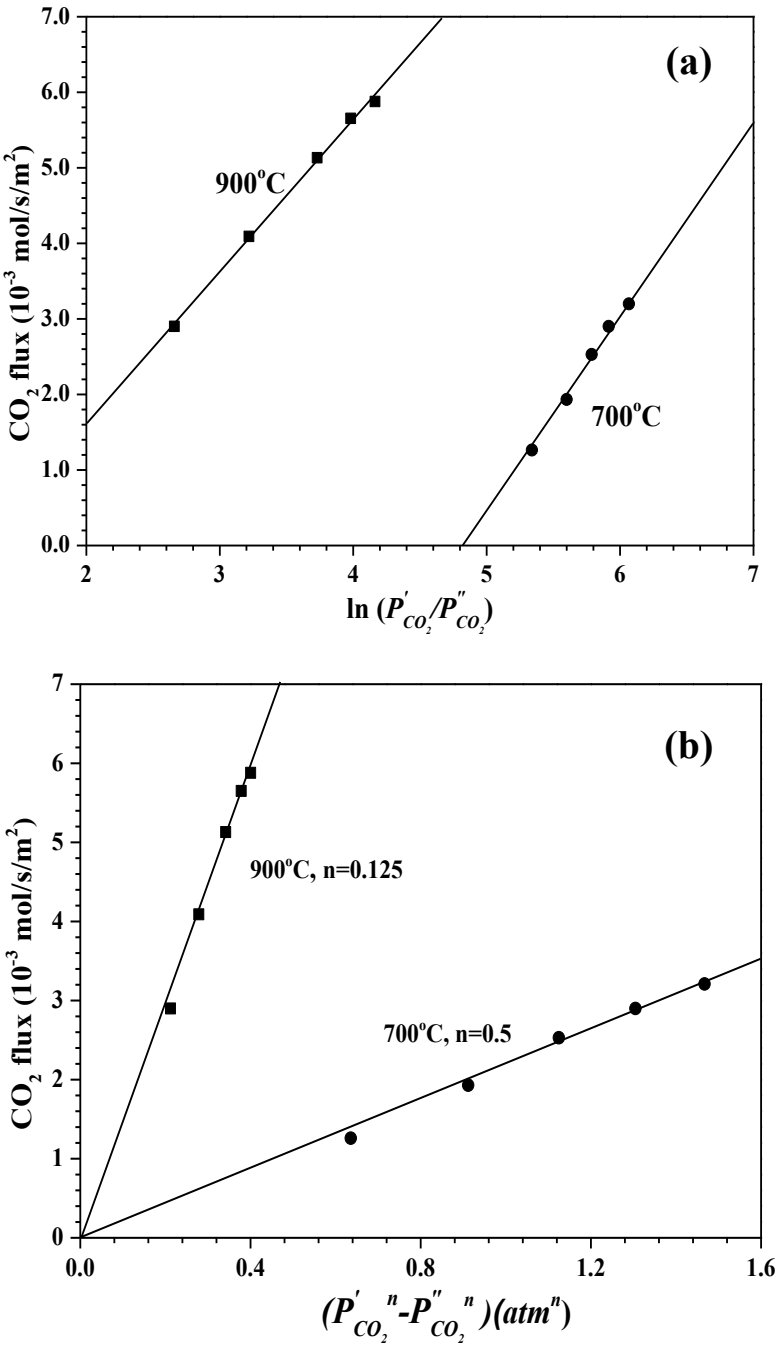

Figure 4.5 CO_2 permeation flux through SDC-carbonate dual-phase membrane versus (a) logarithmic CO_2 partial pressure gradient $ln\left(\frac{P"CO_2}{P'CO_2}\right)$ and (b) $(P'_{CO_2}{}^{n} - P"_{CO_2}{}^{n})$ with CO_2:N_2 feed (Data in at 900°C were obtained with atmospheric pressure, and at 700°C with high pressure)

The CO_2 permeation stability of SDC-carbonate membranes was examined with both atmospheric and high pressure CO_2: N_2 feeds and are shown in Figure 4.6. The membrane tested at 700°C was exposed to a 2.5 atm CO_2 partial pressure with a total feed pressure of 5 atm. The membrane exhibits steady-state CO_2 permeation of approximately 2.91×10^{-3} mol/s/m^2 for more than 80 hours. The membrane tested at 900°C was exposed to atmospheric pressure and a 0.5 atm CO_2 partial pressure and exhibits remarkably stable permeation behavior for two full weeks of testing with a high CO_2 permeation flux between 5.06-5.51$\times10^{-3}$ mol/s/m^2 for more than 330 hours of exposure.

Of the previous studies on the permeation stability of the dual-phase membrane, only LCGFA-carbonate membranes have been shown to maintain chemical and permeation stability after long term exposure to a high CO_2 concentration feed gas without the presence of O_2 [Norton et al., 2014]. The oxygen permeation flux for SDC-carbonate membranes, however, is roughly 30 times higher than that measured for LCGFA-carbonate at 900°C, due to the increased ionic conductivity of the ceramic phase of the membrane. LSCF-carbonate membranes showed long-term permeation stability, however, the presence of O_2 was required to maintain the structural integrity of the ceramic phase [Norton et al., 2014]. Without the presence of O_2, the ceramic phase rapidly decomposes into oxide and carbonate phases on the membrane surfaces, resulting in a substantial drop in CO_2 flux. $Bi_{1.5}Y_{0.3}Sm_{0.2}O_{3-\delta}$ (BYS)-carbonate membranes have shown transient CO_2 permeation behavior for the first 50 hours of testing at 700°C due to

a change in ceramic support structure before reaching steady-state for the remainder of the study [Lu & Lin, 2013].

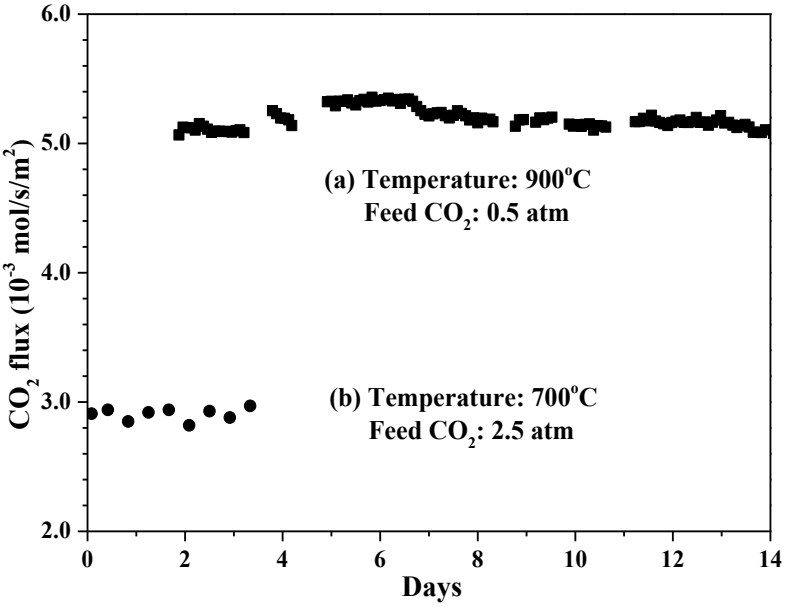

Figure 4.6 Time dependence of CO_2 permeation flux of SDC-carbonate membrane: (a) at 900°C (atmospheric pressure CO_2: N_2 feed) and (b) at 700°C (high pressure CO_2:N_2)

Figure 4.7 shows SEM images of the cross-section, feed, and sweep side of the SDC-carbonate membrane after high pressure testing at 700°C. The membrane maintains its dense nature as shown in Figure 4.7a. Figures 4.7b and 4.7c show that both surfaces of the membrane remain dense and crack-free after nearly 100 hours of exposure to a 4 atm total pressure gradient. Also of importance is that there is no obvious residual carbonate layer on the membrane surface. Therefore, the capillary force of the molten carbonate in the ceramic support is enough to withstand the pressure gradient across the membrane. After testing, membranes were removed from the custom-made permeation cell and maintained their structural integrity and showed no signs of fracture.

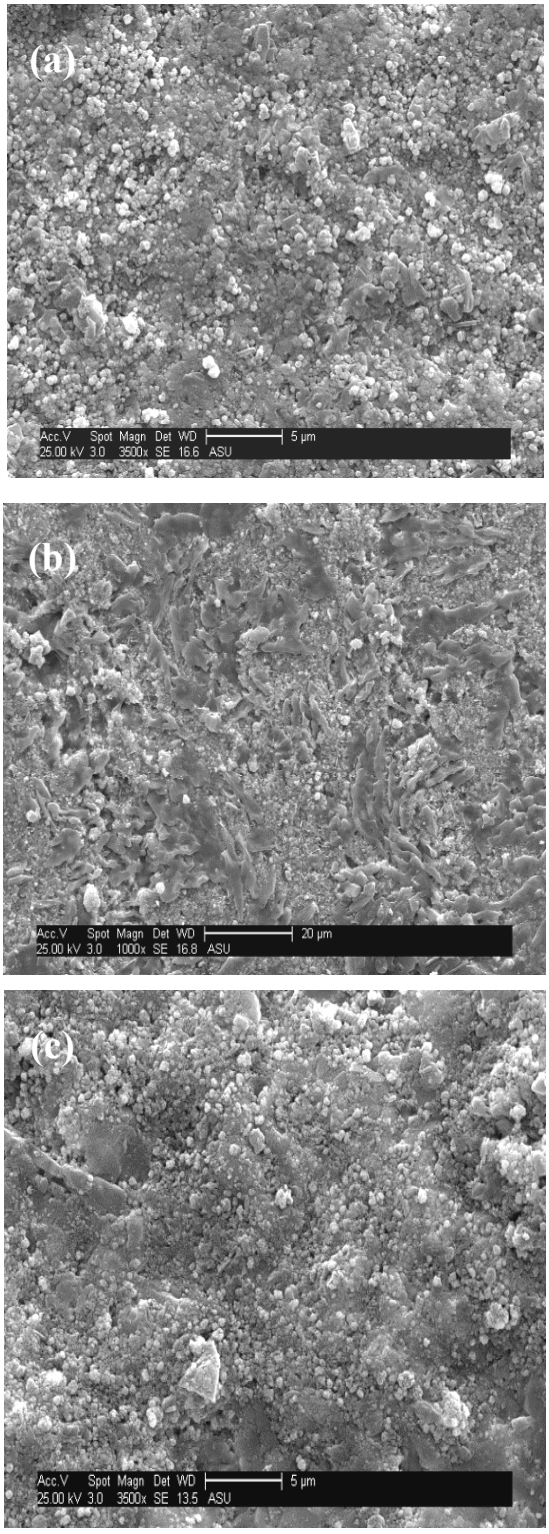

Figure 4.7 SEM images of SDC-carbonate membrane surfaces after high pressure permeation test with CO_2:N_2 feed: (a) cross-section, (b) feed side, and (c) permeate side

4.3.3 Carbon Dioxide Permeation and Stability with Simulated Syngas Feed

In addition to verifying tolerance in varying CO_2 environments, it is important to demonstrate whether dual-phase membranes are able to withstand harsh conditions in order to serve as a potential alternative for pre-combustion CO_2 capture. Figure 4.8a shows the effect of temperature on the CO_2 permeation flux of a SDC-carbonate membrane exposed to simulated syngas (composition 50% CO, 35% CO_2, 10% H_2, 5% N_2) in the temperature range of 500-900^oC as well as the effect of total pressure by applying a 1-5 atm feed pressure of the same composition. A CO_2 permeation flux of 0.68 and 5.11×10^{-3} mol/s/m^2 was measured at 500 and 900^oC, respectively, at a feed CO_2 partial pressure of 0.5 atm. As shown by the Arrhenius plot, the membrane exhibits an exponential dependence to increasing temperature for the entire temperature range in question, resulting in a measured apparent activation energy of 54 kJ/mol.

At 700^oC, a similar dependence to CO_2 pressure gradient across the membrane is observed as previously shown in Figure 4.5b. As the CO_2 partial pressure across the membrane increases, Equation 4.6 also describes well the permeation data with syngas feed with constant n=0.5. The slope of the straight line in Figure 4.8b is 0.29, slightly higher than the value achieved with CO_2: N_2 feed (slope is 0.27). Such difference could indicate an effect of the presence of reducing gases (CO and H_2) in the feed on oxygen ionic conductivity of SDC. However, considering about 10% error in measuring CO_2 permeation flux, such effects are negligible.

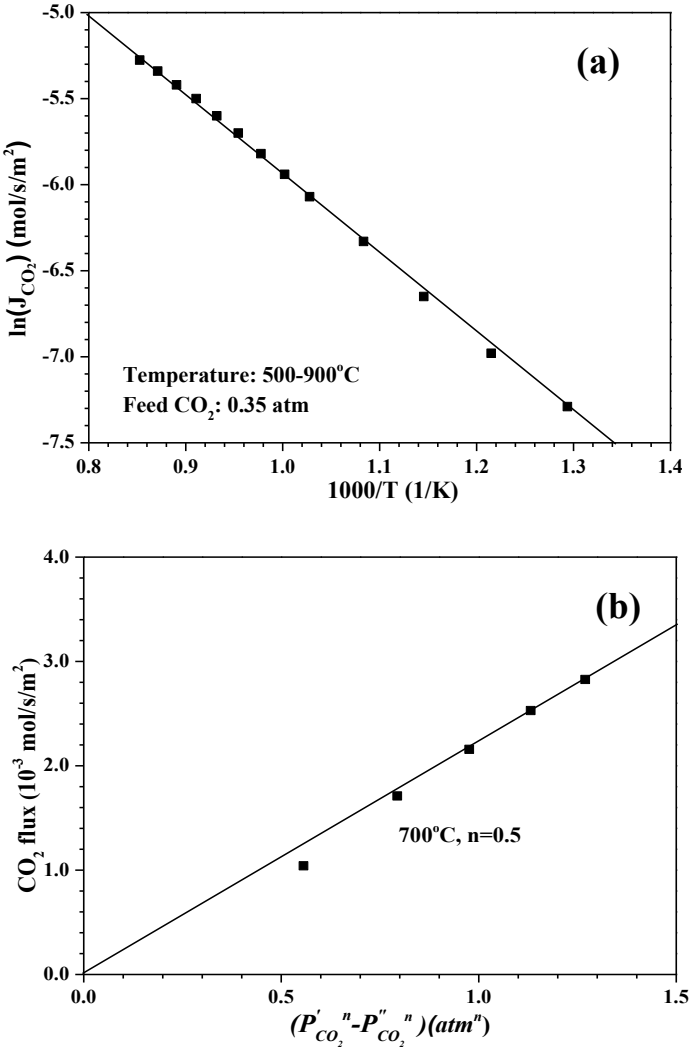

Figure 4.8 Effect of (a) temperature and (b) trans-membrane CO_2 partial pressure gradient on CO_2 permeation flux of SDC-carbonate membranes under high pressure permeation conditions with simulated syngas feed

Figure 4.9 shows the long-term stability of the membrane exposed to simulated syngas at 700°C at atmospheric and elevated system pressures. The CO_2 permeation stability of SDC-carbonate exposed to atmospheric pressure was examined under steady state conditions for more than 30 days. The permeation flux varies throughout the study,

ranging from 1.93-2.6×10^{-3} mol/s/m^2 before stabilizing at approximately 2.31×10^{-3} mol/s/m^2 for the last 10 days of the study. Membranes exposed to a total feed pressure of 5 atm reach a higher permeation flux of over 3×10^{-3} mol/s/m^2 after 5 days of exposure. Previously, LCGFA-carbonate membranes have shown chemical stability after 24 hours of exposure to simulated syngas, but this is the first reported permeation stability data in reducing conditions [Norton et al., 2014]. Zhang et al. [Zhang et al., 2012] reported CO_2 permeation data for SDC-carbonate exposed to H_2, but observed rapid decomposition likely resulting from decomposition of the molten carbonate phase at high temperature.

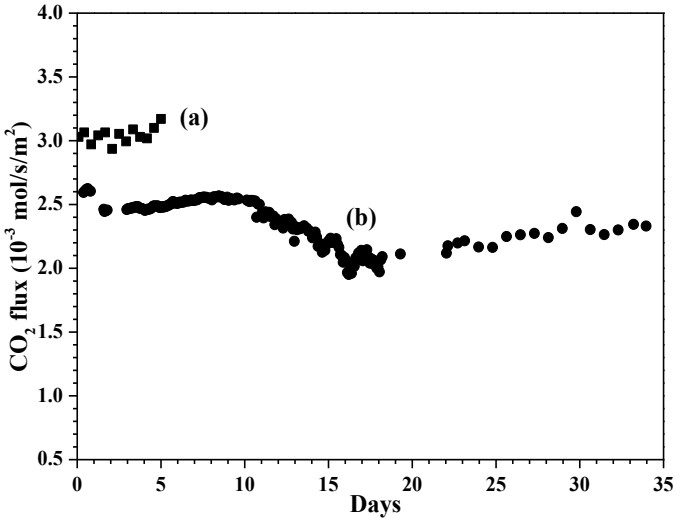

Figure 4.9 Time dependence of CO_2 permeation flux of SDC-carbonate membrane with simulated syngas feed at 700°C: (a) high pressure feed at total feed pressure of 5 atm and P'_{CO2}=1.8 atm, (b) atmospheric pressure feed with P'_{CO2}=0.35 atm

Figure 4.10 shows XRD patterns of the surfaces of two SDC-carbonate membranes after permeation with simulated syngas at 700°C for 35 days. As shown, the sweep side

of both membranes maintains the pure fluorite structure. After long-term exposure to simulated syngas, a decrease in 2 theta for the (111) and (222) peaks is now observed indicating increase in the lattice parameters of the SDC crystals. This is likely resulting from formation of more oxygen vacancy in solid SDC after long-term exposure to low oxygen partial pressure atmosphere. Increase of oxygen vacancy concentration leads to increment of lattice parameters of SDC crystals [Zolochevsky et al., 2012]. Also on the feed side of the membrane, there is also the presence of Sm_2O_3 peaks, which results from decomposition of the fluorite structure on the immediate membrane surface after long term exposure to H_2-containing environments. This decomposition would explain the transient behavior of the long-term permeation flux shown in Figure 4.9.

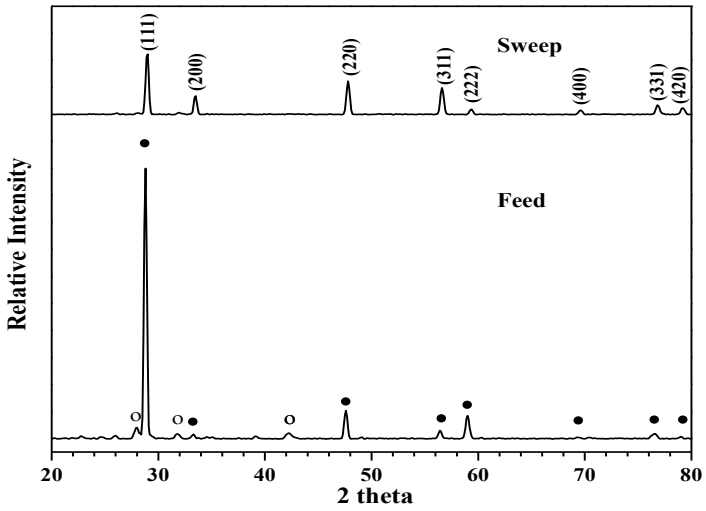

Figure 4.10 XRD patterns of the feed and sweep side of: SDC-carbonate membrane after 36 day atmospheric pressure permeation experiments with simulated syngas feed at 700°C, (peak identification: • = fluorite, ° = Sm_2O_3 phase).

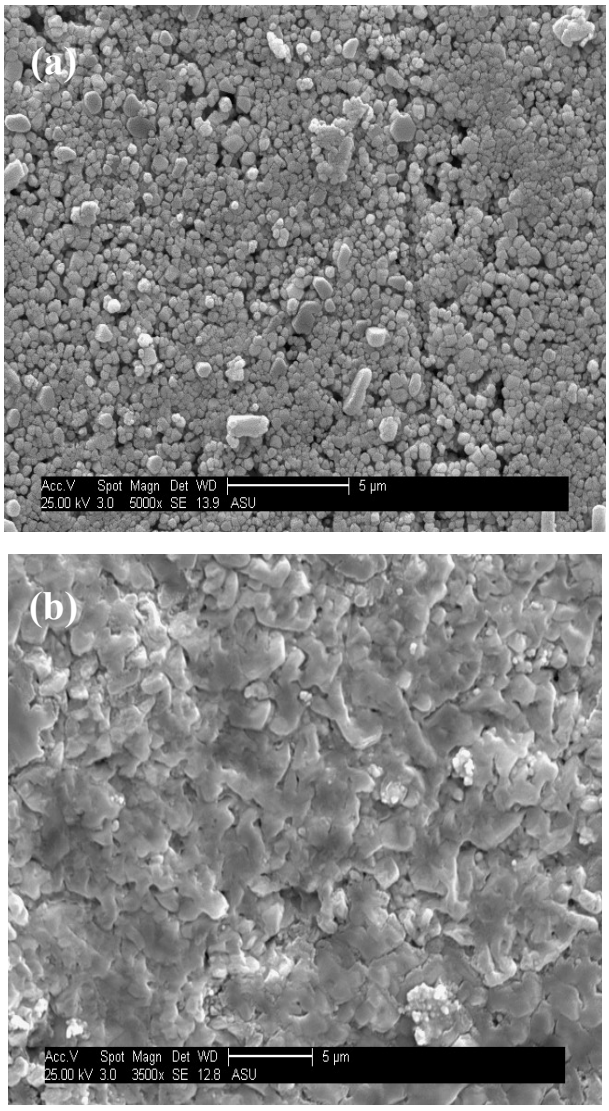

Figure 4.11 SEM images of SDC-carbonate membrane after 6 day permeation test with simulated syngas feed at 700^{o}C (total feed pressure of 5 atm and P'$_{CO2}$=1.8 atm), (a) feed side exposure to syngas; (b) cross section

Figure 4.11 shows SEM images of feed side exposed to syngas and cross section of SDC-MC membrane after the test. Compared to the membrane tested in CO_2 and N_2 as shown in Figure 4.7, feed side of the membrane becomes porous as shown in Figure 4.11a. Combined with XRD pattern, it is believed that this is due to decomposition of

ceramic solid phase in H_2. In Figure 4.11b cross section of the membrane exhibits a dense structure. All the carbonates are held in support pores. Decomposition of the membrane is only limited to the surface exposed to H_2 containing atmosphere. While the membrane shows signs of decomposition into metal oxide phases after long-term exposure, the SDC-carbonate membrane maintained long-term stability in both permeation flux and selectivity after more than one month of exposure to H_2-containing simulated syngas at 700^oC. The results show that the bulk part of the membrane remained in the hermetic SDC-carbonate dual-phase structure allowing selective transport of only CO_2.

4.4 Conclusions

Hermetic ceramic-carbonate dual-phase membranes made of ionic conducting porous samarium doped ceria (SDC) and a Li/Na/K molten carbonate mixture can be prepared by the direct infiltration method. The SDC-carbonate membranes exhibit highly selective CO_2 permeation flux with logarithmic dependence on CO_2 pressure gradient and exponential dependence on temperature. The activation energy for CO_2 permeation of the SDC-carbonate membrane is close to that for oxygen ionic conduction in SDC, confirming rate-controlling of oxygen ionic conduction in CO_2 permeation in the dual-phase membrane. CO_2 permeation characteristics of the SDC-carbonate membrane with CO_2: N_2 feed is the same as that with simulated syngas feed. The results show that the presence of other gases in the feed does not affect CO_2 permeation properties of the

membranes. The SDC-carbonate dual-phase membranes exhibit stable CO_2 permeation with CO_2: N_2 mixture or simulated syngas feed at pressure ranging from 1 to 5 atm for various testing periods of time as along as up to 35 days. SDC-carbonate dual-phase membrane exhibit both high CO_2 flux and long-term stability. The next chapter aims to synthesize thin dual-phase membrane derived from SDC.

CHAPTER 5

ASYMMETRIC THIN SAMARIUM DOPED CERIUM OXIDE-CARBONATE DUAL-PHASE MEMBRANE FOR CARBON DIOXIDE SEPARATION

5.1 Introduction

A new concept of dual-phase (metal-carbonate) membranes perm-selective to CO_2 at high temperature was first reported by Lin and coworkers [Chung et al., 2005]. The metal-carbonate dual-phase membranes were synthesized with stainless steel [Chung et al., 2005] and silver [Xu et al., 2012]. However, the membranes either suffer a stability problem due to reaction between metal phase and molten carbonates at high temperature or require removal of oxygen from the permeate products. To improve the membrane stability and allow the membrane permeating CO_2 without O_2, Lin and coworkers [Anderson & Lin, 2010] prepared ceramic-carbonate dual-phase membranes by replacing the metal support with ionic conducting or mixed-conducting metal oxide ceramics. Dual-phase membranes using various mixed or oxygen ionic conducting porous supports have been prepared by several research groups [Wade et al., 2011, Rui et al, 2012, Zhang et al., 2012].

In Chapter 4, CO_2 permeation properties and stability of samarium doped ceria (SDC)–carbonate dual phase membranes were studied. Ceramic-carbonate dual-phase membranes using $La_{0.6}Sr_{0.4}Co_{0.8}Fe_{0.2}O_{3-\delta}$ (LSCF) [Anderson & Lin, 2010], $Bi_{1.5}Y_{0.3}Sm_{0.2}O_{3-\delta}$ (BYS) [Rui et al., 2012], $La_{0.85}Ce_{0.1}Ga_{0.3}Fe_{0.65}Al_{0.05}O_{3-\delta}$ (LCGFA)

[Norton et al., 2014] and SDC [Norton et al., 2014] as ceramic supports were successfully synthesized in our lab. CO_2 permeation fluxes of these membranes are plotted in Figure 5.1 and permeation properties are summarized in Table 5.1.

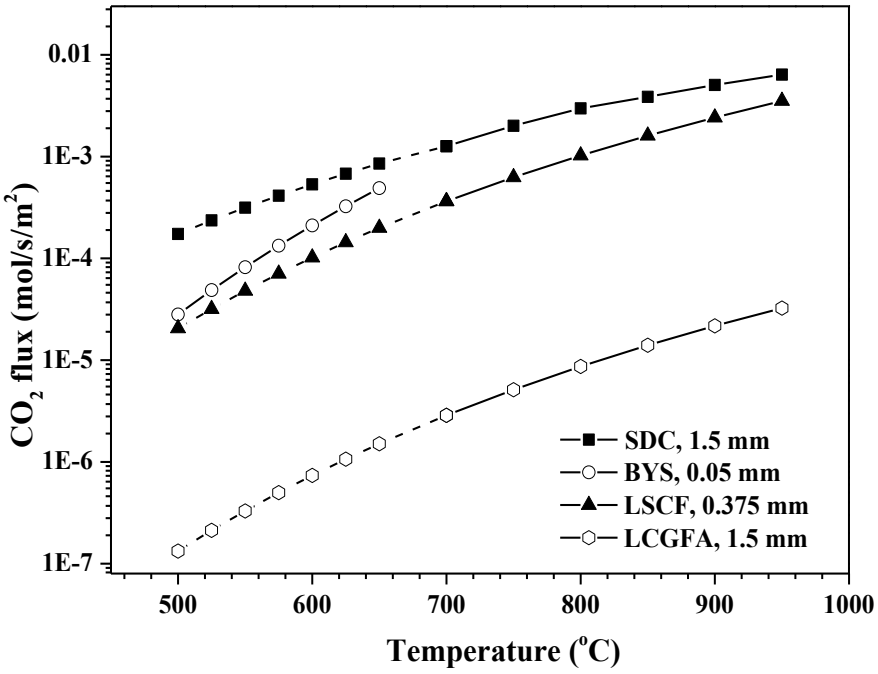

Figure 5.1 CO_2 permeation fluxes of ceramic-carbonate dual-phase membranes of the lab, data in dash are estimated from Ea, P'_{CO_2}=0.5atm (CO_2: N_2 feed), F_{He}=100 ml/min

Table 5.1

CO_2 permeation properties of ceramic carbonate dual-phase membranes

Ceramic	Thickness (mm)	Temp. (°C)	CO_2 flux (10^{-3} mol/s/m^2)	Stability	σ_i (S/cm)	Ref.
SDC	1.5	950	6.41	~330 h	0.155	Norton et al., 2014
BYS	~0.05	650	0.49	~ 50 h	0.137	Rui et al, 2012
LSCF	0.375	900	2.42	50-60 h	0.173	Anderson & Lin, 2010
LCGFA	1.5	900	0.156-0.18	~275 h	0.002	Norton et al., 2014

SDC-carbonate dual-phase membrane exhibits the best performance considering both CO_2 flux and stability. Reducing membrane thickness could effectively increase CO_2 permeation flux. To improve thin dual-phase membrane, it is important to study methods to prepare thin SDC-carbonate membranes on proper support base. The basic requirements for such base support are that (1) it should be porous providing minimum mass transport resistance, (2) it should be oxygen ionic conducting so support-carbonate plug, if formed, would not provide much transport resistance for CO_2, (3) it should not wet carbonate to avoid infiltration of carbonate into the base support, and (4) it should be compatible with the porous SDC top-layer. Following the work of Chapter 3, supported thin SDC-carbonate dual-phase membrane would be prepared on macroporous, oxygen ionic conducting, carbonate non-wettable base as shown in Figure 5.2.

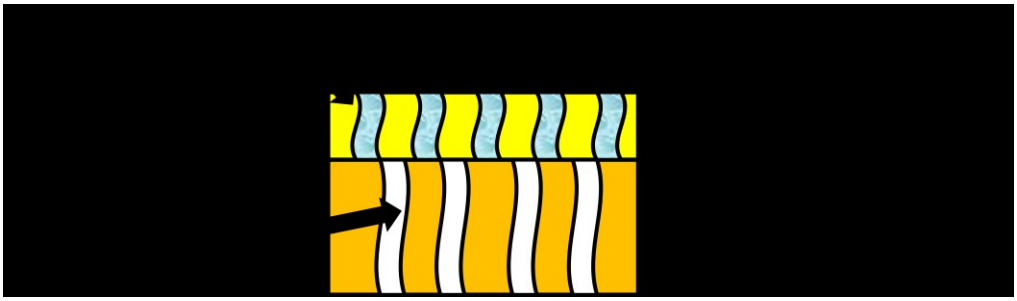

Figure 5.2 Schematic configuration of thin SDC-carbonate dual-phase membrane

The work examined the use of thin SDC layers prepared by dip-coating or co-pressing strategies on macroporous BYS or SDC/BYS base supports for synthesis of thin SDC-carbonate membranes and studied the properties of thin SDC-carbonate membranes on these supports. Objective of Chapter 5 is to present synthesis and

characterization of supported thin SDC-carbonate dual-phase membranes. High temperature gas permeation properties of the membranes are studied as well.

5.2 Experimental

5.2.1 Membrane synthesis

5.2.1.1 Powders and porous supports

Powders of $Bi_{1.5}Y_{0.3}Sm_{0.2}O_{3-\delta}$ (BYS) and $Ce_{0.8}Sm_{0.2}O_{1.9}$ (SDC) were prepared by the citrate method [Rui et al., 2012, Norton et al., 2014]. Stoichiometric amounts of the corresponding metal nitrates, i.e., $Bi(NO_3)_3 \cdot 5H_2O$ (98%, Sigma-Aldrich), $Y(NO_3)_3 \cdot 6H_2O$ (99.9%, Sigma-Aldrich), $Ce(NO_3)_3 \cdot 6H_2O$ (99.5%, Alfa-Aesar) and $Sm(NO_3)_3 \cdot 6H_2O$ (99.9%, Sigma-Aldrich), were fully dissolved in a dilute nitric acid solution (10 vol% of concentrated HNO_3), followed by addition of anhydrous citric acid (99.5%, Alfa Aesar). The solutions were heated to 90–110°C forming sticky gel-like solid and performed a fast and uniform self-ignition of the organics at 400°C. After self-ignition, both powders were further calcined at 900°C for 6 hours.

Macroporous disks of BYS, SDC or SDC/BYS were prepared by placing about 3.5 g of powder of BYS, SDC or mixture of SDC/BYS, with addition of about 5 wt% graphite (Alfa Aesar, APS 7-11 micron), in a stainless steel mold (22 mm in diameter), and pressed at 200 MP for 5 min. The green disks of BYS, SDC or SDC/BYS were then respectively sintered at 750^{o}C, 1100^{o}C and 950^{o}C for 24 hrs. Addition of graphite powders will ensure that the support base contains macro-pores.

5.2.1.2 Supported thin SDC layers on porous supports

To make support with structure shown in Figure 5.2, supported thin SDC layers were prepared from suspension coating or co-pressing strategies. SDC suspension was made according to the method described in Chapter 2 and 3. SDC powders (made from citric method), mixed with dilute nitric acid (pH= 3-4) at a weight ratio of 1:2, were ball milled in polyethylene (PE) pots with ZrO_2 balls for 5-7 days. After the ball-milling process, the SDC suspension was diluted to 5 wt% and 10 wt% by adding more nitric acid. PH of the suspensions was adjusted to 10-12. SDC suspensions were dip-coated on porous BYS supports. PVA was used as drying control chemical additive (DCCA) to prevent crack formation on the membranes during the drying step. The amount of PVA solution added into the suspensions was determined to be at a volume ratio of 3:20 (15 vol%) and 1:4 (25 vol%). The dip-coated disks were dried in air at a relative humidity (RH) of 50%-60% and a temperature of 40°C for 24 hrs. After drying, the membranes were sintered in air at 750°C for 6 h with a heating and cooling rate of 1°C/min. For co-pressing method, about 0.2-0.3 g of SDC powders ball-milled for 72 hrs (to reduce particle size) was packed into the stainless steel mold and pressed under a hydraulic pressure of 5 MP for 10 s. Then about 3.5 g BYS powders without ball-milling, with addition of 5 wt% graphite, was added on top of the SDC layer with a pressure of 150 MP for 5 min, as shown in steps 1-4 in Figure 5.3. The green body was removed from the mold and sintered at 950^{o}C for 20 hrs with ramping rate of 1^{o}C/min.

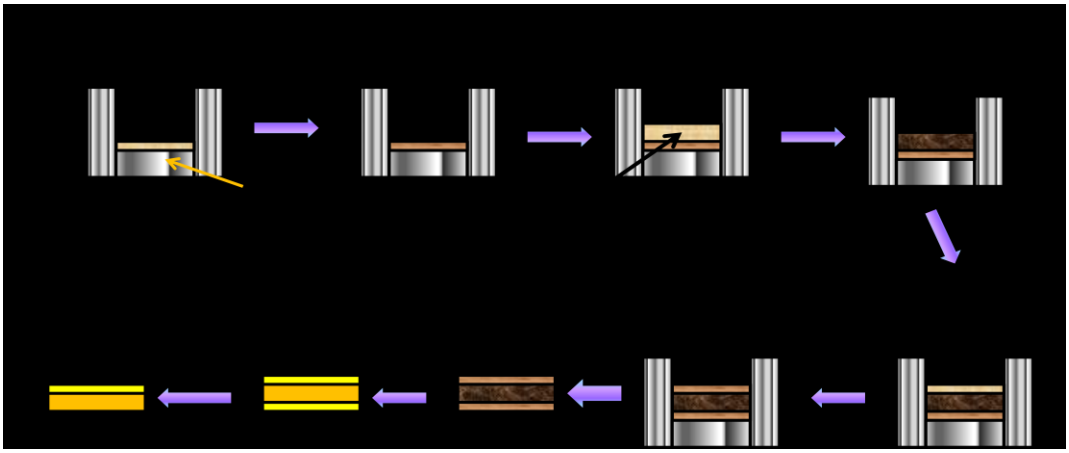

Figure 5.3 Schematic drawing of preparation of thin SDC layers on SDC/BYS supports by co-pressing method.

Asymmetric porous supports consisting of thick, macroporous SDC/BYS support sandwiched by two thin SDC layers (to balance sintering stress) were prepared by similar method shown in Figure 5.3. After formation of SDC and SDC/BYS layers in the mold (step 4 in Figure 5.3), 0.2-0.3 g ball-milled SDC powders were again added on the top and all three layers were uniaxially pressed under a pressure of 200 MP for 5 min. Asymmetric porous supports with a three-layer sandwich structure were achieved. The green body was removed from the mold, and sintered at 950°C for 20 hrs with heating and cooling rate of 60°C per hour. One side of SDC layer was then polished off by a SiC paper (Struers, #800) to obtain the support with structure shown in Figure 5.2. All the disks prepared are about 20 mm in diameter and about 2 mm in thickness.

5.2.1.3 Supported thin SDC-carbonate dual-phase membranes

Thin dual-phase membrane was obtained via a direct infiltration of molten carbonates into the top SDC layer of asymmetric porous support [Chung et al., 2005].

Lithium (Li), sodium (Na), and potassium (K) carbonates (Fisher Scientific, Li_2CO_3, 99.2%; Na_2CO_3, 99.9%; K_2CO_3, 99.8%) were mixed in 42.5/32.5/25 mole percent ratio and heated to 550°C in a box furnace. Before infiltration, the asymmetric support was preheated in the furnace for 30 minutes above the molten carbonate and then was dipped, with SDC layer facing down, into the molten carbonate. The support was held in contact with molten carbonate for 20 minutes to allow the molten carbonate to infiltrate into the thin porous SDC top-layer via capillary action. A continuous carbonate layer covered on the surface of the SDC support, and was removed by the "sponge" soaking method reported in Chapter 3. Finally membrane was cooled down to room temperature at a rate of 1°C/min. As-synthesized thin SDC-carbonate dual-phase membrane is denoted as thin SDC-MC.

5.2.2 Membrane characterization and high temperature CO_2 permeation measurements

Helium permeances of porous supports were measured by the unsteady state permeation method. The porosity of the base supports was obtained by the liquid nitrogen method [Harry & Johnson, 2004]. The sizes of the supports before and after sintering were measured by a caliper. Molten carbonate wettability of SDC/BYS supports was checked by observing molten carbonate liquid drops on the supports at 600°C. Phase structure of powders, supports and dual-phase membranes were determined by X-ray diffraction (XRD) (Bruker AXS, D8 Focus Diffractometer, CuKα). The morphology of the membranes was examined by scanning electron microscopy

(SEM, Phillips, FEI XL-30). High temperature CO_2 permeation tests were carried out in a home-made permeation set-up as shown in Figure 3.2. The thin dual-phase membrane was sealed with graphite seals in the middle of a high temperature cell. CO_2 (50 ml/min, STP) and N_2 (50 ml/min, STP) were introduced to the feed side, and He (100 ml/min, STP) to the downstream as sweep gas during the heating and permeation measurements. Before heating the system, inert gases of N_2 (50 ml/min, STP) to the feed side and He (50 ml/min, STP) to the sweep side were introduced for 20 min to eliminate oxygen in the membrane cell and protect the graphite seals from decomposition.

The system was heated at a rate of 1°C/min to 550°C. After allowing the system to remain at 550°C for 2 h reaching steady state, data collection began. Measurements were taken in 25°C (1°C/min ramp) increments, starting from 550°C and upward to 700°C. Once reaching the desired temperature, the system was kept at that temperature for one hour before data collection. Membrane long term stability was tested by measuring CO_2 permeation at 700^{o}C for over 100 hrs. The gas composition in the sweep gas was measured by a HP 5890 Series II gas chromatograph with a TCD detector with an Alltech Hayesep DB 100/120 column of 30'×1/8"×0.85" SS. The amount of N_2 detected in the sweep gas during permeation experiments allowed determination of CO_2 leak through the seal. Corrected CO_2 flux was made by subtracting the CO_2 associated with the leak. Gas leakage through the membrane or the seal is assumed to follow the Knudsen diffusion mechanism. Leaking nitrogen flux was around 3-5 % of that total

amount of CO_2 measured. For each condition, we measured 2 to 3 data. The errors of the data are within 10%.

5.3 Results and discussion

5.3.1 Membrane synthesis

5.3.1.1 Asymmetric porous supports

Figure 5.4 shows XRD patterns of ceramic powders of BYS and SDC after sintering at 900°C. XRD patterns of the powders of BYS and SDC are of cubic fluorite structure, consistent with previous studies [Rui et al., 2012, Zhang et al., 2012].

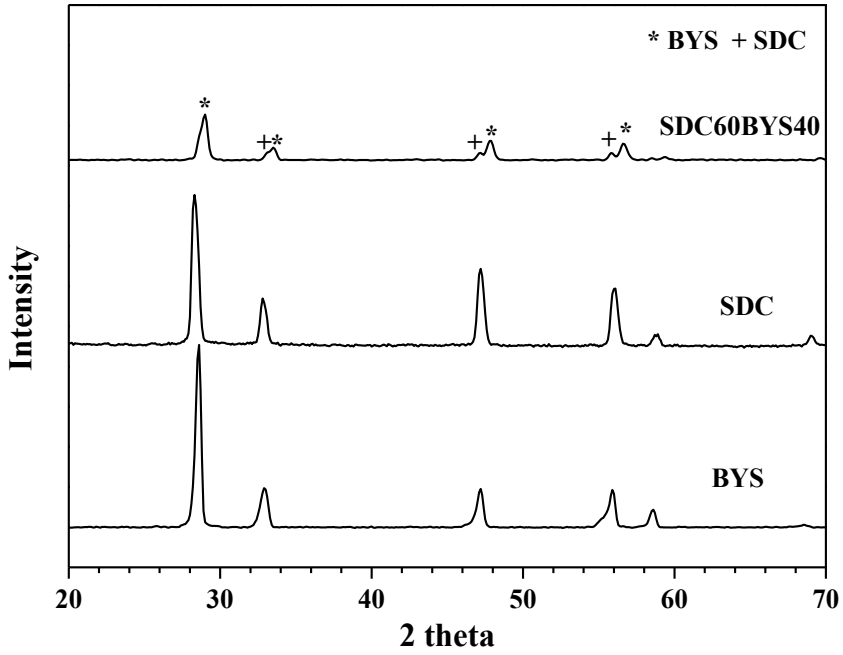

Fig. 5.4 XRD patterns of powders of BYS and SDC after sintering at 900°C and composite SDC60BYS40 support after sintering at 950°C

Asymmetric porous supports were originally prepared by dip-coating SDC suspension on porous BYS supports. Thin SDC layer derived from 10 wt% suspension

always peeled off just after drying process while membranes prepared from 5 wt% suspension were of good quality and went through calcination process. Big concentration suspension produced a thicker dip-coated layer. A larger stress will be developed during drying and cause peeling off issue [Lu & Lin, 2011]. Figure 5.5 shows the morphologies of SDC membranes made of 5 wt% suspensions on BYS base:

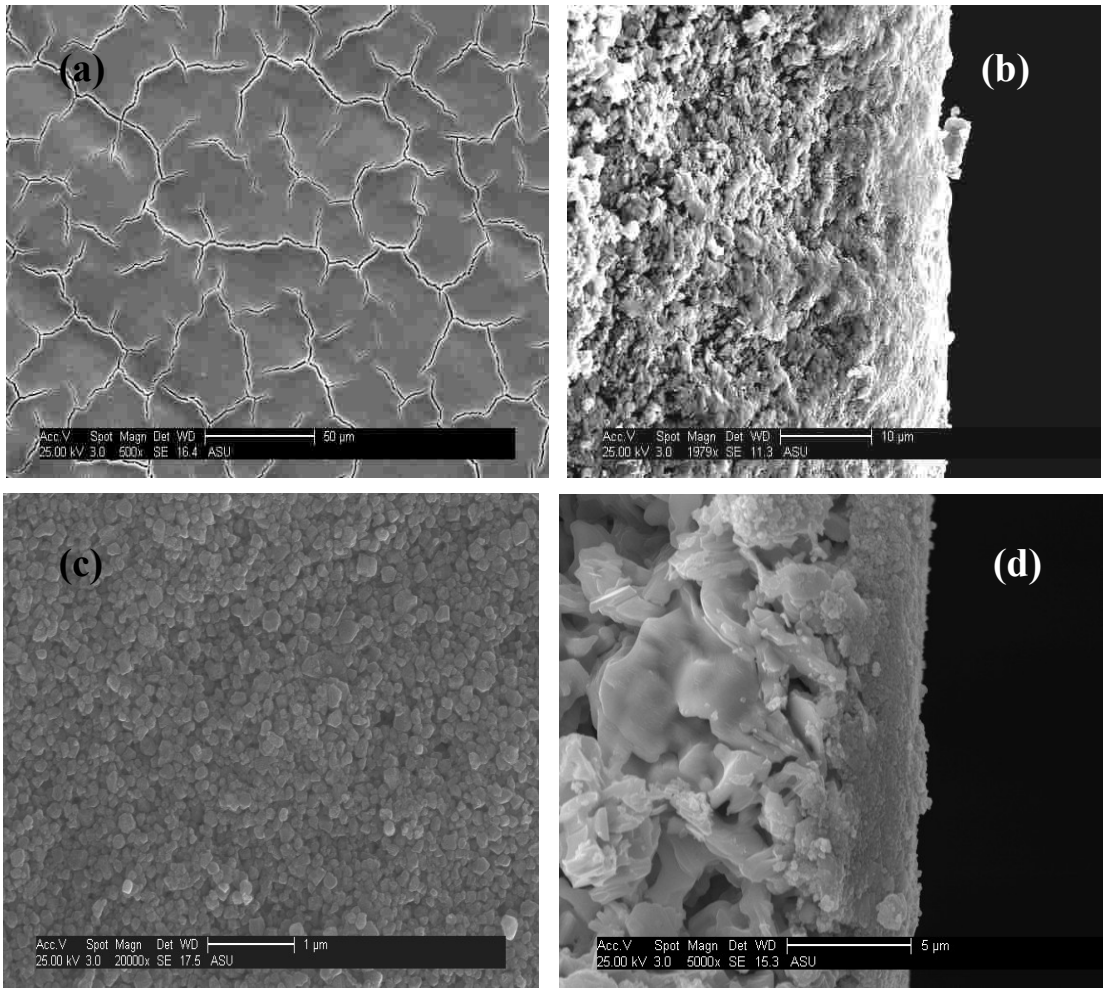

Figure 5.5 Scanning electron microscopy (SEM) images of SDC membranes on BYS supports prepared from suspension with 25 vol% PVA: (a) surface morphology, (b) cross section and with 15 vol% PVA: (c) surface morphology, (d) cross section

Cracks are observed on surface of the membrane prepared from the suspension with more PVA (Figure 5.5a). Thin SDC membrane obtained from suspension using 15 vol% PVA as DCCA is defect free and of good quality as shown in Figure 5.5c and 5.5d. The layer is around 5 μm thick. The PVA molecules tend to form big aggregates in the suspension. More PVA tends to leave larger space after sintering and causes defect formation. Asymmetric porous support derived from 5 wt% suspension coating was denoted as t-SDC/BYS.

Asymmetric porous supports containing one thin SDC layer and a thick BYS support were also prepared by co-pressing a thin SDC layer directly on pure BYS base support followed by sintering. However, the support was seriously warped after sintering at 950^{o}C, as shown in Figure 5.6. BYS and SDC have different sintering-ability as reflected by their different melting point of 1100^{o}C for BYS [Zeng & Lin, 2001] and 2200^{o}C for SDC [Zhang et al., 2012]. Thus, sintering at 950^{o}C results in more shrinkage in BYS than SDC and causes the warp towards BYS side.

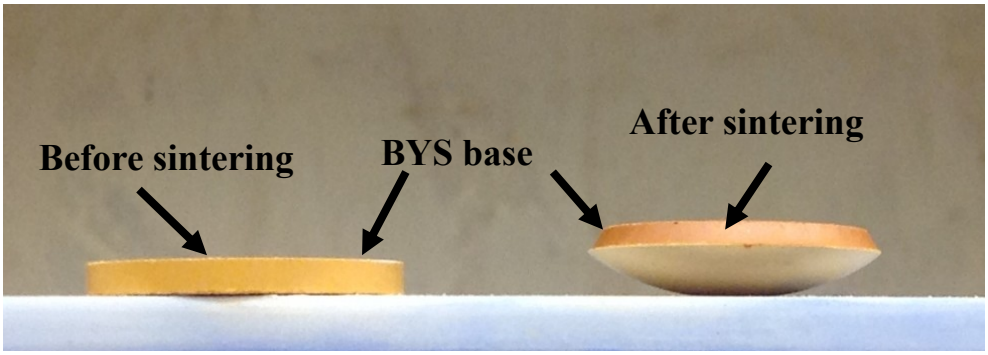

Figure 5.6 Morphology of the thin SDC top-layer prepared on pure BYS support before and after sintering (BYS is facing up).

To overcome the issue, SDC powder was mixed with BYS to prepare SDC/BYS base support. In this way, addition of SDC in the base support helps elevate its sintering temperature and ensure better sintering comparability with the top thin SDC layer. SDC/BYS base supports with SDC ranging from 20, 40 and 60 vol%, denoted as SDC20BYS80, SDC40BYS60 and SDC60BYS20, were prepared. The characteristics of the BYS/SDC supports are summarized in Table 5.2. Helium permeances and porosities of SDC/BYS supports with different mixing ratio are plotted in Figure 5.7. Pure BYS and SDC supports are also included as comparison.

SDC60BYS40 exhibits the highest permeance and porosity and it could provide minimum gas transport resistance through the membrane. As shown in Table 5.2, morphology change (disk diameter) of SDC60BYS40 after sintering is almost same as that of pure SDC support. Addition of SDC powders in BYS same as the solid phase improve sintering compatibility between base support and top layer. As shown in Figure 5.4, SDC60BYS40 shows a XRD pattern that combines the characteristic patterns of pure BYS and SDC and no impurities are observed. This indicates that BYS and SDC in the support are present as separate phases and the powder mixtures are chemically stable after high temperature sintering.

To examine molten carbonate wettability to the supports, Figure 5.8 show porous support disks holding carbonate solid powder at room temperature (Figure 5.8a) and after heat-treatment in air at 600 °C (Figure 5.8b). Compared with Figure 5.8a, clear liquid

drop of melting carbonates can be observed on top of BYS support and no residuals are found on SDC support. The BYS is carbonate non-wettable [Rui et al., 2012] and SDC is carbonate wettable [Norton et al., 2014]. Melting carbonate droplets are observed on SDC60BYS40 support exhibits its carbonate non-wettability. Although molten carbonate is wettable to SDC, existence of non-wettable BYS powder apparently modifies the surface property of the support. The support pores become carbonate non-wettable and avoid being filled by molten carbonate during infiltration. High permeance, carbonate non-wettable SDC60BYS40 was chosen as the base support for thin dual-phase membrane. Crack free and flat asymmetric porous supports consisting of SDC60BYS40 sandwiched by two macroporous SDC layers were obtained after sintering. The support is denoted as SDC-SDC60BYS40. Helium permeance of the asymmetric support is around 10-15% lower than that of base support due to resistance offered by the thin layers.

Table 5.2

Characteristics of SDC/BYS supports

Support	D of green disk (mm)	D after sintering (mm)	He Permeance (10^{-6} mol/s/m^2/Pa)	ε	Carbonate wettability
Pure BYS	22	18	0.001	5%	Non-wettable
SDC20BYS80	22	18.9	0.15	28%	Non-wettable
SDC40BYS60	22	20	1.48	40%	Non-wettable
SDC60BYS40	22	21.2	8.81	46%	Non-wettable
Pure SDC	22	21.3	8.55	45%	Wettable

D, Diameter; ε, porosity

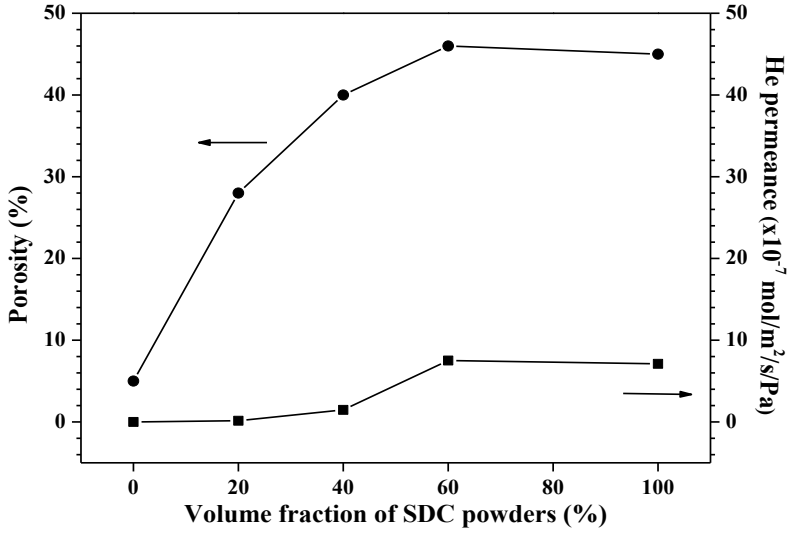

Figure 5.7 Porosity and helium permeance dependence on volume fraction of SDC powders in SDC/BYS support

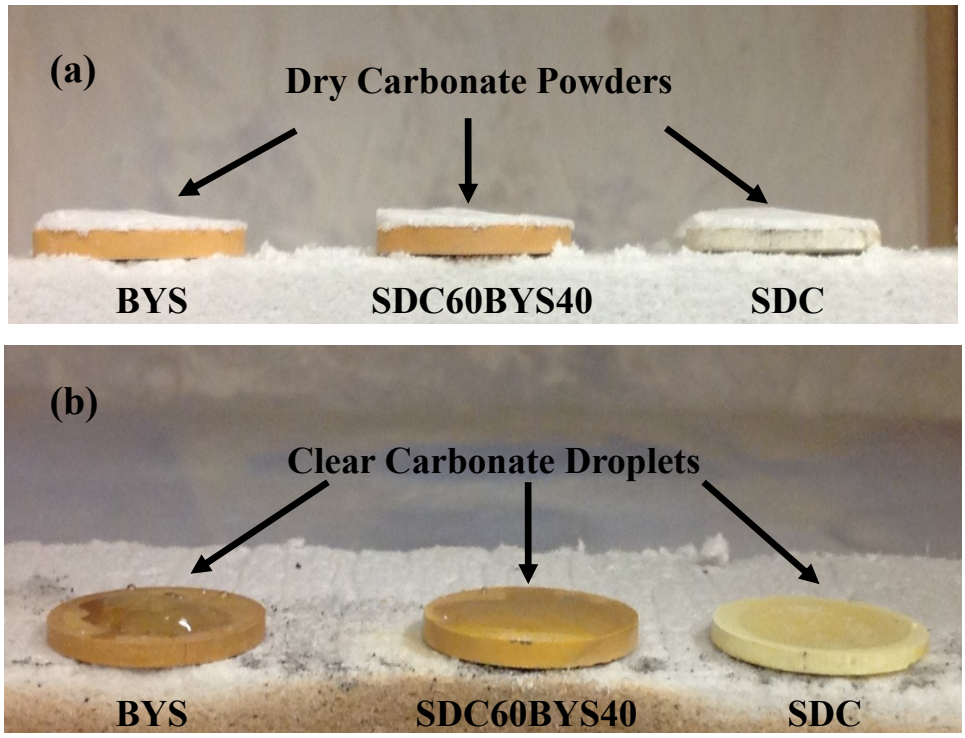

Figure 5.8 Examination of molten carbonates wettability on the various BYS, SDC60BYS40 and SDC supports (a) dry carbonate powders on top of the supports at room temperature and (b) same supports heated and staying at 600 ℃

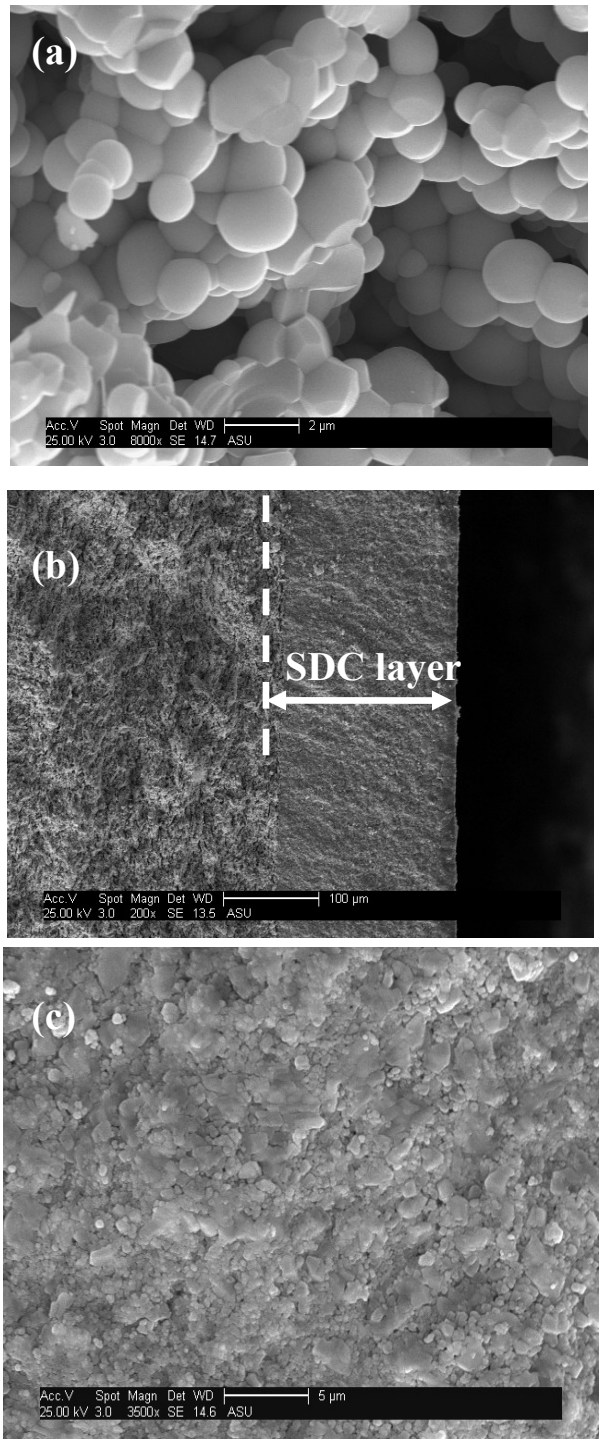

Figure 5.9 SEM images of: (a) surface, (b) cross section of thin SDC layer about 150 µm thick co-pressed on SDC60BYS40 support and (c) cross-section of the SDC layer after molten carbonate infiltration.

Figure 5.9a shows the SEM image of surface morphology of macroporous SDC membrane on SDC60BYS40 base support. The membrane is homogenous and of good quality. The thin membrane demonstrates the similar morphology as that of thick SDC membrane presented in Chapter 4. Figure 5.9b presents cross section of thin SDC membrane on the support. The thickness of the top layer is around 150 μm. The support is flat and not warped as shown in Figure 5.6. Addition of SDC in base support successfully improves sintering comparability of two layers. No cracks are observed between the top SDC layer and SDC60BYS40 base support.

5.3.1.2 Thin SDC-carbonate dual-phase membranes

The thin dual-phase membranes were prepared by directly infiltrating the molten carbonate into the asymmetric support. Carbonate residual layer formed after infiltration was removed by the method previously reported in Chapter 3. Thin dual-phase membrane constructed with d-SDC/BYS always cracked and peeled off as shown in Figure 5.10. The possible reason is that sintering temperature of the membrane is low and causes weak mechanical affinity of thin SDC membrane to BYS base. After infiltration, the stress developed during cooling might crack and peel SDC top layer. Increase sintering temperature will condense BYS support [Zeng & Lin, 2001]. Lower porosity hence a smaller capillary force [Chung et al., 2005] makes forming thin SDC membrane via suspension coating unfeasible.

Figure 5.9c shows the morphology of the cross section of the top layer of SDC-SDC60BYS40 support after infiltration. The support pores are dense and completely filled with molten carbonate. Thin membrane exhibits 4 orders of magnitude reduction in helium permeance compared to the support before carbonate infiltration. A dense thin SDC-MC membrane was successfully prepared on SDC60BYS40 and denoted as d-SDC/SDC60BYS40

Figure 5.10 Image of thin SDC-carbonate dual-phase membrane peeled from BYS support after infiltraion

5.3.2 High temperature CO_2 permeation tests

Table 5.3 summarizes experimental parameters for the high temperature permeation tests for d-SDC/SDC60BYS40. Figure 5.11a shows temperature dependence on CO_2 flux. The measurements were done in the temperature range of 550-700^oC with 25^oC intervals and helium flow rate was fixed at 100 ml/min. CO_2 permeation flux increases from 1.33 to 6.55×10^{-3} mol/s/m^2 when the temperature changes from 550^oC to 700^oC. Figure 5.11b exhibits CO_2 permeation long-term stability of thin SDC-MC membrane at 700^oC. The membrane was exposed to CO_2: N_2 (50: 50) feed with a total pressure of 1

atm. The membrane exhibits a stable CO_2 flux about 6.55×10^{-3} mol/s/m^2 for 180 hrs. The test was discontinued due to system leakage from decomposition of graphite seals. The selectivity of the membrane of CO_2 to N_2 was around 35.

Figure 5.12a and 5.12b show pressure effect on CO_2 permeation through d-SDC/SDC60BYS40 membrane. The tests were performed at 700 ^oC with a total feed pressure of 1 atm. Figure 5.12a shows feed side CO_2 partial pressure (P'_{CO_2}) effect. Sweep helium flow rate was fixed at 100 ml/min. P'_{CO_2} was adjusted by changing feed side CO_2 flow rate from 10 ml/min to 90 ml/min. CO_2 permeation flux increases from 2.45 to 9.17×10^{-3} mol/s/m^2 with upstream CO_2 partial pressure from 0.1 to 0.9 atm. Figure 5.12b exhibits sweep side CO_2 partial pressure (P''_{CO_2}) effect. Feed side CO_2 partial pressure was maintained at 0.5 atm. Different P''_{CO_2} were obtained by changing sweep side helium flow rate from 75 ml/min to 175 ml/min. CO_2 permeation flux decreases with increase of downstream CO_2 partial pressure. A smaller P''_{CO_2} (higher helium flow rate) leads to a larger CO_2 flux. In both cases, adjusting CO_2 partial pressure indeed changes trans-membrane partial pressure difference.

Table 5.3

Experimental parameters of CO_2 permeation tests for d-SDC/SDC60BYS40

Test parameters	Temp. (^oC)	P'_{CO_2} (atm)	F_{He} (ml/min)
Temperature	550-700	0.5	100
Long-term stability	700	0.5	100
P'_{CO_2}	700	0.1-0.9	100
P''_{CO_2}	700	0.5	75-175

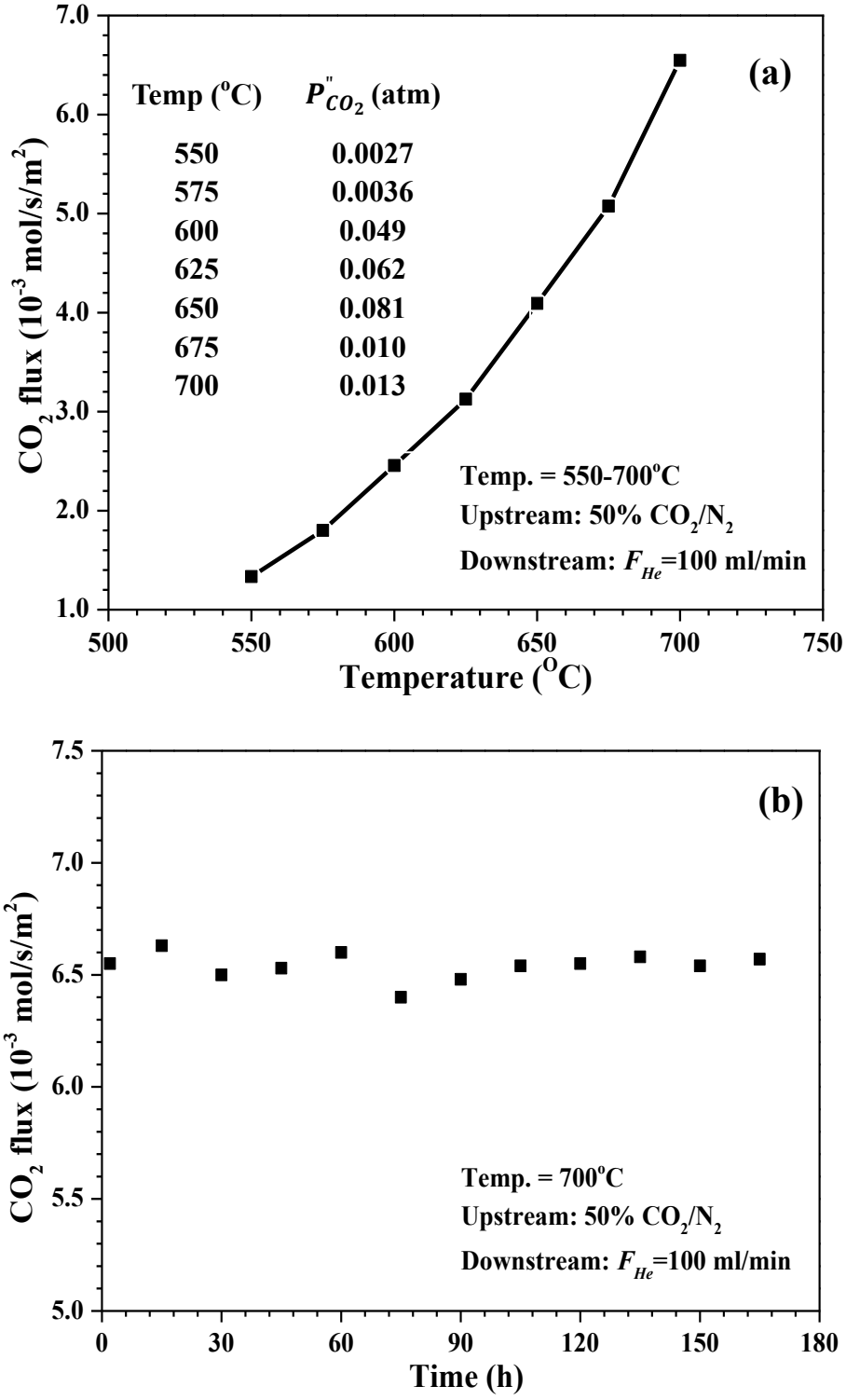

Figure 5.11 CO_2 permeation flux through d-SDC/SDC60BYS40 support as a function of: (a) temperature and (b) permeation time

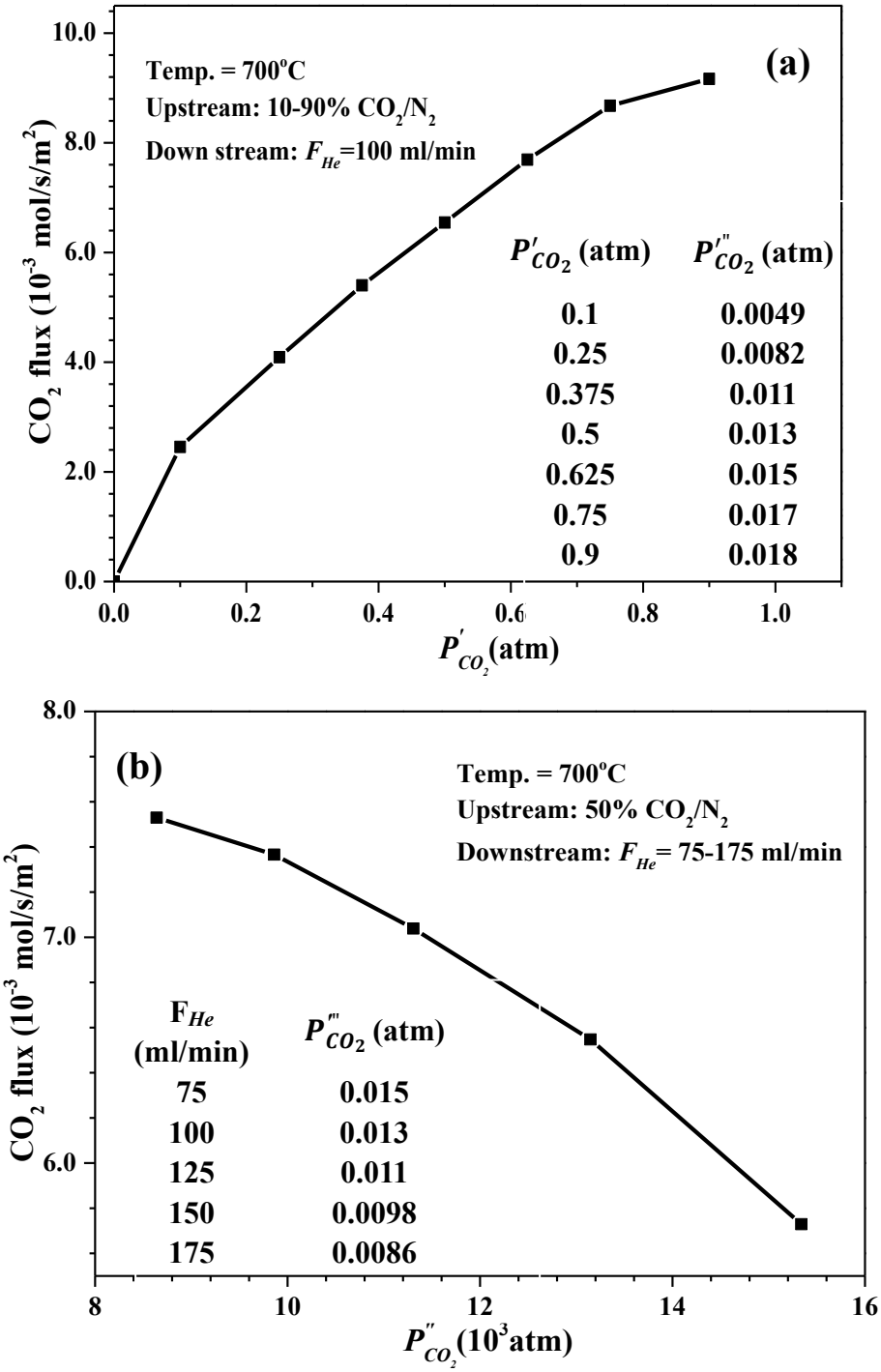

Figure 5.12 CO_2 permeation flux through d-SDC/SDC60BYS40 support as a function of: (a) feed side upstream CO_2 partial pressure, P'_{CO2} and (b) permeate side downstream CO_2 partial pressure, P''_{CO2}

Previous study [Norton et al., 2014] exhibited that CO_2 permeation flux for the dual-phase membrane could be correlated to trans-membrane CO_2 partial pressure difference by:

$$J_{CO_2} = \frac{kRT}{4F^2L}[P'_{CO_2}{}^{n} - P''_{CO_2}{}^{n}] \quad (5.1)$$

where k is a permeance coefficient (or referred to as total conductance) defined by [Ortiz-Landeros et al., 2013]

$$k = \frac{\left(\frac{\varepsilon}{\tau}\right)_p \sigma_c \left(\frac{\varepsilon}{\tau}\right)_s \sigma_i}{\left(\frac{\varepsilon}{\tau}\right)_p \sigma_c + \left(\frac{\varepsilon}{\tau}\right)_s \sigma_i} \quad (5.2)$$

and R is the ideal gas constant, T is the system temperature, F is Faraday's constant, L is the membrane thickness, P'_{CO2} and P''_{CO2} are the feed and sweep CO_2 partial pressures, respectively, ε and τ denote the porosity and tortuosity of either the molten carbonate phase which occupies the ceramic support pore (p) or the solid ceramic phase (s), n is pressure index number which is related to temperature.

Figure 5.13 plots CO_2 flux (combining data at different feed side CO_2 partial pressure and sweep side helium flow rates) versus $(P'_{CO_2}{}^{n} - P''_{CO_2}{}^{n})$ and n is equal to 0.5 at 700°C [Norton et al., 2014]. The plot gives a straight line going through the origin of the coordinate and CO_2 flux proportionally increases with $(P'_{CO_2}{}^{n} - P''_{CO_2}{}^{n})$ confirming CO_2 pressure dependence of the CO_2 permeation flux through the SDC-carbonate membrane. The slope of the corresponding straight line in Figure 5.13 is 0.011 mol/s/m^2/atm$^{0.5}$. In previous study [Norton et al., 2014], for thick SDC-carbonate dual-phase membrane tested at 700°C, the slope for line of CO_2 flux

versus pressure difference is 0.002 mol/s/m^2/atm$^{0.5}$. Carbonate ionic conductivity in the molten carbonate phase is much larger than the oxygen ionic conductivity for SDC [Norton et al., 2014]. CO_2 permeation through SDC-carbonate dual-phase membrane is majorly rate-limited by oxygen ionic conduction in the SDC phase. At given experimental conditions, CO_2 flux could be ascribed to:

$$J_{CO_2} \propto \frac{\left(\frac{\varepsilon}{\tau}\right)_s \sigma_i}{L} \cdot T \tag{5.3}$$

D-SDC/SDC60BYS40 membrane prepared in this work is 0.15 mm thick and sintered at 950^{o}C. While the thick membranes were 1.5 mm thick and sintered at 1100^{o}C [Norton et al., 2014]. Difference in membranes thickness and pore structure leads to the variation in slopes.

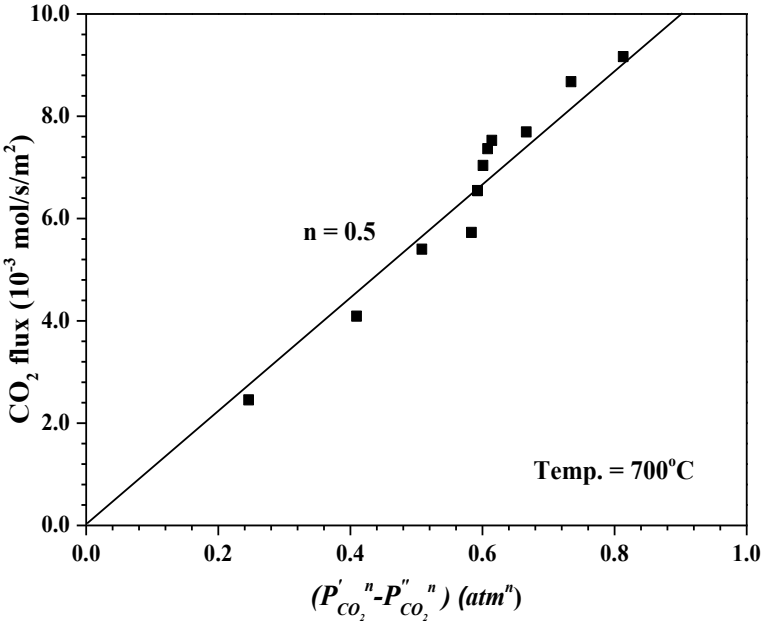

Figure 5.13 CO_2 permeation flux through SDC-carbonate dual-phase membrane versus $(P'_{CO_2}{}^{n} - P''_{CO_2}{}^{n})$

Table 5.4 compares CO_2 permeation fluxes of thin dual-phase membranes. D-SDC/SDC60BYS40 exhibits a higher CO_2 flux than d-YSZ/BYS even it has a larger thickness. Using higher ionic conductive ceramic phase effectively increases CO_2 flux of thin dual-phase membrane. D-SDC/SDC60BYS40 also possesses a better pore structure (porosity comparison) facilitating ion transport through the membrane resulting in a higher flux. [Ortiz-Landeros et al., 2013].

Table 5.4

Comparison of CO_2 flux through thin dual-phase membranes

Ceramic phase	Membrane thickness (μm)	Temp. (°C)	CO_2 flux (10^{-3} mol/s/m^2)	σ_v (S/cm)	ε	Ref.
d-SDC/SDC60BYS40	150	700	6.55	0.017	35%	This work
d-YSZ/BYS	~10	650	3.9	0.009	46%	Chapter 3

ε, porosity

Figure 5.14 compares CO_2 permeation fluxes of thin SDC-MC membrane and other SDC-based dual-phase membranes with similar open porosity of 0.36 [Zhang et al., 2012, Dong et al., 2013, Norton et al., 2014]. CO_2 permeation properties of the membranes are summarized in Table 5.5. Thin SDC-MC membrane achieves the highest CO_2 permeation flux among three disk-shape dual-phase membranes via taking advantage of reducing thickness. CO_2 permeation through dual-phase membranes is controlled by oxygen ionic transport. Smaller membrane thickness shortens ion conducting path and reduces ion transport resistance. An enhanced ionic transport is allowed in the

membrane and accelerates uptake and release of CO_2 at upstream and downstream. Therefore a higher CO_2 permeation flux will be achieved.

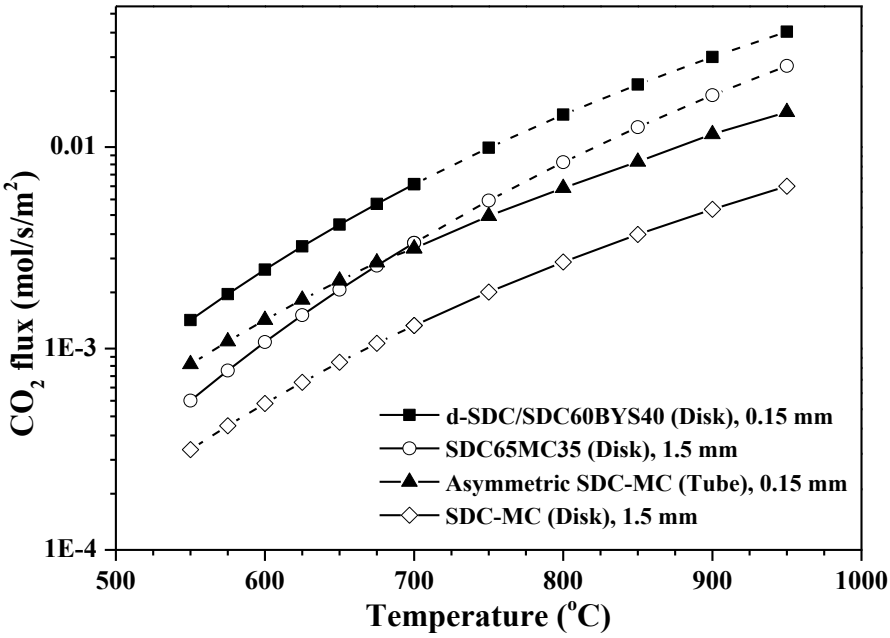

Figure 5.14 Comparison of CO_2 flux for thin SDC-MC membrane developed in this work with other thick SDC dual-phase membranes reported in the literature

Thin SDC-MC membrane also exhibits higher flux than asymmetric tubular SDC-MC membrane with similar thickness. Recently, Lin and coworkers [Ortiz-Landeros, et al., 2013] reported that support pore structure also affects carbon dioxide permeation through the dual-phase membranes. In Figure 5.14, SDC65MC35 exhibits higher CO_2 flux than SDC-MC with similar morphology just because the ceramic support prepared by "co-precipitation" and "template-sacrificial" synthesis had very different microstructure [Zhang et al., 2012] from the membrane made by uniaxially pressing [Norton et al., 2014]. Asymmetric SDC-MC membrane was prepared by

centrifugal casting [Dong et al., 2013]. Microstructure of the SDC layer, such as tortuosity, particle packing pattern etc., might be very different from that of the pressing one. Thin SDC-MC membrane seems to possess a better pore structure for gas permeation and has a higher CO_2 flux.

Table 5.5

CO_2 permeation properties of SDC-based dual-phase membranes

Membrane (shape)	Thick (mm)	T (°C)	CO_2 flux (10^{-3} mol/s/m^2)	ε(%)	Synthesis method
d-SDC/SDC60BYS40 (Disk)	~0.15	550-700	1.38-6.55	35	Co-pressing
SDC65MC35 (Disk)	1.5	550-700	0.55-3.35	36.6	Co-precipitation and sacrificial template
Asymmetric SDC-MC (Tube)	~0.15	700-900	3.14-11.6	35±5	Centrifugal casting
SDC-MC (Disk)	1.5	700-950	1.3-6.40	36	Uniaxially pressing

As shown in Figure 5.14, thin SDC-MC membrane exhibits a CO_2 flux around 5 times larger than the thick membrane. Based on transport mechanism, for the dual-phase membranes with same ceramic phase and microstructure, gas permeation of the membrane is controlled by bulk transport. CO_2 permeation flux is reciprocally proportional to membrane thickness. In theory, thin SDC-MC membrane of 0.15 mm thick should achieve a CO_2 permeation flux 10 times larger than the thick SDC-MC membrane (1.5 mm). However, improvement of permeation flux for thin membrane is only about 5 times. Similar phenomenon was also observed for thin YSZ-MC implying surface reaction becomes a factor as thickness decreases.

5.4 Conclusions

Thin SDC-carbonate dual-phase membranes could not be prepared directly on porous BYS base. Sintering incomparability between SDC and BYS makes asymmetric porous support warp (co-pressing) or dual-phase membrane peel off after infiltration (suspension coating). Blending ceramic powders same as solid phase of dual-phase membrane and carbonate non-wettable ceramics at an appropriate ratio proves effective for base support preparation. The support consisting of mixing powders provides better sintering comparability between ceramic top-layer and base and essential carbonate non-wettability for thin dual-phase membrane synthesis. In this work, SDC and BYS powders are mixed at a volume ratio of 60 to 40 serving as the base. Asymmetric porous supports composed of thick, macroporous SDC60BYS40 support sandwiched by double SDC thin layers (to balance sintering stress) are prepared by co-pressing method. Hermetic thin SDC-MC membrane is achieved via direct infiltrating Li/Na/K carbonate mixtures into supported thin SDC layers. The membrane is around 150 μm thick. CO_2 permeation through the membrane exhibits increasing dependence on temperature (550-700°C). The membrane has a maximum CO_2 flux of 6.55×10^{-3} mol/s/m^2 at 700°C and maintains a stable flux for 180 hrs. CO_2 permeation flux also demonstrates increasing dependence with trans-membrane CO_2 partial pressure difference (ratio of carbon dioxide pressure in the feed to that in the sweep). CO_2 permeation for thin SDC-MC membrane is larger than other SDC based dual-phase membranes. Reduction

in thickness could effectively improve the gas flux. The thin membrane has a lower permeance than estimated value based on bulk diffusion transport indicating effects of the surface reaction on CO_2 permeation for the thin dual-phase membrane.

CHAPTER 6

SUMMARY AND RECOMMENDATIONS

6.1 Summary

This dissertation presented synthesis and characterization of thin ceramic-carbonate dual-phase membranes for high temperature CO_2 separation. Gas permeation properties of the membranes were studied as well. Suspension and sol-gel coating methods were developed for ceramic top-layer synthesis. Porous support for thin ceramic-carbonate dual-phase membrane must be carbonate non-wettable to maintain porous after infiltration. Thin YSZ-carbonate dual-phase membrane was constructed with asymmetric porous support consisting of macroporous YSZ membrane supported on BYS base. Thin membrane of 10 μm thick a CO_2 flux 10 times higher than the thick dual-phase membrane. $Ce_{0.8}Sm_{0.2}O_{1.9}$ (SDC0-carbonate dual-phase membrane exhibited best CO_2 permeation flux and stability among the membranes developed in the lab. D-SDC/SDC60BYS40 was successfully prepared and the membrane achieved a higher CO_2 flux.

The first objective of the work is to develop methods for synthesizing asymmetric porous supports with multi-layer structure. In Chapter 2, suspension and sol-gel coating methods were developed. Mesoporous YSZ membrane of 1 μm and macroporous YSZ membrane of 10 μm were respectively prepared.

The second objective of the work is to synthesize supported thin ceramic-carbonate dual-phase membrane and study membrane characteristics and gas permeation properties. In Chapter 3, the membrane was constructed with two-layer asymmetric support consisting of an oxygen ionic-conducting top-layer supported on a porous base. The base support must be carbonate non-wettable and ionic conductive. Carbonate non-wettability helps to maintain base support porous after infiltration and molten carbonate is held in the thin ionic-conducting top-layer only. Ionic conductivity of the support assures a continuous ionic transport in the ceramic solid phase without preventing gas permeation even limited molten carbonate penetrates into the base support. Macroporous YSZ membrane was prepared on $Bi_{1.5}Y_{0.3}Sm_{0.2}O_{3-\delta}$ (BYS) by suspension coating. D-YSZ/BYS of 10 μm thick was synthesized via a direct infiltration method. A continuous carbonate layer formed on membrane after infiltration and was removed by the "sponge" soaking method to ensure transport of neutral CO_2. D-YSZ/BYS had a CO_2 flux of 3.89×10^{-3} mol/s/m^2 at 650°C 5-10 times larger than other thick dual-phase membranes. Reducing membrane thickness effectively increases CO_2 flux. The thin membrane however has a lower flux than value estimated from bulk transport indicating surface reaction effect on CO_2 permeation when membrane thickness decreases.

The third objective of this dissertation is to optimize thin ceramic-carbonate dual-phase membrane. The work was reported in Chapter 4 and 5. In Chapter 4, CO_2 permeation properties and stability of samarium doped ceria (SDC)-carbonate dual-phase

were studied. Bulk membrane of 1.5 mm thick exhibited highest CO_2 permeation flux and long-term stability among the dual-phase membranes developed in the lab. SDC was chosen as the ceramic solid phase. Chapter 5 reported synthesis of thin SDC-carbonate dual-phase membranes. The membrane could not be directly prepared on pure BYS base via suspension coating or co-pressing methods due to sintering incomparability between SDC and BYS.

Blending ceramic powders same as solid phase of dual-phase membrane and carbonate non-wettable ceramics at an appropriate ratio proves effective for base support preparation. The support provides better sintering comparability and essential carbonate non-wettability and SDC60BYS40 is prepared. Asymmetric porous support consisting of SDC60BYS40 sandwiched by thin SDC porous layers was obtained via co-pressing method. D-SDC/SDC60BYS40 of 150 μm was achieved via direct infiltrating Li/Na/K carbonate mixtures into supported thin SDC layers. CO_2 permeation flux through the membrane showed increase dependences on temperature and trans-membrane CO_2 partial pressure difference. The membrane exhibits higher CO_2 flux than d-YSZ/BYS and other SDC based dual-phase membranes due to higher ionic conductivity and thickness reduction, respectively.

6.2 Recommendations

Based on the experimental and theoretical studies reported in the dissertation, several recommendations are suggested for future research as follows:

6.2.1 Study of permeation stability and mechanism

Thin ceramic-carbonate dual-phase membranes have exhibited higher CO_2 permeation flux. However, the work does not report much on permeation stability. Decomposition of graphite seals at high temperature limit long-term stability test. It is recommended to perform similar stability tests as presented in Chapter 4-exposed to reductive (simulated syngas), high pressure environment. To fulfill stability test, the sealing materials able to withstand high temperature should be developed. Metal or ceramic seals should be taken in consideration. With different high temperature permeation setup, Norton et al. [Norton et al., 2014] directly used melted carbonate to seal the membranes and permeation test last over 30 days without leakage. The stablity test could also be performed with new setup. This helps improve membrane performance and evaluate its potential for industrial application.

Permeation mechanism for thin dual-phase membrane is still unclear. Gas permeation flux not reaching the value estimated by bulk diffusion transport and activation energy inconsistent with the thick one indicate surface reaction effect for gas transport of dual-phase membrane when thickness decreases. It is recommended to synthesize the membranes with various thicknesses. By comparing the permeation properties, it helps to determine if there is a critical thickness for gas transport through the ceramic-carbonate dual-phase membrane. Results help develop transport model considering both bulk transport and surface reaction kinetics.

6.2.2 Exploration of materials for porous base

Porous base support must be carbonate non-wettable to ensure molten carbonate infiltrated into ceramic top-layer only forming thin, hermetic ceramic-carboante dual-phase membrane. In this work, only $Bi_{1.5}Y_{0.3}Sm_{0.2}O_{3-\delta}$ (BYS) exhibits carbonate non-wettability and serves as support base. However, BYS has a lower melting point and shows sintering incomparability with ceramics requiring high sintering temperature, such as SDC which makes synthesis of asymmetric porous support difficult. BYS also suffers phase transform [Rui et al., 2009] at high temperature and makes it unstable for long-term stability test. Blending ceramic powders and BYS with a proper ratio seems to address the issue. Chemical stability of powder mixtures remains a concerning and it is time consuming to identify optimum mixing rate and sintering temperature. It is recommended to explore materials carbonate non-wettable with higher melting point and better stability. The ceramic support could be generally applied to dual-phase membranes using various ceramic as solid phase. One suggestion is to synthesize ceramic powders using bismuth oxide as dopant and check carbonate wettability.

6.2.3 Synthesis of asymmetric supports with controlled pore structure

Due to smaller thickness and integrity with base support, it is hard to characterize pore structure of thin ceramic top-layer. Recently, Lin and coworkers [Ortiz-Landeros et al., 2013] reported pore structure effect on CO_2 permeation through dual-phase membranes. To improve thin dual-phase membrane performance, it is desirable to

synthesize ceramic top-layer with controlled structure (porosity, tortuosity et al.) and identify optimum framework of the support. It is recommended to use methods with controlling factors for support synthesis, such as spinning coating and extrusion. Pore former such as graphite powders could also be used to manipulate porosity of the ceramic supports. Other than liquid nitrogen or SEM, new characterization methods are also recommended for pore structure identification. A fundamental study on the effect of ceramic: carbonate ratio on CO_2 permeation properties for thin dual-phase membrane could also be conducted.

6.2.4 Permeation stability in water vapor containing environment

Thin SDC-carbonate dual-phase membrane has exhibited good permeation stability after long-term exposure to dry gas feed-CO_2: N_2 and syngas. However, stability of the membrane in water containing gas streams was not studied. For practical industrial process, such as gasification in pre-combustion, CO_2 often comes out mixing with water vapor. To evaluate industrial application potential for thin ceramic-carbonate dual-phase membrane, it is recommended to study its permeation stability in CO_2 wet environment where water vapor tends to react with molten carbonate forming hydro-carbonate and affects carbon dioxide permeation for the membrane.

In the lab, water gas shift reaction has been performed with thick SDC-carbonate dual-phase membrane. The membrane demonstrated permeation stability over 100 h exposed to CO, H_2O (vapor), CO_2 and H_2 gas mixtures. The ceramic-carbonate

dual-phase membrane already exhibited certain stability in CO_2 wet environment. Permeation tests for thin dual-phase membrane could also be performed with CO_2 and H_2O (vapor) mixtures at normal pressure ($\triangle P=0$) or high pressure ($\triangle P>1$) feed to study vapor effect in details.

6.2.5 Study of different molten carbonate

Till now, all dual-phase membranes in our lab were only synthesized with $Li_2/Na_2/K_2CO_3$ (42.5/32.5/25 mol%) carbonate mixtures. This particular mixture has melting point of only 397 ^oC which facilitates infiltration process and also exhibits a higher ionic conductivity. However, at high temperatures (850°C+) and low partial pressures of carbon dioxide, the mixture tends to decompose into CO_2 and the corresponding metal oxides (M_2O, where M = Li, Na, K). Decomposition of molten carbonate within the membrane leads to the formation of defects, hence allowing N_2 (or other unwanted gases) to permeate. The mixture is also reactive to some metal oxide serving as ceramic phase and the reaction will form the defects or compounds unable to transport oxygen ion [Norton et al., 2014].

To solve the issue, it is recommended to study molten carbonate mixtures with different compositions. The new mixture should also have a high conductivity and a low melting point, but remain stable with ceramic phase at high temperature. Several combinations of Li/Na/K, Li/K, Li/Na carbonates have been studied, and the characteristics of these have been reported by Janz et al. [Janz et al., 1979]. Potential

candidates for use in the dual-phase membrane could be selected based on the aforementioned findings. Permeation model [Norton el al., 2014] exhibits that gas permeation for ceramic-carbonate dual-phase membranes is also relative to physical structure and ionic conductivity in liquid molten carbonate phase. Studying permeation properties with different carbonate mixtures also helps to further understand transport mechanism of ceramic-carbonate dual-phase membrane.

REFERENCES

Aaron, D., Tsouris, C. (2005). Separation of CO_2 from Flue Gas: A Review. *Separation Science and Technology*, 40, 321-348.

Abdel-Salam O. E., Winnick, J. (1976). Simulation of an Electrochemical Carbon Dioxide Concentrator. *AIChE Journal*, 22, 1042-1050.

Anderson, M., Lin, Y. S. (2006). Synthesis and Characterization of Carbonate-Ceramic Dual-Phase Membranes for Carbon Dioxide Separation, Proc. 9th Internal. Conf. on Inorganic Membranes. R. Bredesen and H. Rader (Eds), 678.

Anderson, M., Lin, Y. S. (2010). Carbonate–ceramic dual-phase membrane for carbon dioxide separation. *Journal of Membrane Science*, 357, 122-129.

Anderson, M., Wang, H., Lin, Y.S. (2012). Inorganic membranes for carbon dioxide and nitrogen separation. *Reviews in Chemical Engineering*, 28, 101-121.

Armin, J. A. R., Ebner, D. (2009). State-of-the-art adsorption and membrane separation process for carbon dioxide production from carbon dioxide emitting industries. *Separation Science and Technology*, 44, 1273–1421.

Arnold, M., Wang, H., Feldhoff, A. (2007). Influence of CO_2 on the oxygen permeation performance and the microstructure of perovskite-type $(Ba_{0.5}Sr_{0.5})$ $(Co_{0.8}Fe_{0.2})$ $O_{3-\delta}$ membranes. *Journal of Membrane Science*, 293, 44–52.

Barsema, J. N., van der Vegt, N. F. A., Koops, G. H., Wessling, M. (2005). Ag-functionalized carbon molecular-sieve membranes based on polyelectrolyte/polyimide blend precursors. *Advanced Functional Materials*, 15, 69-75.

Bernal, M. P., Coronas, J., Menendez, M., Santamaria, J. (2004). Separation of CO_2/N_2 mixtures using MFI-type zeolite membranes. *AlChE Journal*, 50, 127–135.

Bernardo, P., Drioli, E., Golemme, E. (2009). Membrane Gas Separation: A Review/State of the Art. *Ind. Eng. Chem. Res.*, 48, 4638-4663.

Bhave, R. R. (1991). Inorganic membranes: Synthesis, characteristics and applications. New York: Van Nostrand Reinhold.

Biedenkopf, P., Bischoff, M. M., Wochner, T. (2000). Corrosion phenomena of alloys and electrode materials in molten carbonate fuel cells. *Materials and Corrosion*, 146, 287-302.

Birkby, I., Stevens, Ron. (1996). Applications of Zirconia Ceramics. *Key Engineering Materials*, 122, 527-552.

Bounaceur, R., Lape, N., Roizard, D., Vallieres, C., Favre, E. (2006). Membrane processes for post-combustion carbon dioxide capture: A parametric study. *Energy*, 31, 2556-2570.

Bouwmeester, H. J. M., Kruidhof, H., Burggraaf, A. J., Gellings, P. J. (1992). Oxygen semipermeability of erbia-stabilized bismuth oxide. *Solid State Ionics*, 53-56, 460-468.

Brinker, C. J., Scherer, G. W. (1990). Sol-Gel Science. Academic Press, Boston.

Bouwmeester H. J. M., Burggraaf, A. J. (1996). Dense Ceramic Membranes for Oxygen Separation, in "Fundamentals of Inorganic Membrane Science and Technology", Eds A.J. Burggraaf, L. Cot, Chapter 10, Elsevier.

Carolan, M. F., Michaels, J. M. (1990). Growth rates and mechanism of electrochemical vapor deposited yttria-stabilized zirconia films. *Solid State Ionics*, 37, 189-195.

Chang, C. H., Gopalan, R., Lin, Y. S. (1994). A comparative study on thermal and hydrothermal stability of alumina, titania and zirconia membranes. *Journal of Membrane Sc*ience, 91, 27-45.

Cheng, S., Gupta, V. K., Lin, Y. S. (2005). Synthesis and hydrogen permeation properties of asymmetric proton-conducting ceramic membranes. *Solid State Ionics*, 176, 2653-2662.

Chung, S. J., Park, J. H., Li, D., Ida, J. I., Kumakiri, I., Lin, Y. S. (2005). Dual-phase metal-carbonate membrane for high-temperature carbon dioxide separation. *Industrial & Engineering Chemistry Research*, 44, 7999-8006.

Cooper, C. A., Lin, Y. S. (2002). Microstructural and gas separation properties of CVD modified mesoporous g-alumina membranes. *Journal of Membrane Science*, 195, 35-50.

Cuffe, L., MacElroy, J. M. D., Tacke, M., Kozachok, M., Mooney, D. A. (2006). The development of nanoporous membranes for separation of carbon dioxide at high temperatures. *Journal of Membrane Science*, 272, 6-10.

De Vos, R. M., Maier. W. F., Verweij, H. (1999). Hydrophobic silica membranes for gas separation. *Journal of Membrane Science*, 158, 277-288.

Dong, X., Zhang, G., Liu, Z., Zhong, Z., Jin W., Xu, N. (2009). CO_2-tolerant mixed conducting oxide for catalytic membrane reactor, *Journal of Membrane Science*, 340, 141-147.

Dong, X.L., Ortiz-Landeros, J., Lin, Y. S. (2013). Asymmetric tubular ceramic-carbonate dual phase membrane for high temperature CO_2 separation. *Chemical Communications*, 49, 9654-9656.

Farhikhten, S., Maghsoudipour, A., Raissi, B. (2010). Synthesis of nanocrystalline YSZ (ZrO_2–$8Y_2O_3$) powder by polymerized complex method. *Journal of Alloys and Compounds*, 491, 402-405.

Figueroa, J. D., Fout, T., Plasynski, S., McIlvried, H., Srivastava, R. D. (2008). Advances in CO_2 capture technology – the U.S. Department of Energy's Carbon Sequestration Program. *International Journal of Greenhouse Gas Control*, 2, 9-20.

Garcia, G., Figueras, A., Casado, J., Llibre, J., Mokchah, M., Petot-ervas, G., Calderer, J. (1998). Yttria-stabilized zirconia obtained by MOCVD: applications. *Thin Solid Films*, 317, 241-244.

Gopalan, R., Chang, C. H., Lin, Y. S. (1995). Thermal stability improvement on pore and phase structure of sol-gel derived zirconia. *Journal of Material Science*, 30, 3075-3081.

Gu, X., Dong, J., Nenoff, T. M. (2005). Synthesis of defect-free FAU-type zeolite membranes and separation for dry and moist CO_2/N_2 mixtures. *Industrial & Engineering Chemistry Research*, 44, 937-944.

Gu, Y., Oyama, S. T. (2007). Ultrathin, hydrogen-selective silica membranes deposited on alumina-graded structures prepared from size-controlled boehmite sols. *Journal of Membrane Science*, 306, 216-227.

Gurauskis, J., Lohne, O. F., Lein, H. L., Wiik, K. (2012). Processing of thin film ceramic membranes for oxygen separation. *Journal of the European Ceramic Society*, 32, 649-655.

Gurauskis, J., Lohne, O. F., Wiik, K. (2012). $La_{0.2}Sr_{0.8}Fe_{0.8}Ta_{0.2}O_{3-\delta}$ based thin film membranes with surface modification for oxygen production. *Solid State Ionics*, 225, 703-706.

Han, J., Zeng, Y., Xomeritakis, G., Lin, Y. S. (1997). Electrochemical vapor deposition synthesis and oxygen permeation properties of dense zirconia-yttria-ceria membranes. *Solid State Ionics*, 98, 63-72.

Harry, K. G., Johnson, A. (2004). A non-destructive technique for measuring ceramic porosity using liquid nitrogen. Journal of Archaeological Science, 31, 1567-1575.

Hayashi, J.-I., Yamamoto, M., Kusakabe, K., Morooka, S. (1995). Simultaneous improvement of permeance and permselectivity of 3,3',4,4'-biphenyltetracarboxylic dianhydride-4,4'-oxydianiline polyimide membrane by carbonization. *Industrial & Engineering Chemistry Research*, 34, 4364-4370.

He, X., Hägg, M. B. (2011). Hollow fiber carbon membranes: Investigations for CO_2 capture. *Journal of Membrane Science*, 378, 1–9.

He, X., Lie, J. A., Sheridan, E., Hägg, M. B. (2011). Preparation and characterization of hollow fiber carbon membranes from cellulose acetate precursors. *Industrial & Engineering Chemistry Research*, 50, 2080-2087.

Herbert, V., His, C., Guille, J., Vilmiont, S., Wen, T. L. (1991). Preparation and characterization of precursors of Y_2O_3 stabilized ZrO_2 by metal-organic compounds. *Journal of Material Science*, 26, 5184-5188.

Heshmatpour, F., Aghakhanpour, R. B. (2011). Synthesis and characterization of nanocrystalline zirconia powder by simple sol–gel method with glucose and fructose as organic additives. *Powder Technology*, 205, 193-200.

Hsieh, H. P. (1996). Inorganic membranes for separation and reaction. Amsterdam: Elsevier.

Hu, L., Wang, C., Huang, Y. (2010). Porous yttria-stabilized zirconia ceramics with ultra-low thermal conductivity. *Journal of Material Science*, 45, 3242-3246.

Hu, L., Wang C., Hu Z., Lu, S., Sun, C., Huang, Y. (2011). Porous yttria-stabilized zirconia ceramics with ultra-low thermal conductivity. Part II: temperature dependence of thermo physical properties. *Journal of Material Science,* 46, 623-628.

Hu, T., Dong, G., Li, H., Chen, V. (2013). Improved CO_2 separation performance with additives of PEG and PEG–PDMS copolymer in poly (2, 6-dimethyl-1, 4-phenyleneoxide) membranes. *Journal of Membrane Science*, 432, 13–24.

Ida, J.-I. Lin, Y. S. (2003). Mechanism of high temperature CO_2 sorption on lithium zirconate. *Environmental Science and Technology*, 37, 1999-2004.

IPCC. (2007). Climate Change: Synthesis Report. Contribution of Working Groups I, II and III to the Fourth Assessment Report of the Intergovernmental Panel on Climate Change. IPCC, Geneva, Switzerland.

Janz, J., Allen, C., Bansal, P., Murphy, R., Tomkins, R. (1979) Physical Properties Data Compilations Relevant to Energy Storage; Molten Salts: Data on Single and Multi Component Salt System, Washington, DC: National Bureau of Standards.

Kai, T., Kazama, S., Fujioka, Y. (2009). Development of cesium-incorporated carbon membranes for CO_2 separation under humid conditions. *Journal of Membrane Science*, 342, 14-21.

Kanezashi, M., O'Brien, J., Lin, Y. S. (2007). Thermal stability improvement of MFI-type zeolite membranes with doped zirconia intermediate layer. *Microporous and Mesoporous Materials*, 103, 302-308.

Kang, M. P., Winnick, J. (1985). Concentration of carbon dioxide by a high-temperature electrochemical membrane cell. *Journal of Applied Electrochemistry*, 15, 431-439.

Kawamura, H., Yamaguchi, T., Nair, B. N., Nakagawa, K., Nakao, S. -I. (2005). Dual-ion conducting lithium zirconate-based membranes for high temperature CO_2 separation. *Journal of Chemical Engineering of Japan*, 38, 322-328.

Kharton, V. V., Kovalevsky, A. V., Viskup, A. P., Shaula, A. L., Figueiredo, F. M., Naumovich, E. N., Marques, F. M. B. (2003). Oxygen transport in $Ce_{0.8}Gd_{0.2}O_{2-\delta}$-based composite membranes. *Solid State Ionics*, 160, 247–258.

Kim, J., Lin, Y. S. (1998). Sol-gel synthesis and characterization of yttria stabilized zirconia membranes. *Journal of Membrane Science*, 139, 75-83.

Kim, J., Lin, Y. S. (1999). Synthesis and Characterization of Suspension-Derived, Porous Ion-Conducting Ceramic Membranes. *Journal of the American Ceramic Society*, 82, 2641-2646.

Kim, J., Lin, Y. S. (2000). Palladium-Modified Yttria-Stabilized Zirconia Membranes. *Industrial & Engineering Chemistry Research*, 39, 2124-2126.

Kim, S., Ida, J., Guliants, V., Lin, Y. S. (2004). Functionalized mesoporous silica membrane for the separation of carbon dioxide. *International Journal of Environmental Technology and Management*, 4, 21-31.

Koresh, J. E., Sofer, A. (1993). Molecular Sieve Carbon Permselective Membrane. Part I. Presentation of a New Device for Gas Mixture Separation. *Separation and Purification Technology*, 18, 723-734.

Koros, W. J., Mahajan, R. (2000). Pushing the limits on possibilities for large scale gas separation: which strategies? *Journal of Membrane Science*, 175, 181–196.

Kovalevsky, A. V., Yaremchenko, A. A., Kolotygin, V. A., Shaula, A. L., Kharton, V. V., Snijkers, F. M. M., Buekenhoudt, A., Frade, J. R., Naumovich, E. N. (2011). Processing and oxygen permeation studies of asymmetric multilayer $Ba_{0.5}Sr_{0.5}Co_{0.8}Fe_{0.2}O_{3-\delta}$ membranes. *Journal of Membrane Science*, 380, 68-80.

Kueper, T. W., Visco, S. J., De Jonghe, L. C. (1992). Thin-film ceramic electrolytes deposited on porous and non-porous substrates by sol-gel techniques. *Solid State Ionics*, 52, 251-259.

Kuo, C. W., Lee, Y. H., Hung, I. M., Wang, M. C., Wen, S. B., Fung, K. Z., Shih, C. J. (2008). Crystallization kinetics and growth mechanism of 8 mol% yttria-stabilized zirconia (8YSZ) nano-powders prepared by a sol–gel process. *Journal of Alloys and Compounds*, 453, 470-475.

Kusakabe, K., Kuroda, T., Murata, A., Morooka, S. (1997). Formation of a Y-type zeolite membrane on a porous alumina tube for gas separation. *Industrial & Engineering Chemistry Research*, 36, 649-655.

Kusakabe, K., Sakamoto, S., Saie, T., Morooka, S. (1999). Pore structure of silica membranes formed by a sol-gel technique using tetraethoxysilane and alkyltriethoxysilanes. *Separation and Purification Technology*, 16, 139-146.

Leenaars, A. F. M., Keizer, K., Burggraaf, A. J. (1984). Microstructural investigations on non-supported membranes. *Journal of Material Science*, 19, 1077-1088.

Lehman, R., Gentry, J. S., Glumac, N. G. (1998). Thermal stability of potassium carbonate near its melting point. *Thermochimica Acta*, 316, 1–9.

Leo, A., Liu, S., Diniz da Costa, J. C. (2009). Development of mixed conducting membranes for clean coal energy delivery. *International Journal of Greenhouse Gas Control,* 3, 357-367.

Lin, Y. S., de Haart, L. G. J., de Vires , K. J., Burggraaf, A. J. (1990). A Kinetic Study of the Electrochemical Vapor Deposition of Solid Oxide Electrolyte Films on Porous Substrates. *Journal of Electrochemistry Society*, 137, 3960-3966.

Lin, Y. S., de Vries, K. J., Brinkman, H. W., Burggraaf, A. J. (1992). Oxygen semipermeable solid oxide membrane composites prepared by electrochemical vapor deposition. *Journal of Membrane Science*, 66, 211-226.

Lin, Y. S., Burggraaf, A. J. (1993). Experimental studies on pore size change of porous ceramic membranes after modification. *Journal of Membrane Science*, 79, 65-82.

Lin, Y. S. (2001). Microporous and dense inorganic membranes: current status and prospective. *Separation and Purification Technology*, 25, 39-55.

Lin, Y. S., Kumakiri, I., Nair, B. N., Alsyouri, H. (2002). Microporous inorganic membranes. *Separation and Purification Technology* , 61-62, 337-346.

Liu, S., Tan, X., Li, K., Hughes, R. (2002). Synthesis of strontium cerates-based perovskite ceramics via water-soluble complex precursor routes. *Ceramics International*, 28, 327-335.

Liu, Z., Zhang, G., Dong, X., Jiang, W., Jin, W., Xu, N. (2012). Fabrication of asymmetric tubular mixed-conducting dense membranes by a combined spin-spraying and co-sintering process. *Journal of Membrane Science*, 415-416, 313-319.

Lobera, M. P., Serra, J. M., Foghmoes, S. P., Sogaard, M., Kaiser, A. (2011). On the use of supported ceria membranes for oxyfuel process/syngas production. *Journal of Membrane Science*, 385, 154-161.

Lu, B., Lin, Y. S. (2013). Synthesis and characterization of thin ceramic-carbonate dual-phase membranes for carbon dioxide separation. *Journal of Membrane Science*, 444 (2013) 402-411.

Mamantov, G., Braunstein, J., Mamantov, C. B. (1981). Advances in Molten Salt Chemistry, Plenum Press: New York, Vol.4.

Meng, G., Cao, C., Yu, W., Peng, D., de Vries, K., Burggraaf, A. J. (1991). Formation of ZrO_2 and YSZ Layers by Microwave Plasma Assisted MOCVD Process. *Key Engineering Materials*, 61-62, 11-16.

Mercera, P. D. L., van Ommen, J. G., Doesburg, E. B. M., Burggraaf, A. J., Roes, J. R. H. (1991). Stabilized tetragonal zirconium oxide as a support for catalysts Evolution of the texture and structure on calcination in static air. *Applied Catalysis,* 78, 79-96.

Merkel, T. C., Lin, H, Wei, X., Baker, R. (2010). Power plant post-combustion carbon dioxide capture: An opportunity for membranes. *Journal of Membrane Science*, 359, 126-139.

Minh, N. Q., Takahashi, T. (1995). Science and Technology of Ceramic Fuel Cell. Elsevier, Amsterdam.

Moon, J. H., Park, Y. J., Kim, M. B., Hyun, S. H., Lee, C. H. (2005). Permeation and separation of a carbon dioxide/nitrogen mixture in a methyltriethoxysilane templating silica/α-alumina composite membrane. *Journal of Membrane Science*, 250, 195-205.

MTI. (2007). The Future of Coal-Options for a Carbon Constrained World. MTI Interdisciplinary Study.

Mori, T., Wang, Y., Drennan, J., Aucheterlonie, G., Li, J.-G., Ikegami, T. (2004). Influence of particle morphology on nanostructural feature and conducting property in Sm-doped CeO_2 sintered body. *Solid State Ionics*, 175, 641-649.

Nair, N. B., Yamaguchi, T., Kawamura, H., Nakao, S., Nakagawa, K. (2004). Processing of Lithium Zirconate for Applications in Carbon Dioxide Separation: Structure and Properties of the Powders. *Journal of the American Ceramic Society*, 87, 68–74.

Nicolas, C. H., Sublet, J., Schuurman, Y., Pera-Titus, M. (2011). Role of adsorption and diffusion path ways on the CO_2/N_2 separation performance of nanocomposite B-MFI-alumina membranes. *Chemical Engineering Science*, 66, 6057–6068.

Norton, T. T., Lu, B., Lin, Y.S. (2014). Carbon dioxide permeation properties and stability of samarium doped ceria-carbonate dual-phase membrane. *Journal of Membrane Science*, to be submitted.

Norton, T. T., Ortiz-Landeros, J., Lin, Y.S. (2014). Stability of La-Sr-Co-Fe oxide-carbonate dual-phase membrane for CO_2 separation at high temperature. *Industrial & Engineering Chemistry Research*, 53, 2432–2440.

Norton, T. T., Ortiz-Landeros, J., Lin, Y.S. (2014). High performance ceramic-carbonate dual-phase membrane for pre-combustion carbon dioxide capture at high temperature. In preparation.

Okubo, T., Inoue, H. (1989). Single gas permeation through porous glass modified tetraethoxysilane. *AIChE Journal*, 35, 845-848.

Okubo, T., Nagamoto, H. (1995). Low-temperature preparation of nanostructured zirconia and YSZ by sol-gel processing. *Journal of Material Science*, 30, 749-757.

Okubo, T., Takahashi, T., Sakadata, M., Nagamoto, H. (1996). Crack-free porous YSZ membrane via controlled synthesis of zirconia sol. *Journal of Membrane Science*, 118, 151-157.

Ortiz-Landeros, J., Norton, T., Lin, Y. S. (2013). Effects of Support Pore Structure on Carbon Dioxide Permeation of Ceramic-Carbonate Dual-Phase Membranes. *Chemical Engineering Science*, 104, 891-898.

Ostwal, M., Singh, R. P., Dec, S. F., Lusk, M. T., Way, J. D. (2011). 3-Aminopropyltriethoxysilane functionalized inorganic membranes for high temperature CO_2/N_2 separation. *Journal of Membrane Science*, 369, 139–147.

Ping, E. W., Zhou, R. F., Funke, H. H., Falconer, J. L., Noble, R. (2012). Seeded-gel synthesis of SAPO-34 single channel and monolith membranes for CO_2/CH_4 separations. *Journal of Membrane Science*, 415–416, 770–775.

Poshusta, J., Tuan, A. V., Pape, E., Noble, R., Falconer, J. (2000). Separation of light gas mixtures using SAPO-34 membranes. *AIChE Journal*, 46, 779-789.

Powell, C.E., Qiao, G. G. (2006). Polymeric CO_2/N_2 gas separation membranes for the capture of carbon dioxide from power plant flue gases. *Journal of Membrane Science*, 279, 1-49.

Priyatham, T., Bauri, Ranjit. (2010). Synthesis and characterization of nanocrystalline Ni–YSZ cement anode for SOFC. *Materials Characterization,* 61, 54-58.

Roberson, M. L. (2008). The upper bound revisited. *Journal of Membrane Science*, 320, 390-400.

Rui, Z., Anderson, M., Lin, Y. S., Li, Y. D. (2009). Modeling and analysis of carbon dioxide permeation through ceramic-carbonate dual-phase membranes. *Journal of Membrane Science*, 345, 110-118.

Rui, Z., Ji, H. B., Lin, Y. S. (2011). Modeling and analysis of ceramic-carbonate dual-phase membrane reactor for carbon dioxide reforming with methane. *International Journal of Hydrogen Energy*, 36, 8292-8300.

Rui, Z., Anderson, M., Li, Y., Lin, Y. S. (2012). Ionic conducting ceramic and carbonated dual phase membranes for carbon dioxide separation. *Journal of Membrane Science*, 417-418, 174-182.

Sakamoto, Y., Nagata, K., Yogo, K., Yamada, K. (2007). Preparation and CO_2 separation properties of amine-modified mesoporous silica membranes. *Microporous Mesoporous Materials*, 101, 303-311.

Sammes, N. M., Tompsett, G. A., Nafe, H., Aldinger, F. (1999). Bismuth based oxide electrolytes-structure and ionic conductivity. *Journal of the European Ceramic Society*, 19, 1801-1826.

Scholes, C. A., Smith, K. H., Kentish, S. E., Stevens, G. W. (2010). CO_2 capture from pre-combustion processes-Strategies for membrane gas separation. *International Journal of Greenhouse Gas Control*. 4, 739-755.

Sea, B., Lee, K.-H. (2001). Molecular sieve silica membrane synthesized in mesoporous g-alumina layer. *Bulletin of the Korean Chemical Society*, 22, 1400-1402.

Shekhawat, Luebke, D. R., Pennline, H. W. (2003). A Review of Carbon Dioxide Selective Membranes. National Energy Technology Laboratory, Morgantown, WV,.

Shiflett, M. B., Foley, H. C. (2000). On the preparation of supported nanoporous carbon membranes. *Journal of Membrane Science*, 179, 275-282.

Shin, D. W., Hyun, S. H., Cho, C. H., Han, M. H. (2005). Synthesis and CO_2/N_2 gas permeation characteristics on ZSM-5 zeolite membranes. *Microporous and Mesoporous Materials*, 85, 313-323.

Steele, B. C. H. (1987). Ceramic Electrochemical Reactors, Current Status and Application. Ceramionics, Surrey, England.

Steel, K., Koros, W. (2005). An investigation of the effects of pyrolysis parameters on gas separation properties of carbon materials. *Carbon*, 43, 1843-1856.

Sunarso, J., Baumann, S., Serra, J. M., Meulenberg, W. A., Liu, S., Lin, Y. S., Diniz da Costa, J. C. (2008). Mixed ionic-electronic conducting (MIEC) ceramic-based membranes for oxygen separation. *Journal of Membrane Science*, 320, 13-41.

Tan, X., Liu, N., Meng, B., Sunarso, J., Zhang, K., Liu, S. (2012). Oxygen permeation behavior of $La_{0.6}Sr_{0.4}Co_{0.8}Fe_{0.2}O_3$ hollow fiber membranes with highly concentrated CO_2 exposure. *Journal of Membrane Science*, 389, 216-222.

Thery, P. Y., Poulain, M., Dupeux, M., Braccini, M. (2009). Spallation of two thermal barrier coating systems: experimental study of adhesion and energetic approach to lifetime during cyclic oxidation. *Journal of Material Science*, 44, 1726-1733.

Tomita, T., Nakayama, K., Sakai, H. (2004). Gas separation characteristics of DDR type zeolite membrane. *Microporous and Mesoporous Materials*, 68, 71-75.

Tsai, C.-Y., Tam, S.-Y, Lu, Y., Brinker, C. J. (2000). Dual-layer asymmetric microporous silica membranes. *Journal of Membrane Science*, 169, 255-268.

Tseng, H.-H., Shiu, P.-T., Lin, Y.-S. (2011). Effect of mesoporous silica modification on the structure of hybrid carbon membrane for hydrogen separation. *International Journal of Hydrogen Energy*, 36, 15352-15263.

Uhlhorn, R. J. R., Huis In't Veld, M. H. B. J., Keizer, K., Burggraaf, A. J. (1989). High permselectivities of microporous silica-modified γ-alumina membranes. *Journal of Materials Science Letters*, 8, 1135-1138.

Venna, S. R., Carreon, M. A. (2011). Amino-functionalized SAPO-34 membranes for CO_2/CH_4 and CO_2/N_2 separation. *Langmuir*, 27, 2888-2894.

Wade, J. L., Lackner, K. S., West, A. C. (2007). Transport model for a high temperature, mixed conducting CO_2 separation membrane. *Solid State Ionics*, 178, 1530-1540.

Wade, J. L., Lee, C., West, A. C., Lackner, K. S. (2011). Composite electrolyte membranes for high temperature CO_2 separation. *Journal of Membrane Science*, 369, 20-29.

Wang, H., Zhang, L., Gavalas, G. R. (2000). Preparation of supported carbon membranes from furfuryl alcohol by vapor deposition polymerization. *Journal of Membrane Science*, 177, 25-31.

Wang, L. S., Barnett, S. A., (1993). Sputter-deposited medium-temperature solid oxide fuel cells with multi-layer electrolytes. *Solid State Ionics*, 61, 273-276.

Watanabe, A., Kikuchi, T. (1986) Cubic-hexagonal transformation of yttria-stabilized δ-bismuth sesquioxide, $Bi_{2-2x}Y_{2x}O_3$(x=0.215-0.235). *Solid State Ionics*, 21, 287-291.

Watanabe, K., Yuasa, M., Kida, T., Shimanoe, K., Teraoka, Y., Yamazoe, N. (2008). Dense/Porous Asymmetric-Structured Oxygen Permeable Membranes Based on $La_{0.6}Ca_{0.4}CoO_3$ Perovskite-Type Oxide. *Chemistry of Materials*, 22, 6965-6973.

Wen, T. L., Herbert, V., Vilminot, S., Bernier, J. C. (1991). Preparation of nanosized yttria-stabilized zirconia powders and their characterization. Journal of Material Science, 26, 3787-3791.

White, J. C., Dutta, P. K., Shqau, K., Verweij, H. (2010). Synthesis of ultrathin zeolite Y membranes and their application for separation of carbon dioxide and nitrogen gases. *Langmuir*, 26, 10287-10293.

Xia, C., Cao, H., Wang, H., Yang, P., Meng, G., Peng, D. (1999). Sol–gel synthesis of yttria stabilized zirconia membranes through controlled hydrolysis of zirconium alkoxide. *Journal of Membrane Science*, 162, 181-188.

Xia, C., Liu, M. (2001). Low-temperature SOFCs based on $Gd_{0.1}Ce_{0.9}O_{1.95}$ fabricated by dry pressing. *Solid State Ionics*, 144, 249-255.

Xomeritakis, G., Liu, N. G., Chen, Z., Jiang, Y.-B., Kohn, R., Johnson, P. E., Tsai, C.-Y., Shah, P. B., Khalil, S., Singh, S., Brinker. C. J. (2007). Anodic alumina supported dual-layer microporous silica membranes. *Journal of Membrane Science*, 287, 157-161.

Xomeritakis, G., Tsai, C. Y., Jiang, Y. B., Brinker, C. (2009). Tubular ceramic-supported sol-gel silica based membranes for flue gas carbon dioxide capture and sequestration. *Journal of Membrane Science*, 341, 30-36.

Xu, N., Li, X., Franks, M. A., Zhao, H., Huang, K. (2012). Silver-molten carbonate composite as a new high-flux membrane for electrochemical separation of CO_2 from flue gas. *Journal of Membrane Science*, 401-402, 190-194.

Xu, Q., Huang, D., Chen, W., Lee, J., Kim, B., Wang, H., Yuan, R. (2004). Influence of sintering temperature on microstructure and mixed electronic–ionic conduction properties of perovskite-type $La_{0.6}Sr_{0.4}Co_{0.8}Fe_{0.2}O_3$ ceramics. *Ceramics International*, 30, 429-433.

Xu, Q., Huang, D., Chen, W., Lee, J., Kim, B., Wang, H., Yuan, R. (2004). Citrate method synthesis, characterization and mixed electronic–ionic conduction properties of $La_{0.6}Sr_{0.4}Co_{0.8}Fe_{0.2}O_3$ perovskite-type oxides. *Scripta Materialia*, 50, 165-170.

Yamaguchi, T., Niitsuma, T., Nair, B. N., Nakagawa, K. (2007). Lithium silicate based membranes for high temperature CO_2 separation. *Journal of Membrane Science*, 294, 16-21.

Yamamoto, M., Kusakabe, K., Hayashi, J.-I., Morooka, S. (1997). Carbon molecular sieve membrane formed by oxidative carbonization of a copolyimide film coated on a porous support tube. *Journal of Membrane Science*, 133, 195-205.

Yang, H., Xu, Z., Fan, M., Gupta, R., Slimane, R. B., Bland, A. E., Wright, I. (2008). Progress in carbon dioxide separation and capture: A review. *Journal of Environmental Sciences*, 20, 14-27.

Yin, Q., Lin, Y. S. (2007). Beneficial effect of order-disorder phase transition on oxygen sorption properties of perovskite-type oxides. *Solid State Ionics*, 178, 83-89.

Yoshioka, T., Nakanishi, E., Tsuru, T., Asaeda, M. (2001). Experimental studies of gas permeation through microporous silica membranes. *AIChE Journal*, 47, 2052-2063.

Zeng, Y., Lin, Y. S. (2001). Synthesis and properties of copper and samarium doped yttria-bismuth oxide powders and membranes. *Journal of Material Science*, 36, 1271-1276.

Zhang, L., Li, X., Wang, S., Romito,K. G., Kevin Huang, K. (2011). High conductivity mixed oxide-ion and carbonate-ion conductors supported by a prefabricated porous solid-oxide matrix, *Electrochemistry Communications*, 13, 554-557.

Zhang, L., Mao, Z., Thomason, J. D., Wang, S., Huang, K. (2012). Synthesis of a Homogenously Porous Solid Oxide Matrix with Tunable Porosity and Pore Size. *Journal of the American Ceramic Society*, 95, 1832-1837.

Zhang, L., Xu, N., Li, X., Wang, S., Huang, K., Harris, W. H., Chiu, W. K. S. (2012). High CO2 permeation flux enabled by highly interconnected three-dimensional ionic channels in selective CO_2 separation membranes. *Energy & Environmental Science*, 5, 8310-8317.

Zhang, L., Gong, Y., Yaggie, J., Wang, S., Romito, K., Huang, K. (2014) Surface modified silver-carbonate mixed conducting membranes for high flux CO2 separation with enhanced stability. *Journal of Membrane Science*, 453, 36-41.

Zhou, Z., Yang, J., Zhang, Y., Chang, L., Sun, W., Wang, J. (2007). NaA zeolite/carbon nanocomposite thin films with high permeance for CO_2/N_2 separation. *Separation and Purification Technology*, 55, 392-395.

Zhu, B., Liu, X., Zhou, P., Yang, X., Zhu, Z., Zhu, W. (2001). Innovative solid carbonate-ceria composite electrolyte fuel cells. *Electrochemistry Communications*, 3, 566-571.

Zhu, B. (2003) Functional ceria-salt-composite materials for advanced ITSOFC applications. *Journal of Power Sources*, 114, 1-9.

Zhu, B., Liu, X., Schober, T. (2004). Novel hybrid conductors based on doped ceria and BCY20 for ITSOFC applications. *Electrochemistry Communications*, 6, 378-383.

Zhu, X. J., Huang, B. (2012). Molten carbonate fuel cells. Electrochemical technologies for energy storage and conversion. Chapter 16, 729–775.

Zolochevsky, A., Grabovskiy, A. V., Parkhomenko, L., Lin, Y. S. (2012). Coupling effects of oxygen surface exchange kinetics and membrane thickness on chemically induced stresses in perovskite-type membranes. *Solid State Ionics*, 212, 55-65.

APPENDIX A

SYNTHESIS OF MACROPOROUS YTTRIA STABILIZED ZIRCONIA (YSZ) MEMBRANES ON POROUS ALUMINA SUPPORTS

A1. Preparation of porous alumina supports.

1. Mix 10 g of α-alumina powders (A16, Alco) with 1.5 g DI water and place in the mortar. Grind the powder mixtures to destroy large agglomerates and get homogeneous and non-sticky particles.
2. Weigh 2 g powders and put into a stainless steel die (diameter = 22 mm) and uniaxially press the powders under 150 MP for 5 minute.
3. Dry the green disks in air at a relative humidity (RH) of 50%-60% and a temperature of 40°C for 24 h and then sinter disks as the following program shown in Table A.1
4. Smooth the surface of sintered disks with SiC polishing papers (Struers)

Table A.1

Sinter steps for porous alumina support

Step	Rate (^{o}C/min)	Temperature (^{o}C)	Holding time (hr)
1	1	600	0.1
2	1.6	1260	0.1
3	1.6	200	0.1
4	1	1150	30
5	1	50	End

A2. Preparation of 10 wt% yttria stabilized zirconia (YSZ) suspension

1. Mix the YSZ (TZ-8Y, Tosoh Co.) powders with dilute nitric acid (pH=3-4) at a weight ratio of 1:2. Put the mixture in polyethylene (PE) pots with ZrO_2 balls 0.5 mm in diameter. Weight of the balls is 5 times of that dry YSZ powders.
2. Treat the solution ultrasonically to break the agglomerates before ball-milling.

3. Ball-mill the solution for 7-10 days with a spinning speed of 150-200 r/min.
4. Add more dilute nitric acid with the same pH to adjust the suspension concentration to 10 wt% after the ball-milling process.

A3. Preparation of 3 wt% polyvinyl alcohol (PVA) solution

1. Use PVA as drying control chemical additive (DCCA) to prevent crack formation. Add 95 ml DI water and ml 1 M HNO_3 solution into a 200 ml flask.
2. Add 3 g PVA (Fluka, MW=72,000) powders to solvent and stir without heating for first 15 minutes. Heat to 90-110^{o}C and keep stirring till form a transparent liquid.
3. Filter the solution.

A4. Preparation of macroporous YSZ membranes

1. Mix YSZ suspension and PVA solution with a volume ratio of 4:1. Use a stir bar to make the solutions completely blended and add 2-3 ml suspension in a container.
2. Dip the alumina supports into suspension for 5-10 s. Rotate dipped disk by 90^{o} and wipe the liquid on bottom with a paper tissue carefully after dip-coating.
3. Dry the coated membranes in air at a relative humidity (RH) of 50%-60% and a temperature of 40°C for 24 h. Sinter the membranes at 1000°C for 3 h (ramping rate = 100°C/h). Repeat the dip-coating, drying and sintering processes twice.
4. Characterize the resulting membranes with XRD, SEM and helium permeation tests.

APPENDIX B

SYNTHESIS OF MESOPOROUS YTTRIA STABILIZED ZIRCONIA (YSZ) MEMBRANES ON SUPPORTED MACROPOROUS YSZ MEMBRANES AND POROUS ALUMINA SUPPORTS

B1. Preparation 0.25 M zirconia sol

1. Heat 900 DI water to 90^{o}C.
2. Mix 123 ml zirconium-n-propoxide (Alfa, MW=327.56) with 500 ml HPLC grade isopropanol. Keep stirring the solution at 40-50^{o}C.
3. Add the solution to heated DI water drop by drop. The process lasts 2-3 hours and white zirconia precipitates will form.
4. Filter the precipitates with vacuum suction forming a zirconia cake. Wash the cake in water several times to remove isopropanol.
5. Dilute the cake in 1000 ml DI water and peptize with 125 ml 1M HNO_3 solution.
6. Reflux the solution at 90-100^{o}C for 12 h with stirring.
7. Treat the sol ultrasonically for 30 minutes-re-disperse the particles-before use.

B2. Preparation of 0.07 M yttrium nitrate solution

1. Add 95 ml DI water and ml 1 M HNO_3 solution into a 200 ml flask.
2. Add 2 g $Y(NO_3)_3$ (Alfa) powders in the solvent and stir at 50^{o}C for half to one hour until get a transparent solution.

B3. Preparation of DCCA

1. Use hydroxypropyl cellulose (HPC) and PVA as DCCA. Prepare PVA solution following the procedure described in Appendix A.

2. Prepare HPC solution by adding 0.35 g powder (Aldrich, MW=100,000) to solvent consisting of 95 ml DI water and ml 1 M HNO_3.
3. Stir at 90^{o}C for 3 h until get a clear solution.

B4. Preparation of supported mesoporous YSZ membranes

1. Mix aforementioned zirconia sol, yttrium nitrate solution and DCCA (PVA or HPC) together with a volume ratio of 35: 11: 11. Concentration of the sol is 0.154 M.
2. Dilute the original sol to concentrations of 0.026 M, 0.013 M, and 0.0087 M respectively by adding DI water.
3. Dip-coat the diluted sol-solutions separately on supported macroporous YSZ membranes and porous alumina supports made in Appendix A. Dipping time is 5 s.
4. Dry the dipped disks in air at a relative humidity (RH) of 50%-60% and a temperature of 40°C for 48-72 h. Long drying time allows for a complete dehydration.
5. Calcine the membranes at 450°C for 3 h (ramping rate = 0.5°C/min). Repeat the dip-coating, drying and calcination processes 5 times to ensure the preparation of crack-free mesoporous YSZ membranes.
6. Characterize the resulting membranes with X-ray diffraction, Scanning Electron Microscopy and helium permeation tests to identify properties.

APPENDIX C

SYNTHESIS OF MACROPOROUS YTTRIA STABILIZED ZIRCONIA (YSZ) MEMBRANES ON POROUS YTTRIA AND SAMARIUM DOPED BISMUTH OXIDE (BYS) SUPPORTS

1. Prepare $Bi_{1.5}Y_{0.3}Sm_{0.2}O_{3-\delta}$ (BYS) powders via citric acid method. Table C.1 shows the weight of precursors for synthesizing 0.05 mol products

Table C.1

Raw material compositions for $Bi_{1.5}Y_{0.3}Sm_{0.2}O_{3-\delta}$ (BYS)

Materials	Weight (g)
$Bi(NO_3)_3 \cdot 5H_2O$ (Aldrich, 98%)	36.380
$Y(NO_3)_3 \cdot 6H_2O$ (Aldrich, 99.9%)	5.745
$Sm(NO_3)_3 \cdot 6H_2O$ (Aldrich, 99.9%)	4.445
Citric acid (Alfa Aesar, 99.5%)	28.82

2. Dissolve metal nitrates and citric acid in 1000 ml HNO_3 (10 vol% concentrated one).
3. Stir the solution on the hot plate at 90-110^{o}C and get a transparent liquid. Keep stirring for another 2-3 h to allow for a complete polymerization reaction. Then increase temperature to speed up evaporation until forming sticky gel-like solids. Dry the gel and perform a fast, uniform self-ignition to remove organics at 400^{o}C. Air is supplied to facilitate burning. The whole process should be conducted in a fume hood due to emission of hazard chemicals (NO_x et al.).
4. Further sinter the powders at 900^{o}C for 6 h (ramping rate = 5^{o}C/min) to remove left impurities. Identify phase structure of the powders with X-ray diffraction.
5. Grind the calcined powders in a mortar to get uniform fine particles. Weigh 4 g BYS powders and completely mix with 0.4 g 3 wt% PVA (made in Appendix A). Press the powder mixtures uniaxially in a stainless steel die (diameter = 22 mm) under a pressure of 100 MP for 5 minutes.
6. Dry the disks for 24 h and sinter in air at 750^{o}C for 24 h (ramping rate = 1^{o}C/min).

7. Check molten carbonate wettability to the BYS supports by observing the contact angle of the molten carbonate drop on the support surface at 550°C.
8. Dip-coat 10 wt% yttria stabilized zirconia (YSZ) suspension on porous BYS support. Follow the same procedure as described in Appendix A.
9. Dry the coated membranes and sinter at 750°C for 6 h (ramping rate = 1°C/min). Repeat the dip-coating, drying and sintering processes twice.
10. Characterize the resulting membranes with X-ray diffraction, Scanning Electron Microscopy and helium permeation tests to identify properties.

APPENDIX D

SYNTHESIS OF MACROPOROUS SAMARIUM DOPED CERIUM OXIDE (SDC) MEMBRANES ON POROUS METAL OXIDE SUPPORTS

D1. Preparation of $Ce_{0.8}Sm_{0.2}O_{1.9}$ (SDC) powders

1. Prepare $Ce_{0.8}Sm_{0.2}O_{1.9}$ (SDC) powders by citric acid method. Table D.1 shows the weight of precursors for synthesizing 0.1 mol products

Table D.1

Raw material compositions for $Ce_{0.8}Sm_{0.2}O_{1.9}$ (SDC)

Materials	Weight (g)
$Ce(NO_3)_3 \cdot 5H_2O$ (Alfa, 99.5%)	34.738
$Sm(NO_3)_3 \cdot 6H_2O$ (Aldrich, 99.9%)	8.889
Citric acid (Alfa Aesar, 99.5%)	76.84

2. Dissolve metal nitrates and citric acid in 1000 ml HNO_3 (10 vol% concentrated one).
3. Stir the solution on the hot plate at 90-110^oC and get a transparent liquid. Keep stirring the solution until forming sticky gel-like solids. Dry the gel and perform a fast, uniform self-ignition to remove organics at 400^oC. Air is supplied to facilitate burning. The whole process should be conducted in a fume hood due to emission of hazard chemicals (NO_x et al.).
4. Further sinter the powders at 900^oC for 6 h (ramping rate = 5^oC/min) to remove left impurities. Identify phase structure of the powders with X-ray diffraction.
5.

D2. Preparation of SDC membranes on porous $Bi_{1.5}Y_{0.3}Sm_{0.2}O_{3-\delta}$ (BYS) supports

1. Prepare porous $Bi_{1.5}Y_{0.3}Sm_{0.2}O_{3-\delta}$ (BYS) supports following the same procedure described in Appendix C.
2. Prepare macroporous SDC membrane by suspension-coating method. Prepare SDC

suspension by mixing SDC powders and dilute nitric acid (pH=3-4) and ball mill the solution in polyethylene (PE) pots with ZrO_2 balls (5-7 times weight of SDC powders) for 5-7 days. Set ball-milling rate at 170-190 r/min. Add more dilute nitric acid to adjust solution pH and concentration to 10-12 and 5 wt% respectively after the ball-milling process.

3. Add PVA as DCCA to the suspension with a volume ratio of 3: 20.
4. Dip-coat SDC suspension on porous BYS support. Follow the same procedure as described in Appendix A. Set dipping time for 5 s.
5. Dry the coated membranes and sinter at 750 °C for 6 h (ramping rate = 1 °C/min). Repeat the dip-coating, drying and sintering processes twice.

D3. Preparation of porous SDC/BYS supports

1. Prepare the SDC and BYS powders following the procedures previously described.
2. Mix SDC and BYS powders with different volume ratio. Table D.2 gives the compositions for 10 g powder mixtures (0.5 g graphite added as pore former).

Table D.2

Compositions of SDC and BYS powders for SDC/BYS supports

No.	Volume Ratio (SDC: BYS)	Weight of SDC (g)	Weight of BYS (g)	Denotation
1	20: 80	1.65	7.85	SDC20BYS80
2	40: 60	3.41	6.09	SDC40BYS60
3	60: 40	5.30	4.20	SDC60BYS40
4	80:20	7.32	2.18	SDC80BYS20

3. Weigh 3.5-4 g SDC/BYS powders and pack into a stainless steel die (diameter = 22 mm) and press under 200 MP for 5 minutes. Add 0.2-0.3 g PVA as binder.
4. Dry the disks at a relative humidity of 50-60% and temperature of 40^{o}C for 1 day and then sinter in air at 950^{o}C for 24 h (ramping rate = 1^{o}C/min).
5. Characterize the supports with X-ray diffraction and helium permeation tests and observe molten carbonate contact angle with membrane surface at 550^{o}C.

D4. Preparation of SDC membranes on SDC/BYS supports

1. Prepare SDC membranes on SDC/BYS supports by co-pressing technique. Schematic drawing of the procedure is shown in Figure 5.2.
2. Dry ball-mill some SDC powders for 72 h (spinning rate = 150 r/min) to reduce particle size and use the powders for thin SDC layers.
3. Pack 0.2-0.3 g ball-milled SDC powders into a stainless steel die (diameter = 22 mm) and press under a hydraulic pressure of 5 MP for 10 s.
4. ADD 3.5 g SDC/BYS powder mixtures on pre-formed SDC layer and press under a pressure of 10 MP for 20 s.
5. Finally, add another 0.2-0.3 g ball-milled SDC on top and uniaxially press the powders under a pressure of 200 MP for 5 minutes to get a sandwich-like green disks.
6. Sinter the supports at 950 °C for 24 h (ramping rate = 1^{o}C/min).
7. Remove one of the SDC layers with SiC papers by polishing before infiltration.

APPENDIX E

ROOM TEMPERATURE HELIUM PERMEATION TESTS

E1. Steady state permeation test

1. Connect the permeation setup as shown in Figure G.1 (from Figure 2.1). Set the gauge pressure of the cylinder in the range of 30-40 psi.
2. Seal the membrane in the permeation cell with rubber O-rings. Balance the force exerted for sealing to avoid support breaking. Set the mass flow controller to proper values (10-100 ml/min) according to membrane permeances. Keep valve 4 (V4) closed during the whole test.
3. Check system leakage before test. Fully open valves 1-3 (V1-3) and close the needle valve. After aerating the system for 10-30 s, close V1. If the reading value of pressure sensor does not drop, there is no leakage and membrane is also unbroken.
4. Fully open V1 to V3 and needle valve. System reaches equilibrium state when reading values of pressure sensor do not change. Record P_h (upstream gauge pressure) and $\triangle P$ (gauge pressure difference). In the meantime, measure helium flow rate from bubble flow meter via a stop watch.
5. Close the needle valve to 11, 12.5, 13.5 and 14 turns and repeat step 4. Record values of P_h, $\triangle P$ and flow rate separately at each stable state.
6. Plot the pressure and gas permeance of the membrane in a straight line according to Equation 2.1. Calculate average pore size of the support by Equation 2.2.
7. Close helium cylinder and open V4 to vent the system after the test. Make sure reading values of pressure sensor to be zero.

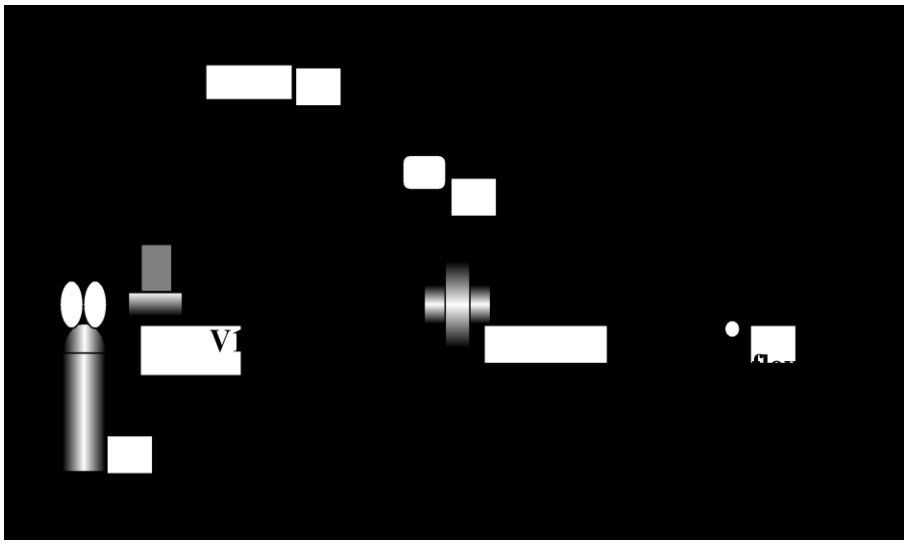

V1-V4: valves 1 to 4

Figure E.1 Schematic drawing of steady state helium permeation setup

E2. Unsteady state helium permeation test

1. Connect the permeation setup as shown in Figure G.2.
2. Evacuate the system with vacuum pump. Open valves (V) 2 to 4 and close valve 1. Wait until reading value of pressure sensors reaches the minimum value.
3. Close V2 to V4 and open V1. Adjust gauge pressure in the range of 30-40 psi. Stable value of the pressure sensor indicates the system is leakage free.
4. Record the value of the sensor as P_1. Open V3 and in the meantime start the stop watch. Close V3 and stop timing after the test. Record reading value of pressure senor as P_2 and time t. Use P_2 minus P_1 to get $\triangle P$. For porous membranes, test time is around 10-20 s. For dense membranes, alteration of pressure value within 0.01 psi in 10-15 minutes indicates dense property of the membrane.

5. Calculate the unsteady state helium permeance using the following Equation G.2.1

$$Q = \frac{\Delta P}{t} \cdot \frac{V_C}{S \cdot R \cdot T} \qquad \text{(G.2.1)}$$

Q = permeance (usually in mol/m^2/Pa)

$\triangle P$ = pressure difference (Pa)

t = time (s)

V_c = volume of the cylinder (m^3)

S = permeation area of the membrane (m^2)

R = gas constant for chosen units (8.314 m^2/kg/s^2/K/mol)

T = temperature (K)

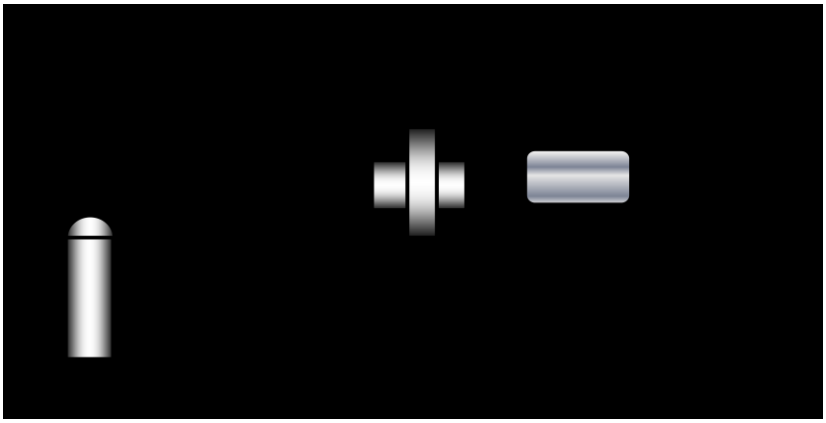

V1-V4: valves 1 to 4

Figure E.2 Schematic drawing of unsteady state helium permeation setup

APPENDIX F

EXAMINATION OF MOLTEN CARBONATE WETTABILITY TO POROUS CERAMIC SUPPORTS

1. Mix various carbonates (Li/Na/KCO_3) with a molar ratio of 42.5/32.5/2. Put the powders in a mortar and grind hard to break big agglomerates getting fine particles. Blend the powders completely and homogeneously.
2. Weigh 0.5-1 g mixture powders and put on top of porous supports. Slightly press the carbonates to form a cake on the surface.
3. Put the supports in a box furnace at room temperature.
4. Increase temperature to the range of 550-600^{o}C and wait for 1-2 h to let carbonate mixtures fully melt.
5. Open the furnace and observe state of melted carbonates on support surface. Due to high temperature, wear the mask field and high temperature gloves during operation.
6. Take photos of states of the supports at high temperature. For carbonate wettable materials, molten carbonates will be sucked into support pores via capillary force leaving nothing on surface. For carbonate non-wettable ceramics, clear liquid drop of molten carbonates will be observed on top.
7. Close the furnace and cool the system down to room temperature.

APPENDIX G

LIQUID NITROGEN METHOD FOR MEASURING POROSITIES

1. Prepare the stand with a sample pan and put on the scale. Measure the dry porous support weight (*D*) as shown in Figure I.1.
2. Immerse the support completely in liquid nitrogen. Wait until reading of the scale is stable. Record the value as immersed support weight (*I*).
3. Remove the support from liquid nitrogen and measure the weight immediately to prevent loss of liquid nitrogen. Record the number as saturated support weight (*S*).
4. Calculate the porosity by Archimedean principle using Equation I.1

$$P = \frac{S - D}{S - I} \tag{I.1}$$

P = Porosity

D = Dry support weight (g)

I = Immersed support weight (g)

S = Saturated support weight (g)

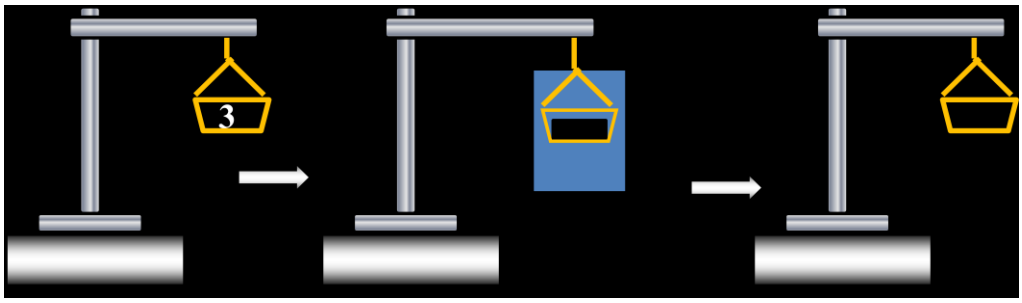

(1) Scale; (2) Steel stand; (3) Ceramic support sample; (4) Sample pan; (5) Liquid nitrogen container; (6) Steel holder with chain

Figure G.1 Schematic drawing of procedure for measuring porosities of the supports by liquid nitrogen method

APPENDIX H

X-RAY DIFFRACTION (XRD) AND SCANNING ELECTRON MICROSCOPY (SEM)

H.1 X-ray Diffraction

1. Use X-ray diffraction (XRD) (Bruker AXS, D8 Focus Diffractometer, CuKα) to characterize the phase structure or chemical stability of ceramic powder mixtures after high temperature treatment.
2. Grind powders samples to break agglomerates and then put into the sample pan. Place disk samples in the sample pan with adhesive tape to avoid movement during the test. Make sure the sample surface is leveling with the edge of the sample pan as shown in Figure J.1. X-ray could have same input and diffraction angles to avoid inaccuracy caused by 2θ deviation.
3. Set 2θ in the range of 20-70^{o} (depending on characteristic peak position of the material) and scanning speed of 1^{o}/min. Start the machine. Collect data and plot relationship between 2θ and peak intensity to get XRD patterns.

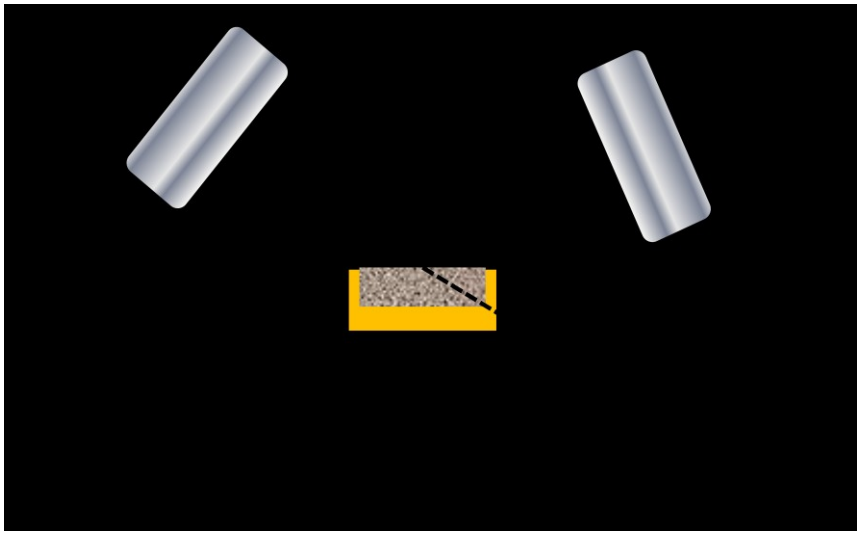

Figure H.1 Schematic drawing of working mechanism for X-ray diffraction (XRD)

H.2 Scanning electron microscopy

1. Use scanning electron microscopy (SEM, Phillips, FEI XL-30) to check morphology of the samples. For surface morphology, prepare the samples of 1 cm by 1cm squares. For cross section, sample height should be no more than 5 mm.
2. Stick the samples to the sample pan with adhesive tape (electronic conducting). Coat the sample surface with Pt/Au. The coating time is 5-7 minutes. Evacuate the system and operate to get images according to the manual.
3. For this particular machine, measuring voltage is 25 kV and spot size is 3. Remove the samples after test and re-evacuate the system.

APPENDIX I

SEALING OF THIN CERAMIC-CARBONATE DUAL-PHASE MEMBRANES FOR HIGH TEMPERATURE PERMEATION TEST

1. Thin ceramic-carbonate dual-phase membranes were sealed in the high temperature permeation cell composed of three parts.
2. Put one piece of graphite seal (7/8”OD×0.55”ID×1/8” Thk, Mercer Gasket &Shim), membrane and the second piece of graphite seal in series in the chamber of part C. The membrane was sandwiched by two pieces of the graphite seals
3. Put part B on top and seal the membrane. Under pressure, graphite seal would deform and make sure to balance the force exerted on the seals to avoid breaking the thin dual-phase membrane.
4. After sealing the membrane inside chamber of part C, put another bigger graphite seal (2 3/8”OD×1 7/8”ID×1/8” Thk, Mercer Gasket &Shim) in the outside slot.
5. Put part A on part C and seal the whole permeation cell.
6. After sealing, put the cell in the furnace and connect the system as shown in Figure 3.2 for high temperature permeation test.